BIOGEOCHEMICAL INVESTIGATION OF CENTRIFUGED FINE TAILINGS DEPOSITS AT AN OIL SANDS MINE IN NORTHERN ALBERTA, CANADA

A Thesis Submitted to the College of

Graduate Studies and Research

In Partial Fulfillment of the Requirements

For the Degree of Master of Science

In the Department of Geological Sciences

University of Saskatchewan

Saskatoon

By

KAITLYN KASSANDRA HEATON

PERMISSION TO USE

In presenting this thesis in partial fulfillment of the requirements for a Postgraduate degree from the University of Saskatchewan, I agree that the Libraries of this University may make it freely available for inspection. I further agree that permission for copying of this thesis in any manner, in whole or in part, for Scholarly purposes may be granted by the professors who supervised my thesis work or, in their absence, by the Head of the Department in which my thesis work was done. It is understood that any copying or publication or use of this thesis or parts thereof for financial gain shall not be allowed without my written permission. It is also understood that due recognition shall be given to me and to the University of Saskatchewan in any scholarly use which may be made of any material in my thesis.

Requests for permission to copy or to make other use of material in this thesis in whole or in part should be addressed to:

Head of the Department of Geological Sciences
University of Saskatchewan
114 Science Place
Saskatoon, Saskatchewan, Canada
S7N 5E2

ABSTRACT

Centrifuged fine tailings (CFT) technology was developed to reduce volumes of fluid fine tailings (FFT) stored in tailings ponds at oil sands mines. Increasing FFT inventories in tailings ponds results from slow settlement of clay minerals suspended in oil sands process-affected water (OSPW). High sodium (Na) concentrations in OSPW increase the electrical double layer (EDL) thickness at clay-mineral surfaces, which hinders aggregation and, therefore, settlement. Production of CFT involves dredging FFT from tailings ponds, amending with polyacrylamide and gypsum, and decanter centrifuging. This process promotes aggregation and flocculation, and decreases gravimetric water content from approximately 70 to 55 % (w/w). The resulting CFT is deposited in thin lifts (< 2 m) into sub-aerial containment areas to facilitate further dewatering via freeze-thaw cycling.

This research was focused on characterizing the biogeochemical conditions and processes within the CFT deposits. These deposits remain tension-saturated and, similar to tailings ponds, anaerobic redox processes including iron (Fe) reduction, sulfate (SO_4) reduction, and methanogenesis likely dominate.

The geochemistry, mineralogy, and microbiology of core samples from two field-scale test deposits and two full-scale production deposits were examined. Results were compared with previously published data from FFT deposits to assess impacts of chemical amendments on biogeochemical processes within CFT deposits.

Pore-water chemistry within the CFT deposits is affected by evaporative concentration of dissolved ions, which leads to high concentrations of salts (Na, 3000 mg L^{-1}; Cl, 1500 mg L^{-1}; SO_4, 5000 mg L^{-1}) and naphthenic acids (NAs 150 mg L^{-1}) near the surface (< 0.3 m) of these deposits. Increases in concentrations of conservative ions (i.e., Cl) indicated that 30 to 40 % of pore water was lost to evaporation at a depth of 0.1 m below surface. Results also suggest that microbially-mediated Fe reduction, SO_4 reduction, and methanogenesis are dominant redox processes within the CFT deposits. Microbes related to genera known to use these terminal electron acceptors were identified by high-throughput DNA sequencing data. Increases in

dissolved Fe and H_2S with depth were also indicative of Fe and SO_4 reduction, respectively. These results provide the first insight into biogeochemical conditions and processes within oil sands CFT deposits.

ACKNOWLEDGEMENTS

An immense thank you to my (co) supervisors, Drs. Matt Lindsay and Joyce McBeth, for all the guidance, encouragement, and mentorship provided throughout my degree - it was invaluable. Thank you so much for supporting my goal of finishing so quickly; I thoroughly appreciate the attention to detail you've shown in providing feedback and comments in the thesis writing process. You have helped to inspire me to consider a more holistic view of environmental problems than I would have done without this experience, which will be valuable in my future career.

Thank you to Dr. Won Jae Chang for reminding me to consider statistics during experimental design and for the comments that helped to strengthen my thesis. Thank you also to my external examiner, Terry Fonstad, for reviewing this thesis and providing many helpful comments.

Funding for this research was provided by Syncrude Canada Ltd and the National Sciences and Engineering Research Council of Canada (NSERC) through an Industrial Research Chair held by Matt Lindsay. A portion of the research described in this paper was performed at the Canadian Light Source, which is funded by the Canada Foundation for Innovation, the NSERC, the National Research Council Canada, the Canadian Institutes of Health Research, the Government of Saskatchewan, Western Economic Diversification Canada, and the University of Saskatchewan.

My field sampling campaign could not have been completed without support. Thank you to Dallas Heisler for liaising information from others at Syncrude. Thank you to Lori Cyprian and Chris Beierling for the Syncrude on-site support, as well as Richard Maslanko and David Duford for Syncrude lab support. Thank you to Dyan Pratt and Spencer, Dave, Chris, Ben, Jake, Ashley, Tiereny, Farhan, and Dallas from Conetec for the assistance with collecting the cores.

I also could not have possibly finished my lab work without the support of several people. Thank you to Danielle Penrod, Jake Nesbitt, Matt Lindsay, Jared Robertson, Yu Han, Amy Pitman, Colin Pitman, and Kathryn Dompierre - I couldn't have completed my first and

second stream sampling without you. Thank you to Darshil Koshti for preparing and measuring samples for PXRD.

I also want to acknowledge Jonathan Vyskocil for processing the DNA sequencing data in mothur and related sequencing support, Matt Lindsay for processing the XANES data, and Jake Nesbitt for teaching me how to use PREEQCi and Match!.

Thank you to Amy Pitman for the sanity check nearly every lunch-hour. Thank you to my family and friends for keeping me inspired that this research is interesting and valuable. And, finally, I am so grateful to Duncan for his unwavering support throughout my degree.

To Duncan.

TABLE OF CONTENTS

LIST OF TABLES

LIST OF FIGURES

LIST OF ABBREVIATIONS

AEO	Acid extractable organics
AER	Alberta Energy Regulator
AOSR	Athabasca oil sands region
BDL	Below detection limit
bp	Base pairs
BTEX	Benzene, toluene, ethylbenzene, xylene
CCD	Charge-coupled device
CFT	Centrifuged fine tailings
CLS	Canadian Light Source
CMCF	Canadian Macromolecular Crystallography Facility
DNA	Deoxyribonucleic acid
DNase	Deoxyribonuclease
EC	Electrical conductivity
EDL	Electrical double layer
Eh	Reduction-oxidation potential of a hydrogen electrode
ESI-FT-ICR-MS	Electrospray ionization Fourier transform ion cyclotron resonance mass spectrometry
EV-1	First full-scale CFT deposit
EV-2	Second full-scale CFT deposit
FeOB	Iron-oxidizing bacteria
FeRB	Iron-reducing bacteria
FFT	Fluid fine tailings
FTIR	Fourier transform infrared
GC	Gas chromatography
GC-MS	Gas chromatography – mass spectrometry
GD	Gypsum truck dump test CFT deposit
HDPE	High density polyethylene
IC	Ion chromatography
ICP-MS	Inductively coupled plasma – mass spectrometry
ICP-OES	Inductively coupled plasma – optical emission spectroscopy
NA	Naphthenic acid
ND	Not detected
NMDS	Non-metric multidimensional scaling
OSPW	Oil sands process-affected water

OTU	Operational taxonomic unit
PAH	Polycyclic aromatic hydrocarbon
PCA	Principal component analysis
PCR	Polymerase chain reaction
PES	Polyesthersulfone
PHC	Petroleum hydrocarbon
PXRD	Powder x-ray diffraction
qPCR	Quantitative polymerase chain reaction
RNA	Ribonucleic acid
RNase	Ribonuclease
SI	Saturation index
SOB	Sulfur-oxidizing bacteria
SRB	Sulfate-reducing bacteria
SXRMB	Soft X-Ray Micro-characterization Beamline
TD	Truck dump test CFT deposit
TEA	Terminal electron acceptor
XANES	X-ray absorption near-edge structure

CHAPTER 1 INTRODUCTION

Heavy unconventional oil with a density greater than 1000 kg m^{-3} and a viscosity exceeding 1 kPa·S is classified as bitumen (Banerjee, 2012). This form of oil is hosted in cretaceous sand deposits in the Athabasca oil sands region (AOSR) of Northern Alberta, Canada. Bitumen extraction and upgrading in the AOSR has altered a large area of boreal forest. The footprint of surface mining operations currently exceeds 715 km^2 (CAPP, 2012), including approximately 200 km^2 of tailings ponds (Kasperski and Mikula, 2011).

Tailings ponds, which are also referred to as settling basins, are large earthen dam-based containment structures used to hold fluid tailings and other bitumen extraction and upgrading by-products. Extraction involves mixing crushed oil sands ore with hot water and solvents to separate the bitumen and sand. The liquid waste stream – known as oil sands process-affected water (OSPW) – contains elevated concentrations of dissolved salts, naphthenic acids (NAs), and unrecovered bitumen and other petroleum hydrocarbons (PHCs; Allen, 2008; Kavanagh et al., 2011). Associated tailings - a suspension of clay and sand particles in OSPW - are hydro-transported to tailings ponds for settlement and storage under a water cover. The sand settles rapidly in beaches, whereas the clay remains suspended in OSPW forming fluid fine tailings (FFT), which typically has initial solids content of 30 to 35 % (w/w).

Clay minerals include hydrous silicate and aluminosilicate phases formed in sheets with opposing negative surface charge. The negative charge is balanced by cations including calcium (Ca), magnesium (Mg), potassium (K), and sodium (Na) at clay mineral surfaces. Sodium hydroxide is added during extraction to increase bitumen recovery. This addition promotes the exchange of monovalent Na for divalent Ca, which increases the thickness of the electrical double layer (EDL) and hinders aggregation. The resulting dispersion of the clay particles helps to enhance bitumen recovery. However, increasing the EDL thickness also impedes settling and dewatering of clay particles within tailings ponds, which has led to increased volumes of FFT stored in tailings ponds.

Oil sands mining operations have increased tailings storage capacity to accommodate increasing FFT inventories. The Alberta Energy Regulator (AER) issued Directive 074 in September of 2009 to mandate a reduction in inventories of FFT stored in the tailings ponds by 50 % within five years (AER, 2009). Reducing these inventories using technologies that enhance FFT dewatering and/or divert FFT from the tailings ponds provides a number of potential benefits including reduced dewatering times and increased rates and volumes of OSPW recycling. Ultimately, reducing FFT inventories minimizes the required capacity of tailings ponds, reduces the volume of fresh water extracted from the Athabasca River, and facilitates progressive reclamation of mines.

Oil sands surface mine operators were permitted to develop and implement technologies to address Directive 074 that best suited their operations. Syncrude Canada Ltd. (Syncrude) piloted centrifugation technology in response to this directive. With this technology, FFT is dredged from the mudline of the tailings pond after one to two years of settlement. Polyacrylamide and gypsum [$CaSO_4 \cdot 2H_2O$] are then added to promote flocculation and coagulation, respectively, and the tailings are then decanter-centrifuged. Polyacrylamide bonds with clay particles and creates larger, heavier aggregates that will more readily settle out of the water column. Gypsum addition reduces the thickness of the EDL by replacing monovalent Na ions with divalent Ca ions at clay mineral surfaces. This ion exchange reaction facilitates closer packing of clay particles, thereby enhancing settlement and dewatering. The resulting centrifuged fine tailings (CFT) are deposited sub-aerially in thin lifts (< 2 m) by truck end-dumping. The CFT in these deposits are allowed to undergo one freeze-thaw cycle before subsequent lifts are placed. This step is integral to the dewatering process. During freezing, water collects in the interstitial space and forms larger ice crystals, and then, as the deposit thaws, the water melts and is expelled toward the surface of the deposit and runs off. At the time of deposition, CFT is characterized by a moisture content of 50 to 58 % (w/w). The moisture content decreases to approximately 30 % (w/w) following consolidation and dewatering by freeze-thaw cycling and self-weight. Centrifuge technology, therefore, enhances geotechnical characteristics of fine tailings, helps reduce FFT inventories, and increases OSPW recycling. However, the impact of this technology on resulting CFT pore-water chemistry and on water released during *in situ* dewatering remains largely unknown. The potential impact of this water

on receiving groundwater or surface water bodies is an important consideration when developing mine closure strategies for mines in the AOSR (Council of Canadian Academies, 2015).

Water quality of the CFT deposits may be directly or indirectly impacted by the chemical amendments. In addition to contributing Ca, gypsum is a source of sulfate (SO_4) and, therefore, has potential to promote microbial SO_4 reduction (Holowenko et al., 2000; Kijjanapanich et al., 2014; Salloum et al., 2002). In contrast, polyacrylamide contains carbon (C) and nitrogen (N) that could stimulate indigenous microbial populations (Kay-Shoemake et al., 1998) and promote methanogenesis (Haveroen et al., 2005). Deposits of CFT are largely water-saturated (i.e. tension-saturated) and anoxic conditions are expected to dominate. This research, therefore, examines anaerobic reduction-oxidation (redox) processes, with particular emphasis on microbial SO_4 reduction and methanogenesis.

Directive 074 was suspended in March 2015 (AER, 2015) and replaced by a Tailings Management Framework that is currently under review (Government of Alberta, 2015). Nevertheless, Directive 074 was the impetus for development of CFT technology, which is expected to continue playing a central role in achieving reduction in FFT inventories at the Mildred Lake mine and, potentially, other operations in AOSR of Northern Alberta, Canada (Council of Canadian Academies, 2015).

1.1 Research Hypotheses and Objectives

This study is the first to examine biogeochemical processes in CFT deposits produced at oil sands mines in Northern Alberta, Canada. The overall goal of this research is, therefore, to develop an overarching understanding of the relationships between chemical, biological, and physical processes and their impact on water chemistry. Two main hypotheses will be tested to understand these relationships: 1) evaporation from the surface of CFT deposits concentrates dissolved ions and produces pore water with high total dissolved solids; and 2) the addition of gypsum shifts the microbial community towards SO_4 reducers. The specific objectives of this study are to:

1) constrain the principal controls on pore-water chemistry;
2) assess the influence of chemical amendments on biogeochemical processes; and
3) develop initial conceptual and geochemical models of CFT deposits.

1.2 Thesis Organization

This thesis is structured in manuscript-style according to guidelines established by the College of Graduate Studies and Research at the University of Saskatchewan. Included are a general introduction (Chapter 1), two manuscripts (Chapters 2 and 3), and overall conclusions (Chapter 4). The first manuscript (Chapter 2) describes the overall biogeochemical characteristics of CFT deposits studied for this M.Sc. thesis. The second manuscript (Chapter 3) compares biogeochemical processes occurring among these CFT deposits, which were produced up to four years apart using differing amounts of chemical amendments.

CHAPTER 2 BIOGEOCHEMICAL CHARACTERISTICS OF CENTRIFUGED OIL SANDS FINE TAILINGS

2.1 Executive Summary

Centrifuged fine tailings (CFT) technology has been developed by oil sands surface mine operators in response to Directive 074. Integration of this material into mine closure landscape requires an understanding of the biogeochemical characteristics of CFT. However, the biogeochemical processes and conditions in CFT deposits have not yet been assessed. This study examined geochemical, microbiological, and mineralogical characteristics of two field-scale test deposits and two full-scale production deposits. Gypsum and polyacrylamide are added to enhance dewatering during centrifugation. These additives may affect the microbially-mediated processes of iron (Fe(III)) reduction, sulfate (SO_4) reduction, and methanogenesis that are expected to occur within the CFT deposits. Relatives of microbial families with known Fe reduction, SO_4 reduction, and methanogenic capabilities were identified. Gypsum contributed additional SO_4 and increased the concentration of calcium (Ca). Evaporative concentration of dissolved ions occurred near the surface of these deposits, where concentrations up to 3700 mg L^{-1} sodium (Na), 2200 mg L^{-1} chloride (Cl), 6400 mg L^{-1} SO_4, and 260 mg L^{-1} total naphthenic acid (NA) were observed. Increased Na concentrations near the surface of the deposits promoted ion exchange at clay mineral surfaces and increased Ca concentrations in CFT pore water near the deposit surface. Although the CFT may satisfy the objectives of Directive 074, chemical amendments added during CFT production increased dissolved ion concentrations and reduced water quality.

2.2 Introduction

Tailings ponds currently cover approximately 200 km^2 of the landscape in the Athabasca Oil Sands Region (AOSR) of Northern Alberta, Canada (Kasperski and Mikula, 2011). Water quality is one of the biggest environmental concerns associated with oil sands tailings deposits (Council of Canadian Academies, 2015). Oil sands process-affected water (OSPW) associated with tailings solids generally contains elevated concentrations of dissolved salts, naphthenic

acids (NAs), trace elements, as well as unrecovered bitumen and other petroleum hydrocarbons (PHCs; Allen, 2008; Kavanagh et al., 2011). Directive 074 was issued in 2009 by the Alberta Energy Regulator (AER) to address increasing tailings inventories within these ponds (AER, 2009). This directive required oil sands surface mine operators to develop approaches to reduce the volumes of fine particles entering tailing ponds. The presence of clay minerals, which represent a substantial component of fluid fine tailings (FFT), is an important factor in the lengthy settlement times for FFT in these ponds.

Clay minerals are characterized by an electrical double layer (EDL), where cations balance the net negative surface charge. The EDL consists of a surface layer containing specifically-adsorbed and non-specifically adsorbed, hydrated cations called the Stern layer. The diffuse layer is a distal second layer of non-specifically adsorbed, hydrated cations attracted to the clay mineral surface by Van der Waals forces. The combined thickness of these two layers is determined by the valence and hydrated radius of the cations within the EDL. Ion exchange reactions, for example sodium (Na) for calcium (Ca), can occur at clay mineral surfaces:

$$Ca \cdot X + 2Na^{+} \rightleftharpoons Ca^{2+} + 2Na \cdot X \qquad 2.1$$

where X represents the clay mineral surface. Because Na^{+} is monovalent, it is added during ore processing to increase the thickness of the EDL, promote clay mineral dispersion, and enhance bitumen recovery. A thicker EDL also hinders aggregation and, therefore, settlement of clay minerals within tailings ponds. Exchange of one Ca^{2+} atom with two Na^{+} atoms decreases the thickness of the EDL and improves settlement. The cation exchange capacities (CECs) for the most common clay minerals found in FFT are 3 to 15 meq 100 g^{-1} for kaolinite and 10 to 40 meq 100 g^{-1} for the illite and chlorite (Kaminsky, 2008; Mitchell and Soga, 2005). Montmorillonite and vermiculite, which have also been identified in FFT, can have CEC values of up to 150 meq 100 g^{-1} (Mitchell and Soga, 2005). However, FFT can have CEC values much higher than those represented by the individual clay components due to the presence of mixed-layer clay minerals (Ignasiak et al., 1983; Kaminsky, 2008; Smith and Ng, 1993).

Centrifuged fine tailings (CFT) are produced by amending fluid fine tailings (FFT) dredged from tailings ponds with polyacrylamide and gypsum [$CaSO_4 \cdot 2H_2O$] and decanter-centrifuging the mixture. Supernatant is recycled for ore processing, and CFT is deposited sub-aerially by truck end-dumping. Polyacrylamide and gypsum are added prior to centrifugation to promote flocculation and coagulation of clay minerals, respectively. The initial moisture content

of CFT produced using this technology is typically 50 to 58 % (w/w); however, subsequent *in situ* dewatering due to freeze-thaw cycling and evaporation can reduce the moisture content to less than 30 % (w/w). Lower water contents generally correspond to increased geotechnical strength, which is required to integrate CFT into the closure landscape.

Studies of the biogeochemical characteristics of CFT have not previously been published. However, the biogeochemical characteristics of FFT – the source material for CFT – are fairly well constrained. The chemistry of water contained in tailings ponds is dominated by that of OSPW, which generally exhibits mildly alkaline pH (8.0-8.4) and elevated electrical conductivity (EC; 0.3-3.5 mS cm^{-1}). The dominant ions contributing to elevated EC include Na (500-1000 mg L^{-1}), bicarbonate (HCO_3^-; 790-1700 mg L^{-1}), chloride (Cl; 500-700 mg L^{-1}), and sulfate (SO_4; 2-530 mg L^{-1}); however, ammonia (NH_3; 4-14 mg L^{-1}) and total NA (40-90 mg L^{-1}) are present at elevated concentrations (Allen, 2008; Chen et al., 2013; Chi Fru et al., 2013; Fedorak et al., 2003; Holowenko et al., 2000; Ramos-Padrón et al., 2011; Salloum et al., 2002; Siddique et al., 2014a; Stasik and Wendt-Potthoff, 2014; Stasik et al., 2014). Methanogenesis and SO_4 reduction are generally the dominant redox processes within FFT deposits (Chen et al., 2013; Holowenko et al., 2000; Ramos-Padrón et al., 2011; Siddique et al., 2014b, 2012, 2008, 2006; Stasik and Wendt-Potthoff, 2014; Stasik et al., 2014), although iron (Fe) reduction is also important (Stasik and Wendt-Potthoff, 2014; Stasik et al., 2014). The addition of polyacrylamide during CFT production has potential to stimulate microbial growth by contributing carbon (C) and nitrogen (N) (Haveroen et al., 2005; Kay-Shoemake et al., 1998), whereas gypsum addition has potential to promote SO_4 reduction (Ramos-Padrón et al., 2011; Salloum et al., 2002), and may, therefore, supress methanogenesis (Holowenko et al., 2000; Ramos-Padrón et al., 2011; Stumm and Morgan, 1996).

The objective of this study was to constrain the geochemical, mineralogical, and microbiological characteristics of oil sands CFT deposits. Measurements of pore-water geochemistry were made on core samples collected from multiple locations within four CFT deposits. Complementary investigations of the geochemistry, mineralogy, and microbiology of CFT solids were performed. Results of this study provide the first insight into the processes influencing pore-water quality within CFT deposits.

2.3 Site Description

The Mildred Lake mine, which is operated by Syncrude Canada Ltd (Syncrude), is located approximately 35 km north of Fort McMurray, Alberta, Canada. The regional climate is characterized by short cool summers and long cold winters (Hackbarth and Nastasa, 1979). Minimum and maximum mean monthly temperatures measured at the Mildred Lake station (57.04° N, 111.56° W) were 18.4°C (July) and -17.4°C (January), respectively, from 1994 to 2015 (Environment Canada, 2015). Mean annual precipitation over this time was 388 mm (σ = 95 mm), with approximately 70 % occurring from April to September when average monthly temperatures were above 0°C (Environment Canada, 2015).

This study was focused on four CFT deposits at the Mildred Lake mine including two field-scale test deposits (57°05'N 111°37'W) and two full-scale production deposits (57°00'N 111°45'W; Figure 2.1). The two test deposits were constructed by truck end-dumping during development of the CFT technology. The first of these deposits (TD) was amended only with polyacrylamide (0.7 to 0.85 kg tonne^{-1} dry weight FFT), whereas the other (GD) was amended with polyacrylamide (0.7 to 0.85 kg tonne^{-1} dry weight FFT) and gypsum (~0.8 kg tonne^{-1} dry weight FFT). The TD deposit measured approximately 100 m long and varied in thickness from less than 1.0 m to 1.4 m. The GD deposit measured 40 m in length and was consistently less than 1.1 m thick. Both test deposits were constructed in 2010 and sampled in June 2014, following four freeze-thaw cycles. The two full scale deposits (EV-1, EV-2) were amended with polyacrylamide (~1.5 kg tonne^{-1} dry weight FFT) and gypsum (~1.5 kg tonne^{-1} dry weight FFT) and also produced by truck end-dumping. The gypsum added to these deposits can, however, vary up to six times higher to manage short-term geotechnical characteristics. Deposition of the first lift in EV-1 began in August 2012 and, following a break between September 2012 and April 2013, was completed in July 2013. Deposition of CFT in EV-2 occurred between May and July 2013. These deposits each cover an area of roughly 10^5 m^2 and were approximately 1.7 m thick when sampled in December 2013 (EV-1) and June 2014 (EV-2). Although the CFT in EV-2 had completed a full freeze-thaw cycle, only portions of the CFT in EV-1 had completed one freeze-thaw cycle at the time of sampling.

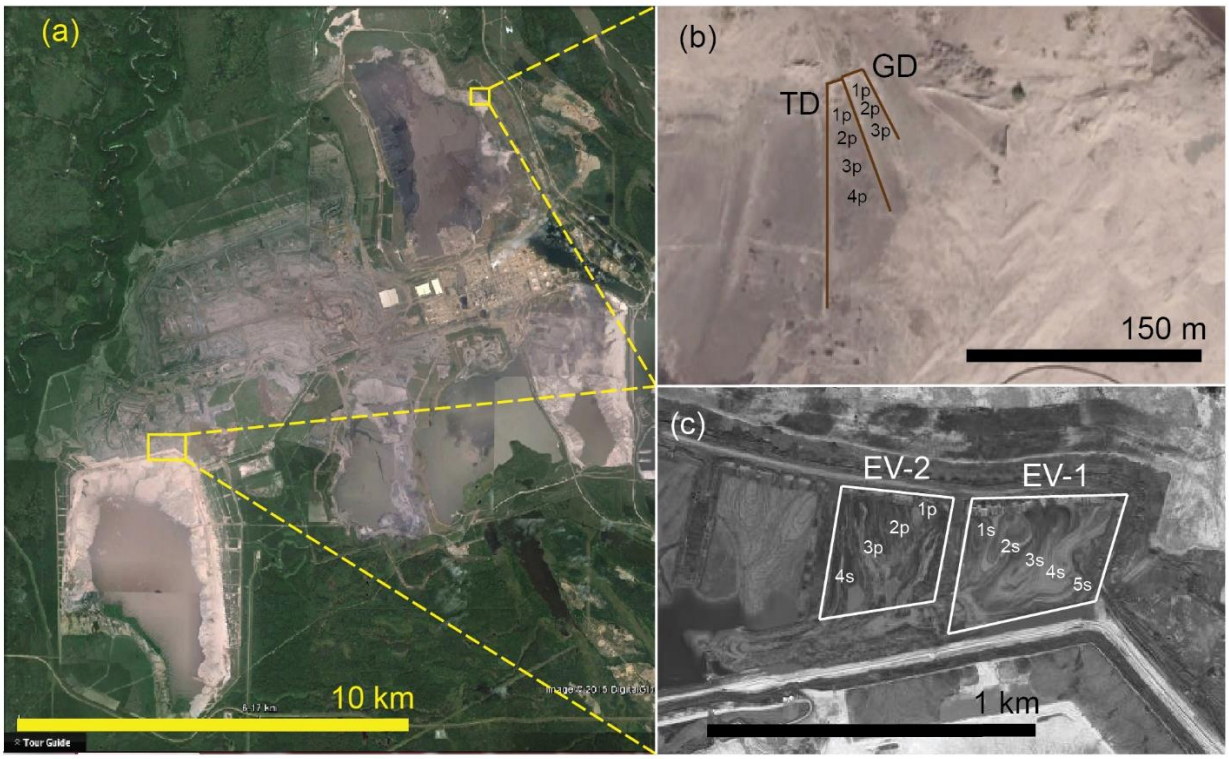

Figure 2.1: (a) Site map of Syncrude's Mildred Lake Mine site highlighting deposit areas. (b) Test Deposits, GD, and TD and the sampling bore holes. The "p" indicates paired cores were collected. (c) Full-scale deposits, EV-1 and EV-2 and their sampling boreholes. The "p" indicates paired cores were collected, the "s" indicates a single core was collected (Images (a) and (b) © 2015 DigitalGlobe, Image (c) supplied by Syncrude)

2.4 Materials and Methods

2.4.1 Sample collection

Core samples were collected along transects of the test deposits (TD, GD) and full-scale deposits (EV-1, EV-2) to examine vertical and lateral variability in the CFT deposits. Paired cores were collected from TD, GD, and EV-2 to ensure sufficient sample would be available for analysis. A piston coring technique similar to that described by Starr and Ingleton (1992) was used to collect continuous core samples. The cores were collected into 7.2 cm diameter aluminum (Al) tubing that was advanced by direct push at approximately 0.6 m depth intervals. The recovered length was measured and divided by the push length to determine a scaling factor, assuming linear compaction across the depth interval. The cores were then sealed with paraffin wax and polyethylene caps, and secured with vinyl tape to minimize oxygen exposure. The cores were shipped on ice to the University of Saskatchewan. The upper 0.6 m of EV-1 was frozen during the December 2013 sampling campaign; therefore, samples were obtained by augering

over this depth interval. The frozen samples were sealed in polypropylene bags and transported frozen to the University of Saskatchewan. All samples were transferred to a freezer and stored at -20°C until analysis.

2.4.2 Pore-water extraction and analysis

Prior to analysis, the frozen core samples were transferred into an anoxic chamber (<5 vol% Hydrogen gas [H_2], balance nitrogen gas [N_2]), allowed to thaw, and then extruded from the core tubing. Depth intervals for pore-water extraction were determined based upon water content and the volume of water required for analysis (~100 mL total). Sub samples from these intervals were transferred into multiple (9 to 20) 50 mL conical tubes and centrifuged at 10,000 rpm (13,800 g) for 30 to 120 minutes, with samples exhibiting lower moisture content requiring a longer centrifugation time. Supernatant from all sub-samples was combined for each depth interval, and measurements of pH, redox potential (Eh), and electrical conductivity (EC) were performed on unfiltered samples immediately after centrifugation. The pH electrode (Thermo ORION, model 8156BNUWP) was regularly calibrated to NIST traceable pH 4, 7, and 10 buffer solutions. Zobell's (Nordstrom, 1977) and Light's (Light, 1972) solutions were used to regularly check performance of the redox electrode (Thermo ORION, model 9678BNWP). Redox potentials were corrected to the standard hydrogen electrode and values are reported as Eh. The EC cell (Thermo ORION, model 011050MD) was regularly checked against a NIST traceable 9.981 mS cm^{-1} standard solution.

Water samples were passed through sterile 0.45 µm polyesthersulfone (PES) syringe filter membranes (Pall Corporation, USA) using sterile syringes (HSW GmbH, Germany) prior to determination of alkalinity, hydrogen sulfide (H_2S), and NH_3. Alkalinity was measured by titrating to the bromocreosol green-methyl red endpoint using 1.6 N sulfuric acid. Dissolved H_2S and NH_3 were determined by spectrophotometry (Hach Company, model DR2800) using the methylene blue (Lindsay and Baedeker, 1988) and salicylate (Hach Company, 2007) methods, respectively.

Dissolved concentrations of inorganic anions and major cations were quantified by ion chromatography (IC; EPA Method 300.0) and inductively coupled plasma – optical emission spectroscopy (ICP-OES; EPA Method 200.7). Trace elements and potassium (K) concentrations were determined by inductively coupled plasma – mass spectrometry (ICP-MS; EPA Method 200.8). Samples for IC analyses were passed through 0.45 µm PES syringe filter membranes and

stored in high density polyethylene (HDPE) bottles at 4°C until analysis. Samples for ICP-MS and ICP-OES analyses from EV-1 were syringe filtered using 0.45 µm PES membranes, whereas those from EV-2, GD, and TD were passed through 0.2 µm PES membranes. This change was made following observations of elevated Al concentrations in some samples from EV-1. Samples for ICP-OES and ICP-MS analysis were acidified to pH less than 2 using trace element grade nitric acid (HNO_3; Omnitrace, EMD Millipore, USA) and stored in HDPE bottles at 4°C until analysis. Finally, dissolved acid-extractable organics (AEO) were determined using Fourier Transform Infrared (FTIR) Spectroscopy (Scott et al., 2008). Samples were passed through 0.45 µm PES membranes and stored in 40 mL amber glass vials with no headspace until analysis. Although results of this method are commonly reported as total NA, it has been shown to overestimate NA concentrations determined by gas chromatograph – mass spectrometry (GC-MS; Scott et al., 2008) and electrospray ionization Fourier transform ion cyclotron resonance mass spectrometry (ESI-FT-ICR-MS; Grewer et al., 2010). Nevertheless, AEO values determined by FTIR spectroscopy are referred to as total NA for the purpose of this study.

2.4.3 Geochemical modelling

The geochemical code PREEQCi (Version 3.1.6-9191; Parkhurst and Appelo, 2013) was used to assess data quality and to assist with data interpretation. Saturation indices (SIs) for relevant minerals were calculated using the included WATEQ4F thermodynamic database (Ball and Nordstrom, 1991). Assessment of data quality in PREEQCi demonstrated that the charge balance error (CBE) of the pore-water chemistry data was generally very good, with most samples (n = 65) having a CBE of ± 6 % and the remainder (n = 9) having a CBE of ± 13 %.

2.4.4 Microbiology

Sub-samples of the CFT samples thawed in the anaerobic chamber (<5 vol% H_2, balance N_2) were obtained using sterile (i.e., free of deoxyribonucleic acid (DNA), ribonucleic acid (RNA), deoxyribonuclease (DNase), and ribonuclease (RNase)) 15 mL conical polyethylene tubes. Ethanol-sterilized tubing snips were used under a flame to trim the bottoms off the tubes. The trimmed tubes were then placed in an autoclaved plastic beaker covered with sterile Al foil and transferred into the anaerobic chamber. The tubes were pushed into the cores of the thawed CFT to collect the sub-samples. The caps were tightened and the bottom ends were sealed with paraffin wax. These tubes were stored in the freezer at -20°C until DNA extraction.

Initial DNA extraction trials were performed using three different commercially available soil DNA extraction kits (PowerSoil and PowerWater kits, Mo Bio Laboratories Inc., Carlsbad, USA; FastDNA Spin Kit for Soil, MP Biomedicals, Santa Ana, USA) with triplicate extractions performed for each kit from a single sub-core sample. Extracted DNA yields were then quantified with a fluorometer (Life Technologies, Qubit 2.0) and a spectrophotometer (Thermo Scientific, Nanodrop 2000). As a result of these tests, the FastDNA Spin kit for Soil DNA extraction was chosen because it provided the highest concentration of DNA with the greatest purity.

The manufacturer's protocol was then optimized to achieve maximum DNA concentration and purity. Modifications included: (1) repeating the extraction step and pooling supernatant before adding the binding matrix (guanidine isothiocyanate 60-70%), (2) performing the ethanol wash step in triplicate, and (3) eluting twice (first with 100 µL, then 50 µL) with the polymerase chain reaction (PCR) grade water provided with the kit. The extracted DNA was quantified again by fluorometry and by spectrophotometry using Take-3 plate with an Epoch spectrophotometer (BioTek, VT, USA). These samples were stored at -20°C until further processing.

Triplicate DNA extractions of samples from the 0.6 m depth level were performed for each deposit. Replicates of these samples with the greatest DNA concentrations were sequenced using the MiSeq (Illumina Inc., San Diego, USA) platform. Approximately 20,000 reads were sequenced for each sample using 515F/806R primers targeting the V4 variable region of the 16S rRNA gene for both Bacteria and Archaea (Research & Testing Laboratories, Lubbock, TX, USA). Technical replicates – comprised of nine individually extracted samples from a single CFT sub-sample that were pooled and concentrated – from two deposits were chosen to send with each sequencing batch to provide a calibration check for the results. Sequences from the replicate with the most returned sequences for each deposit were processed using the mothur software suite standard operating procedure (Schloss et al., 2009). Briefly, the sequences were selected to have less than 300 base pairs (bp) as the amplicon has an average size of 300 to 350 bp. Sequences with homopolymers greater than 8 bps in size and with any ambiguous bps were rejected. Additionally, chimeras were removed using UCHIME (Edgar et al., 2011). To obtain the final dataset, the resulting sequences were aligned to the SILVA database (Pruesse et al., 2007). The sequences were randomly subsampled to 18,000 reads per sample, which equalled the

fewest reads among all sampling locations. This sub-sampling approach eliminated bias caused by samples with anomalously high or low sequencing reads. Operational taxonomic units (OTUs) are a group of sequencing reads that share DNA sequence identity at a specific level of similarity. Here, we have classified OTUs at 97% segment identity match and this is approximately equivalent to a genera level relationship between reads. A Venn diagram was prepared from the final sequencing dataset to identify OTUs that overlap among all four CFT deposits.

2.4.5 Mineralogy

Synchrotron-based powder X-ray diffraction (PXRD) patterns were collected on the Canadian Macromolecular Crystallography Facility (CMCF) beamline 08B1-1 at the Canadian Light Source (CLS). Centrifuged solids were frozen and freeze-dried before being powdered using an agate mortar and pestle in an anoxic chamber. Samples were then transferred into 0.81 mm polyimide capillary tubes (Cole-Parmer) sealed with Loctite 454 prism gel (ethyl cyanoacrylate) adhesive under a continuous flow of argon gas. Incident X-ray energy was selected using a dual crystal monochromator fitted with silicon (Si) (111) crystals, and a Rayonix MX300HE back illuminated CCD (charge-coupled device) detector was used for data collection. The detector distance was set to 0.25 m and alignment was calibrated with a lanthanum hexaboride (LaB_6) standard. Incident photon energy of 18 keV (λ = 0.6888 Å) and exposure time of 90 seconds was used to obtain these PXRD patterns. The two dimensional PXRD patterns were converted to plots of intensity versus two-theta calibrated using GSAS-II (Toby and Von Dreele, 2013). Mineralogical phase identification from the 1D patterns was performed using Match! (v2.4.2).

2.4.6 Solid-phase geochemistry

The bulk chemical composition of CFT samples (n = 33) from all deposits was determined. Samples were oven dried at 60°C for 48 hours before grinding in an agate mortar and pestle. The dried samples were pulverized to 85 % passing a 200 mesh sieve and split for complementary analyses. The first split was digested by lithium metaborate/tetraborate fusion followed by HNO_3 dissolution. The second split was leached in hot aqua regia (1:3 volume ratio of HNO_3:HCl). Major and minor element concentrations from these digests were quantified by ICP-OES and ICP-MS, respectively.

Bulk sulfur (S) and iron (Fe) K-edge X-ray absorption near edge structure (XANES) spectra were measured on the Soft X-ray Micro-Characterization Beamline (SXRMB) at the CLS. Samples were prepared for analysis following the same method used for PXRD. Samples and reference materials were mounted on a copper plate using C tape and transferred to the beamline vacuum chamber for analysis. The beam was focused to a spot size of 1.0 to 3.0 mm wide by approximately 1 mm high. A dual crystal monochromator fitted with two Si (111) crystals was used to scan the incident photon energy from -50 to +200 eV relative to the theoretical S (2472 eV) and Fe (7112 eV) K-edges. X-ray absorption was measured using a four element Si drift detector (Bruker XFlash 4040). Sulfur reference materials included elemental S [S_8], gypsum, L-cysteine [$HO_2CCH(NH_2)CH_2SH$], and pyrite [FeS_2]. Ferrihydrite [$Fe_{10}O_{14}(OH)_2$], goethite [α-FeO(OH)], hematite [Fe_2O_3], pyrite, and magnetite [Fe_3O_4] were used as Fe reference materials. These reference materials were purchased as ACS grade reagents, synthesized (ferrihydrite, goethite, hematite), or obtained from the University of Saskatchewan mineral collection (pyrite, magnetite). Confirmation of the mineralogy and purity of synthesized and natural mineral samples was confirmed by XRD. These spectra were edge-step normalized and analyzed within ATHENA (Ravel and Newville, 2005).

2.5 Results

2.5.1 Pore-water chemistry

pH, Eh, EC, and alkalinity

Pore-water pH ranged from 7.45 to 8.67, with an average value of 7.88 ($\sigma = 0.26$, $n = 62$; Figure 2.2), which is consistent with previous values reported for FFT (Allen, 2008; Chen et al., 2013; Fedorak et al., 2003; Holowenko et al., 2000; Siddique et al., 2014b). Measured pH values averaged 8.0 near the surface of EV-1 but decreased to less than 8.0 at depths greater than 0.5 m. However, samples from 0 to 0.5 m in EV-1 were stored in bags and carbon dioxide (CO_2) degassing could have raised the pH slightly in these samples. In contrast, pH values in EV-2 were generally constant with depth ($\mu = 7.7 \pm 0.2$). The test deposits (GD, TD) exhibited slightly elevated pH values at depth, increasing from pH 7.7 at the surface to approximately pH 8.2 at depths of 1 m.

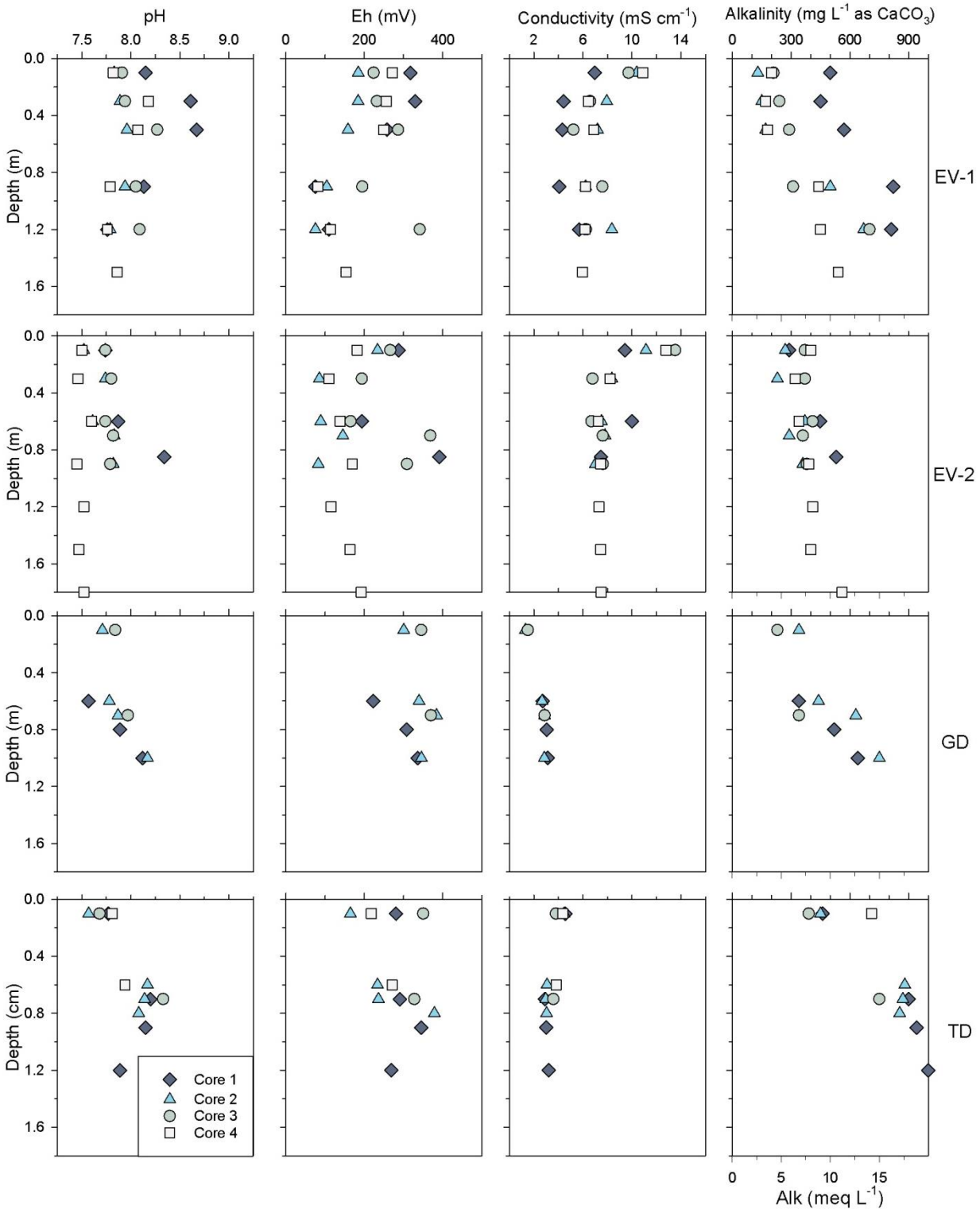

Figure 2.2: Pore-water pH, Eh, EC, and alkalinity with depth for EV-1, EV-2, GD, and TD.

Redox potential (Eh) ranged from 75 to 390 mV and averaged 230 mV (σ = 90 mV) among all samples (n = 62; Figure 2.2). The full-scale deposits (EV-1, EV-2) exhibited lowest

Eh values from 0.6 to 1.2 m depth (~100 mV). Values for the test deposits were fairly consistent with depth, and the values were generally higher (~300 mV) than the full-scale deposits. Although efforts were made to ensure the most accurate measurements, Eh values are higher than what would be expected in an anaerobic system. Although Eh values of +200 mV and lower are generally indicative of anoxic conditions, values associated with SO_4 reduction typically range from 0 to -200 mV, whereas those for methanogenesis are generally less than -200 mV (Boulding and Ginn, 2003). Higher values may result from low concentrations of active redox couples (such as Fe(II)/Fe(III)) in the pore water, the presence of zero-valent S (Couture and Van Cappellen, 2011), and/or exposure to oxygen. The latter may have been an issue for the bagged samples from EV-1. Additionally, Salloum et al. (2002) noted that Eh values for supernatant from centrifuged gypsum-amended FFT exhibited approximately 200 mV higher values compared to the bulk sample. Reported *in situ* Eh values for FFT in lab-based studies are typically around -200 mV (Chen et al., 2013; Salloum et al., 2002).

Electrical conductivity (EC) ranged from 1.3 to 13.5 mS cm^{-1} (n = 62), and large differences between the full-scale (EV-1, EV-2) and test (TD, GD) deposits were observed (Figure 2.2). The full-scale deposits exhibited much higher values, averaging 7.6 mS cm^{-1} (σ = 2.0 mS cm^{-1}), compared to the test deposits where average EC was 3.1 mS cm^{-1} (σ = 0.8 mS cm^{-1}). These differences are attributed to higher rates of gypsum amendment used for full-scale CFT production. Measured EC values exhibited limited variability with depth below 0.3 m in individual deposits. However, EC values increased toward the surface in EV-1 (+3 mS cm^{-1}), EV-2 (+4 mS cm^{-1}), and TD (+1 mS cm^{-1}). Conversely, GD exhibited a small decrease in EC to approximately 1.3 mS cm^{-1} near the surface. The measured values in the test deposits are generally consistent with average values reported for FFT pore water (Allen, 2008; Chen et al., 2013; Salloum et al., 2002).

Alkalinity averaged 470 mg L^{-1} (σ = 220 mg L^{-1}) as $CaCO_3$, but ranged from 130 to 1000 mg L^{-1} among all deposits (n = 61; Figure 2.2). Alkalinity values in EV-2 exhibited a slight increase with depth (from 300 to 400 mg L^{-1}), whereas larger increases were observed with depth in the other deposits. Alkalinity in EV-1 increased from 200 to 500 mg L^{-1}, GD increased from 300 to 600 mg L^{-1}, and TD increased from 400 to 900 mg L^{-1}. Location 1 from EV-1 exhibited about two times higher alkalinity compared to other locations in that deposit (approximately 600 mg L^{-1} and 300 mg L^{-1}, respectively). The higher alkalinity values from EV-1 are more

consistent with those reported for FFT (650-1400 mg L^{-1} as $CaCO_3$; Allen, 2008; Fedorak et al., 2011; Holowenko et al., 2000; Salloum et al., 2002; Siddique et al., 2014a).

Major Cations

Calcium (Ca) concentrations ranged from 10 to 470 mg L^{-1} among all deposits (n = 76; Figure 2.3). The full-scale deposits exhibited mean Ca concentrations of 140 mg L^{-1} (EV-1; σ = 130 mg L^{-1}) and 230 mg L^{-1} (EV-2; σ = 90 mg L^{-1}). Concentrations of Ca generally decreased with depth from approximately 400 mg L^{-1} at surface to approximately 100 mg L^{-1} in EV-1 and approximately 200 mg L^{-1} in EV-2. Much lower Ca concentrations were observed for GD and TD, which exhibited average concentrations of 48 mg L^{-1} (σ = 26 mg L^{-1}) and 30 mg L^{-1} (σ = 25 mg L^{-1}), respectively. Elevated Ca concentrations were exhibited at 0.4 m depth in GD, although other concentrations remain fairly consistent with depth in that deposit (averaged 41 mg L^{-1}). The TD deposit exhibited decreasing Ca concentrations with depth at all sampling locations. This disparity is attributed to higher rates of gypsum amendment used for the full-scale deposits. However, the core from location 1 in EV-1 exhibited similarly low values to the test deposits (<100 mg L^{-1}). Geochemical modelling indicated that the CFT pore water was consistently at or above saturation with respect to calcite and dolomite (Figure 2.4). Pore water was near saturation with respect to gypsum in the full-scale deposits and consistently under-saturated with respect to gypsum in the test deposits. The lower Ca concentrations observed for the test deposits are generally consistent with those reported for FFT (Chen et al., 2013; Holowenko et al., 2000; Salloum et al., 2002; Siddique et al., 2014a; Stasik and Wendt-Potthoff, 2014; Stasik et al., 2014).

Magnesium (Mg) concentrations were typically lower than Ca concentrations and ranged from 10 to 150 mg L^{-1} (n = 76; Figure 2.3). The full-scale deposits exhibited mean Mg concentrations of 40 mg L^{-1} (EV-1; σ = 36 mg L^{-1}) and 62 mg L^{-1} (EV-2; σ = 28 mg L^{-1}), respectively. Concentrations of Mg decreased with depth, from 120 mg L^{-1} near surface in EV-1 to less than 40 mg L^{-1} at depth and from 130 mg L^{-1} near surface in EV-2 to 60 mg L^{-1} at depth. The Mg concentrations in the test deposits averaged 20 mg L^{-1} (σ = 10 mg L^{-1}). Although there was an elevated concentration at 0.4 m depth in GD (40 mg L^{-1}), Mg concentrations remained fairly constant with depth at 20 mg L^{-1}. Conversely, TD also exhibited decreasing concentrations with depth from 40 mg L^{-1} at surface to 20 mg L^{-1} below 0.3 m. Magnesium concentrations in all deposits were generally greater than those reported for FFT (Chen et al., 2013; Holowenko et al.,

2000; Salloum et al., 2002; Siddique et al., 2014a; Stasik and Wendt-Potthoff, 2014; Stasik et al., 2014).

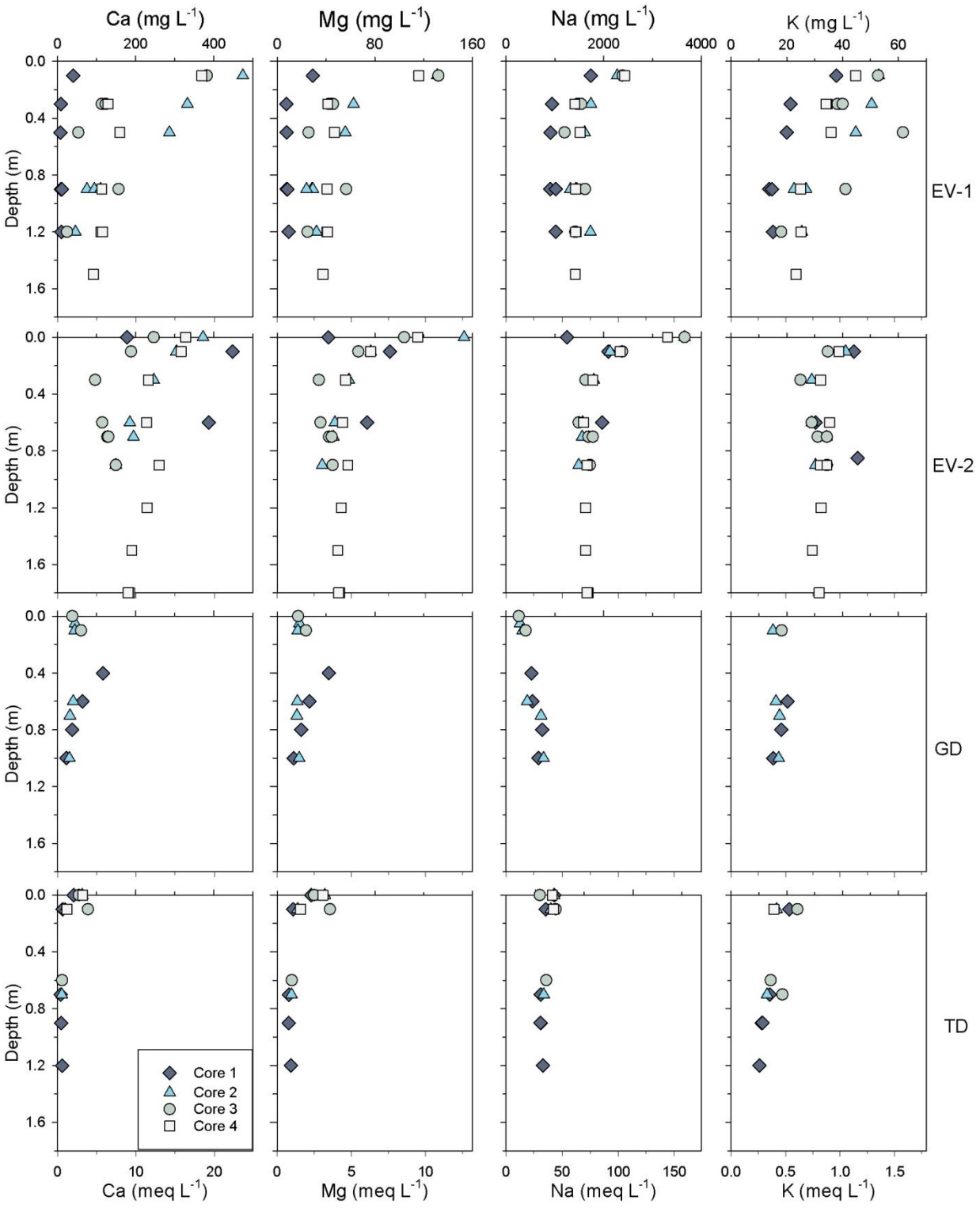

Figure 2.3: Pore-water Ca, Mg, Na, and K concentrations with depth for EV-1, EV-2, GD, and TD.

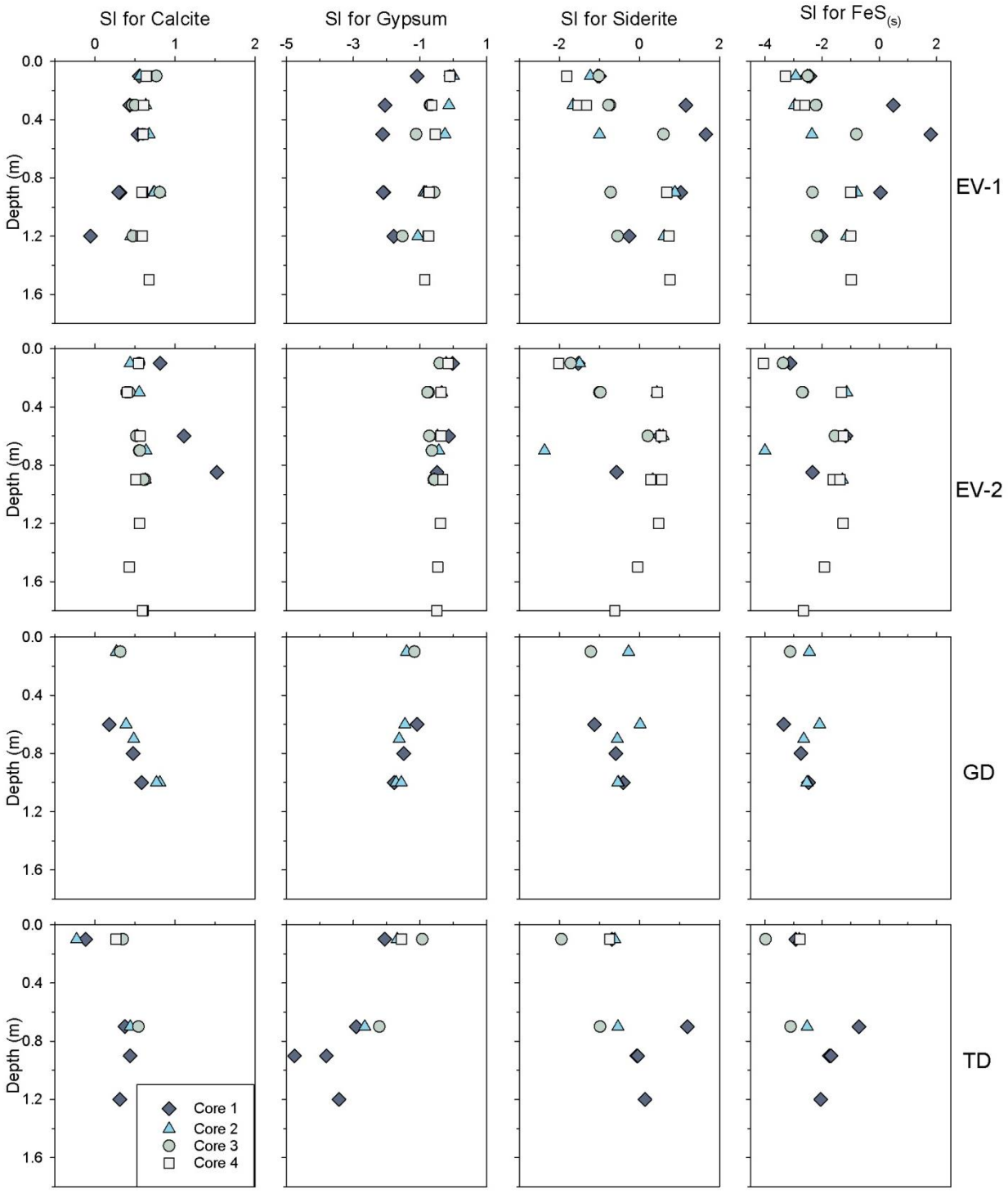

Figure 2.4: Saturation indices for calcite, gypsum, siderite, and $FeS_{(s)}$ with depth for EV-1, EV-2, GD, and TD.

Sodium was consistently the dominant cation in CFT pore water, with a range in concentrations from 260 to 3700 mg L^{-1} (n = 76; Figure 2.3). Concentrations of Na were

substantially higher in the full-scale deposits than in the test deposits; mean concentrations were 1500 mg L^{-1} (σ = 420 mg L^{-1}) in EV-1, 2000 mg L^{-1} (σ = 650 mg L^{-1}) in EV-2, 520 mg L^{-1} (σ = 190 mg L^{-1}) in GD, and 840 mg L^{-1} (σ = 120 mg L^{-1}) in TD. Pore-water Na concentrations were generally constant below 0.3 m in all deposits, with an increase in concentration near surface for EV-1 (+500 mg L^{-1}) and EV-2 (+1000 mg L^{-1}). In contrast, Na concentrations were fairly consistent with depth in TD, but exhibited a slight increase with depth (+400 mg L^{-1}) in GD. Average Na concentrations observed for the test deposits (GD, TD) were generally consistent with typical values reported for FFT (530-1000 mg L^{-1}) (Allen, 2008; Chen et al., 2013; Holowenko et al., 2000; Salloum et al., 2002; Siddique et al., 2014a; Stasik and Wendt-Potthoff, 2014; Stasik et al., 2014), whereas Na concentrations for the full-scale deposits (EV-1, EV-2) were two to four times higher.

Potassium exhibited the lowest concentrations of the major cations, with a range of 10 to 60 mg L^{-1} (n = 65; Figure 2.3). Mean pore-water K concentrations were 34 mg L^{-1} (σ = 10 mg L^{-1}) in the full-scale deposits and 16 mg L^{-1} (σ = 3 mg L^{-1}) in the test deposits. The K concentrations observed in the test deposit are similar to K concentrations of 9-25 mg L^{-1} reported for FFT (Chen et al., 2013; Holowenko et al., 2000; Salloum et al., 2002; Siddique et al., 2014a; Stasik and Wendt-Potthoff, 2014; Stasik et al., 2014). Potassium concentrations exhibited limited variability with depth in GD, but decreased with depth by 30 mg L^{-1} in EV-1, 10 mg L^{-1} in EV-2, and 10 mg L^{-1} in TD.

Chloride and Fluoride

Pore-water chloride (Cl) concentrations ranged from 80 to 2200 mg L^{-1} among all deposits (n = 78; Figure 2.5). The full-scale deposits exhibited mean Cl concentrations of 920 mg L^{-1} (EV-1; σ = 180 mg L^{-1}) and 1060 mg L^{-1} (EV-2; σ = 390 mg L^{-1}). Concentrations of Cl were consistently elevated near surface (> 1000 mg L^{-1} in EV-1 and > 1500 mg L^{-1} in EV-2) but decreased below 0.3 m to 830 mg L^{-1} in EV-1 and 880 mg L^{-1} in EV-2. The test deposits exhibited a mean of 260 mg L^{-1} (GD; σ = 140 mg L^{-1}), and 440 mg L^{-1} (TD; σ = 60 mg L^{-1}). Pore-water Cl concentrations increased with depth in GD from 100 mg L^{-1} near surface to 400 mg L^{-1} at 1.1 m, whereas TD exhibited consistent Cl concentrations with depth. Average Cl concentrations for FFT reported in literature exhibit a wide range from 100 to 700 mg L^{-1} (Allen, 2008; Chen et al., 2013; Holowenko et al., 2000; Salloum et al., 2002; Siddique et al., 2014a; Stasik and Wendt-Potthoff, 2014; Stasik et al., 2014). Although dissolved Cl concentrations for

the test deposits are generally consistent with these values, higher average Cl concentrations for the full-scale deposits exceeded these FFT values.

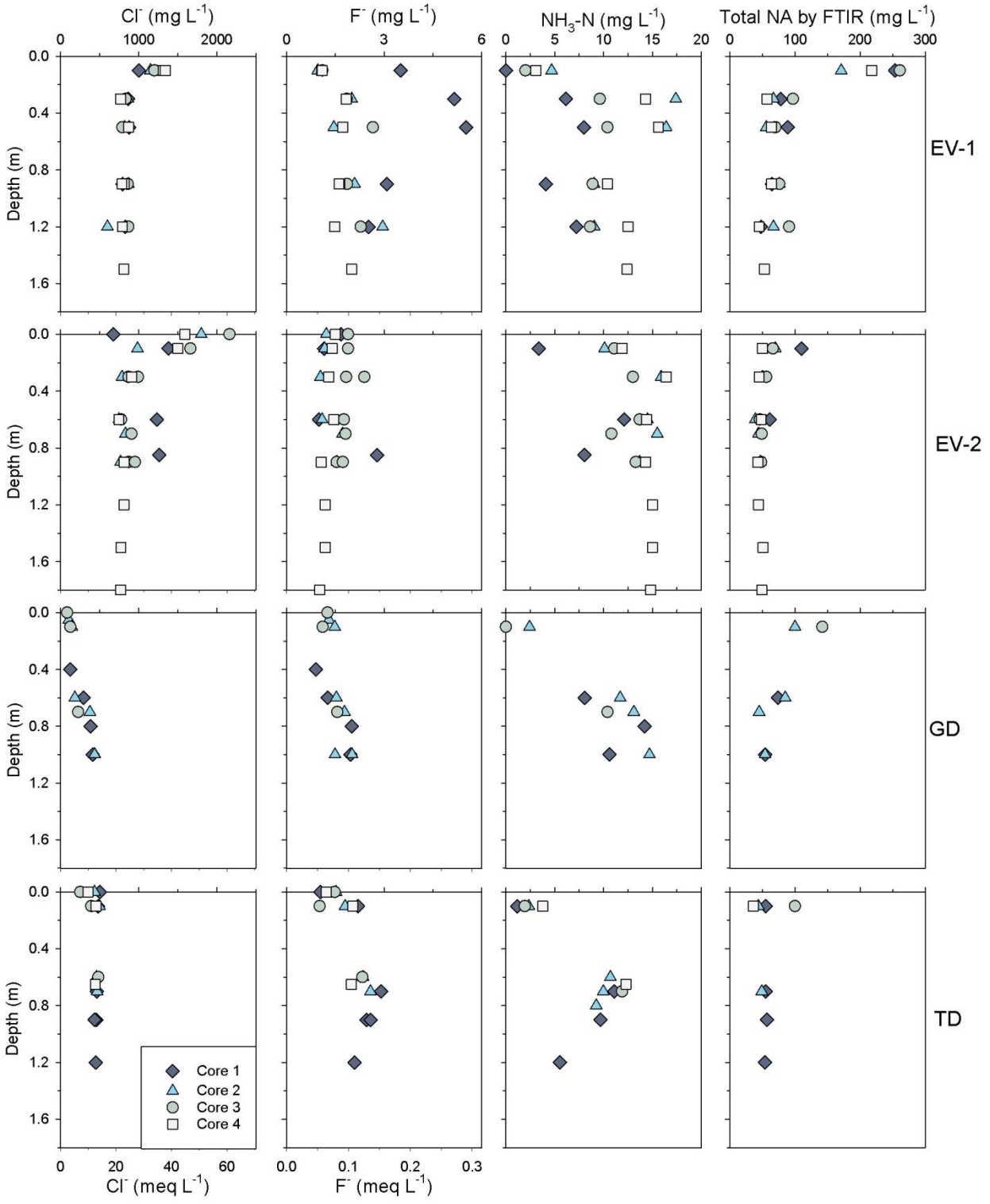

Figure 2.5: Pore-water Cl, F, NH_3, and total NA concentrations with depth for EV-1, EV-2, GD, and TD.

Pore-water fluoride (F) concentrations were much lower than Cl, ranging from 0.9 to 5.5 mg L^{-1} among all deposits (n = 78; Figure 2.5). The mean dissolved F concentration among all CFT deposits was 1.8 mg L^{-1} (σ = 0.8 mg L^{-1}). Concentrations exhibited slight increases from surface to a depth of 0.9 m before slightly decreasing across the remaining depth profile. Of note, location 1 of EV-1 exhibited much higher values than other locations within EV-1 as well as in the other deposits. Concentrations of F are not commonly reported, but Chen et al. (2013) reports that F concentrations are below detection in that lab-based OSPW and FFT study.

Ammonia and acid-extractable organics

Ammonia concentrations ranged from 1 to 17 mg L^{-1} as NH_3-N (n = 60; Figure 2.5), and averaged 10 mg L^{-1} (σ = 4 mg L^{-1}) in pore water from all deposits. This concentration range is in general agreement with reported values for FFT (Allen, 2008; Chen et al., 2013; Fedorak et al., 2003; Holowenko et al., 2000; Salloum et al., 2002; Stasik and Wendt-Potthoff, 2014; Stasik et al., 2014). There was a general increasing trend with depth in EV-1, EV-2, and GD. Pore-water NH_3 concentrations in the full-scale deposits increased from less than 5 mg L^{-1} near surface to 12 mg L^{-1} at 1.4 m in EV-1 and from 9 mg L^{-1} near surface to 15 mg L^{-1} at 1.8 m in EV-2. Concentrations of NH_3 in GD increased from 2.5 mg L^{-1} near surface to 13 mg L^{-1} at 1.1 m depth. Conversely, TD exhibited concentration peak of 12 mg L^{-1} at 0.6 m depth before decreasing to 5 mg L^{-1} at 1.2 m.

Total NA concentrations ranged from 36 to 260 mg L^{-1} (n = 55; Figure 2.5) and exhibited an average concentration of 74 mg L^{-1} (σ = 48 mg L^{-1}) among all deposits. Concentrations were generally consistent below 0.3 m at 68 mg L^{-1} in EV-1, 48 mg L^{-1} in EV-2, and 62 mg L^{-1} in GD, and TD exhibited consistent concentrations throughout the depth profile at 56 mg L^{-1}. Near surface total NA concentrations increased to 230 mg L^{-1} in EV-1, 74 mg L^{-1} in EV-2, and 120 mg L^{-1} in GD. The concentrations observed below 0.3 m in all deposits are generally consistent with the range of 40 to 90 mg L^{-1} reported total NA concentrations in FFT (Allen, 2008; Fedorak et al., 2011; Holowenko et al., 2000; Salloum et al., 2002); however, concentrations observed at shallower depths generally exceeded these values.

Manganese, iron, and sulfur

Pore-water manganese (Mn) concentrations ranged from 0.02 to 1.3 mg L^{-1} among all deposits (n = 56; Figure 2.6). The full-scale deposits exhibited mean Mn concentrations of 0.17 mg L^{-1} in EV-1 (σ = 0.23 mg L^{-1}) and 0.26 mg L^{-1} (σ = 0.31 mg L^{-1}), whereas the test

deposits exhibited mean Mn concentrations of 0.11 mg L-1 in GD (σ = 0.07 mg L^{-1}) and 0.07 mg L^{-1} in TD (σ = 0.07 mg L^{-1}). Concentrations of Mn remained fairly consistent below 0.3 m in all deposits. Higher Mn concentrations were found near surface in EV-1 (0.52 mg L^{-1}), EV-2 (0.72 mg L^{-1}), GD (0.13 mg L^{-1}), and TD (0.12 mg L^{-1}). Published data on dissolved Mn concentrations is limited; however, average Mn concentrations observed in TD and GD were similar to those reported by Chen et al. (2013).

Total dissolved Fe concentrations varied from below the detection limit (BDL) to 2.1 mg L^{-1} in all deposits (n = 56; Figure 2.6). Dissolved Fe exhibited slightly higher concentrations in the full-scale deposits, where mean values were 0.26 mg L^{-1} (σ = 0.40 mg L^{-1}) for EV-1 and 0.60 mg L^{-1} (σ = 0.62 mg L^{-1}) for EV-2, than in the test deposits (μ = 0.07 mg L^{-1}, σ = 0.16 mg L^{-1}). Dissolved Fe concentrations increased slightly with depth in EV-1, EV-2, and TD, but remained relatively consistent with depth in GD. Geochemical modelling indicated that pore water within all CFT deposits was super-saturated with respect to pyrite. Pore water approached saturation with respect to siderite and $FeS_{(s)}$ (Figure 2.4) as total Fe concentrations increased with depth.

Sulfate was the dominant anion with concentrations ranging from 1 to 6400 mg L^{-1} among all deposits (n = 78; Figure 2.6); however, mean SO_4 concentrations in EV-1 and EV-2 were 2300 mg L^{-1} (σ = 1300 mg L^{-1}) and 3200 mg L^{-1} (σ = 1200 mg L^{-1}), respectively. Near surface, SO_4 concentrations were highest at approximately 4000 mg L^{-1} in EV-1 and approximately 6000 mg L^{-1} in EV-2. Concentrations decreased with depth to approximately 0.6 m, whereas values remained relatively constant at greater depths (1500 mg L^{-1} in EV-1; 2500 mg L^{-1} in EV-2). Pore water from location 1 in EV-1 exhibited slightly lower SO_4 concentrations (< 2500 mg L^{-1}) compared to the other cores from that deposit. The test deposits exhibited much lower SO_4 concentrations, with mean concentrations of 570 mg L^{-1} (GD; σ = 220 mg L^{-1}) and 610 mg L^{-1} (TD; σ = 540 mg L^{-1}). Dissolved SO_4 concentrations were also slightly elevated near surface in TD where values reached 1000 mg L^{-1}. In contrast, GD exhibited consistent concentrations throughout the depth profile. Reported SO_4 concentrations for oil sands tailings ponds vary widely from 0 to 550 mg L^{-1}, with FFT pore water on the low end of these values and OSPW on the high end (Allen, 2008; Chen et al., 2013; Chi Fru et al., 2013; Fedorak et al., 2003; Holowenko et al., 2000; Ramos-Padrón et al., 2011; Salloum et al., 2002; Siddique et al., 2014a; Stasik and Wendt-Potthoff, 2014; Stasik et al., 2014).

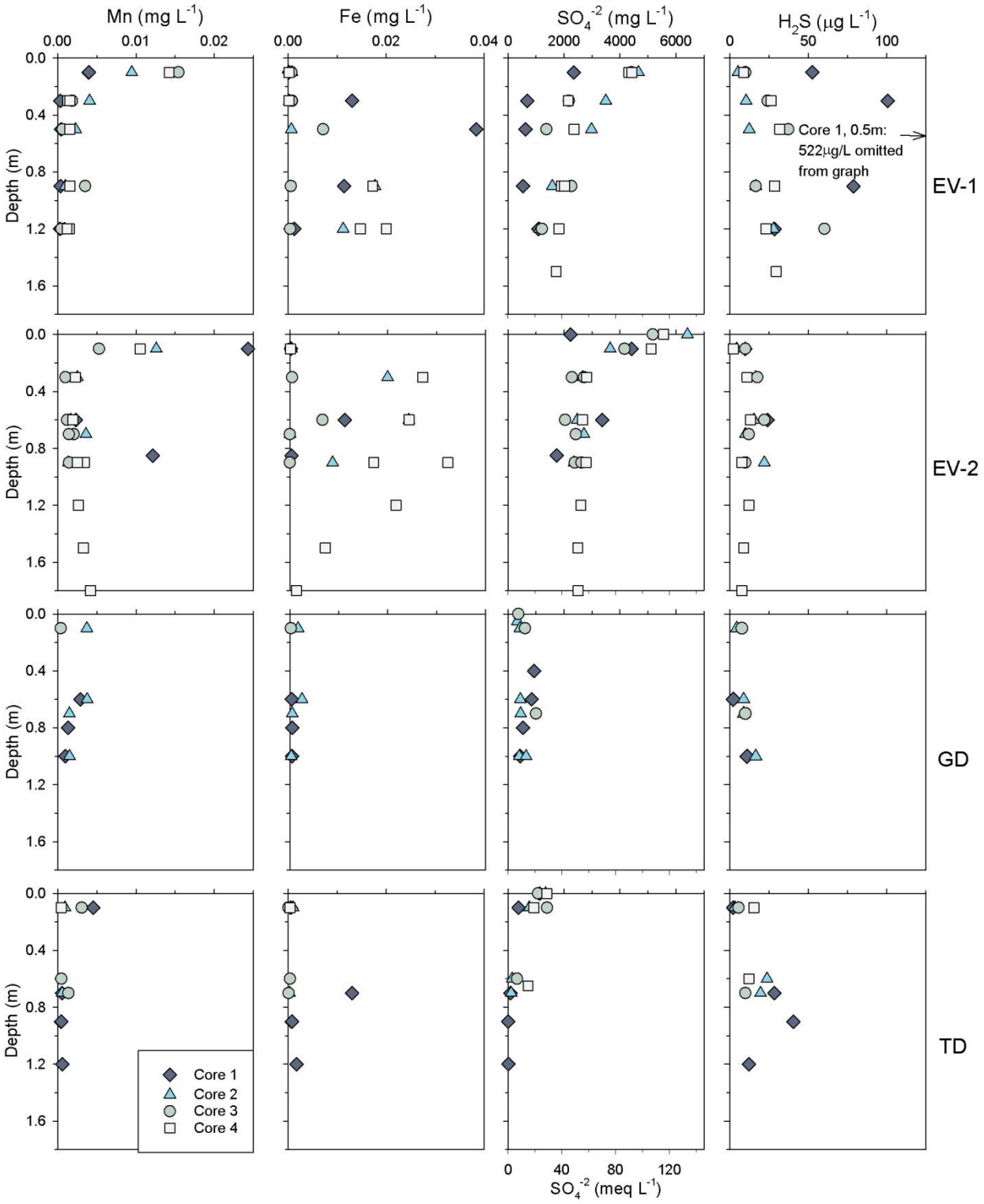

Figure 2.6: Pore-water Mn, Fe, SO_4, and H_2S concentrations with depth for EV-1, EV-2, GD, and TD.

Dissolved H_2S concentrations within all CFT deposits ranged from 2 to 520 µg L^{-1} (n = 59; Figure 2.6), and averaged 28 µg L^{-1} (σ = 68 µg L^{-1}). Dissolved H_2S concentrations generally increased with depth; values in EV-1 and EV-2 increased by approximately 25 µg L^{-1} and 10 µg L^{-1}, respectively. Similar increases were observed for GD (~10 µg L^{-1}) and TD (~20 µg L^{-1}). Location 1 from EV-1 exhibited very high pore-water H_2S concentrations compared to the other cores, including one sample with a measured concentration of 522 µg L^{-1}. Sulfate reduction is likely coupled with oxidation of organic carbon derived from unrecovered bitumen or other PHCs (Cunningham et al., 2001; Edwards et al., 1992; Rothermich et al., 2002). Concentrations of H_2S were reported as 0 to 90 µg L^{-1} by Ramos-Padrón et al. (2011), 0.3 to 5 µg L^{-1} by Chi Fru et al. (2013), and 340 µg L^{-1} by Stasik and Wendt-Potthoff (2014). High H_2S concentrations generally corresponded to lower pore-water SO_4 and elevated total Fe concentrations.

Mass balance

Balance calculations of dissolved anions (i.e. HCO_3, F, Cl, and SO_4; Table 2.1) and major cations (i.e. Ca, Mg, Na, and K; Table 2.2) were performed to assess the role of ion exchange reactions. Anion abundance followed the general order SO_4 > Cl > HCO_3 > F, and cation abundance followed the general order Na > Ca > Mg > K. With the exception of HCO_3, near-surface pore-water samples exhibited greater dissolved ion concentrations than those obtained for depths greater than 0.2 m. Notably, the full-scale deposits (EV-1, EV-2) contained two to three times the total sum of miliequivalents as the test deposits (GD, TD; Table 2.3). The balance column was the sum of the anions minus the sum of the cations, and the surface samples generally exhibited a slightly higher difference in these values.

Table 2.1: Mass balance of major anions. All values in meq L^{-1}.

	HCO_3		F		Cl		SO_4	
Borehole	> 0.2 m	0.1 m	> 0.2 m	0.1 m	> 0.2 m	0.1 m	> 0.2 m	0.1 m
EV-1-1	13.87	9.99	0.20	0.19	23.86	29.26	14.84	51.51
EV-1-2	8.29	2.60	0.12	0.05	24.44	32.44	45.60	97.02
EV-1-3	7.11	4.20	0.11	0.06	23.56	33.85	38.23	91.61
EV-1-4	7.09	4.00	0.09	0.06	22.54	37.80	41.43	92.23
EV-2-1	9.77	5.79	0.10	0.06	35.12	38.92	53.20	92.03
EV-2-2	6.24	5.40	0.07	0.06	22.04	27.76	53.09	75.99
EV-2-3	7.51	7.39	0.10	0.10	25.26	46.82	50.18	86.61
EV-2-4	8.42	7.99	0.06	0.07	22.55	42.31	54.97	106.39
GD-1	11.59	6.79	0.10	0.07	11.16	8.29	10.12	17.53
GD-2	12.84	6.79	0.09	0.08	10.06	4.03	10.05	8.83
GD-3		4.60		0.06		3.50		12.64
TD-1	18.88	9.19	0.13	0.12	12.71	13.45	0.56	7.93
TD-2	17.38	8.99	0.14	0.09	13.17	13.99	2.31	15.74
TD-3	14.99	7.79	0.12	0.05	13.60	11.06	6.72	28.94
TD-4		14.19		0.11		12.72		19.18

Table 2.2: Mass balance for major cations. All values in meq L^{-1}.

	Ca		Mg		Na		K	
Borehole	> 0.2 m	0.1 m	> 0.2 m	0.1 m	> 0.2 m	0.1 m	> 0.2 m	0.1 m
EV-1-1	0.53	2.31	0.71	2.66	47.32	76.56	0.48	1.04
EV-1-2	8.33	23.65	3.47	10.78	71.41	99.17	0.69	1.36
EV-1-3	4.68	19.06	3.21	10.86	63.07	103.96	1.02	1.35
EV-1-4	5.99	18.41	3.40	9.54	62.47	105.70	0.73	1.14
EV-2-1	15.79	22.36	5.44	7.60	81.99	91.34	0.97	1.13
EV-2-2	9.66	15.17	3.88	6.29	69.81	92.65	0.78	1.05
EV-2-3	6.13	9.38	3.30	5.46	72.45	103.52	0.78	0.89
EV-2-4	11.00	15.77	4.40	6.29	72.26	101.78	0.83	0.99
GD-1	1.47	3.16	1.36	2.16	30.62	23.49	0.42	0.52
GD-2	1.63	2.19	1.40	1.38	29.30	14.92	0.43	0.38
GD-3		2.99		1.93		17.62		0.46
TD-1	0.45	0.63	0.81	1.06	31.39	35.36	0.30	0.53
TD-2	0.53	0.94	0.95	1.37	33.62	40.06	0.33	0.42
TD-3	0.56	3.87	0.98	3.55	35.93	44.37	0.47	0.61
TD-4		1.18		1.56		42.32		0.39

Table 2.3: Mass balance summary for major ions. All values in meq L^{-1}.

	Sum Anions		Sum Cations		Balance	
Borehole	> 0.2 m	0.1 m	> 0.2 m	0.1 m	> 0.2 m	0.1 m
EV-1-1	52.77	90.95	49.05	82.55	3.72	8.40
EV-1-2	78.45	132.11	83.90	134.96	-5.44	-2.85
EV-1-3	69.01	129.71	71.97	135.23	-2.97	-5.52
EV-1-4	71.16	134.08	72.59	134.80	-1.43	-0.71
EV-2-1	98.19	136.81	104.19	122.43	-6.01	14.38
EV-2-2	81.45	109.21	84.13	115.16	-2.68	-5.96
EV-2-3	83.04	140.93	82.67	119.25	0.37	21.67
EV-2-4	85.99	156.77	88.49	124.83	-2.50	31.94
GD-1	32.97	32.68	33.87	29.32	-0.90	3.36
GD-2	33.04	19.73	32.76	18.87	0.28	0.86
GD-3		20.79		23.00		-2.21
TD-1	32.29	30.69	32.96	37.59	-0.67	-6.90
TD-2	33.00	38.82	35.44	42.80	-2.43	-3.98
TD-3	35.43	47.84	37.94	52.40	-2.51	-4.56
TD-4		46.19		45.46		0.73

2.5.2 Microbiology

The sequencing data for samples obtained from 0.6 m below surface revealed that the total richness (i.e. unique OTUs) shared between the four deposits was 88 OTUs at 97% similarity (Figure 2.7). A greater number of OTUs were shared between the full-scale deposits (285 overlapping OTUs between EV-1 and EV-2) and the test deposits (274 overlapping OTUs between GD and TD) than any other combination of two deposits. Total OTUs numbered 1807, with 1270 of those OTUs unique to individual deposits. Of the 88 shared OTUs, some of the identified sequences were related to known sulfate- and sulfur-reducing bacteria (SRB), including *Desulfurivibrio* (Sorokin et al., 2008), *Desulfocapsa*, and *Desulfuromonas*, which were also previously identified in a microbial study of gypsum-amended FFT (Ramos-Padrón et al., 2011). Relatives of the following taxa were also identified in high abundance: *Anaerolineaceae*, a family of methanogenic syntrophs that are known to degrade alkanes (Liang et al., 2015); *Alteromondaceae*, a family including aerobic and facultative anaerobic Na-loving bacteria (Ivanova and Mikhailov, 2001); *Thiobacillus*, a genus containing Fe- and S-oxidizing bacteria (FeOB, SOB); and *Comamonadaceae*, a phenotypically diverse family known to include denitrifiers and FeRB (Willems, 2014). *Geobacteraceae*, a family containing known FeRB

(Röling, 2014), was also identified in the shared OTUs; however its abundance was much lower. Although no Archaea were identified as common to all four deposits, relatives of the methanogens *Methanosaeta* and *Methanobacterium* were shared among EV-2, GD, and TD, whereas *Methanoregula* and *Methanolinea* were shared between GD and TD. *Methanosaeta* is one of two genera of acetoclastic methanogens which convert acetate into CH_4 and CO_2 (Smith and Ingram-Smith, 2007). In contrast, Archaea of the genera *Methanobacterium*, *Methanoregula*, and *Methanolina* are hydrogenotrophic and couple CO_2 reduction with H_2 oxidation (Brauer et al., 2010; Imachi et al., 2008; Mori and Harayama, 2011). Some species within *Methanobacterium* are halotolerant (Mori and Harayama, 2011). *Methanosaeta*, *Methanoregula*, and *Methanolinea* were identified in microbial studies of FFT (Ramos-Padrón et al., 2011; Siddique et al., 2014b). A more comprehensive microbial analysis of samples from all four CFT deposits is contained within the third chapter of this thesis.

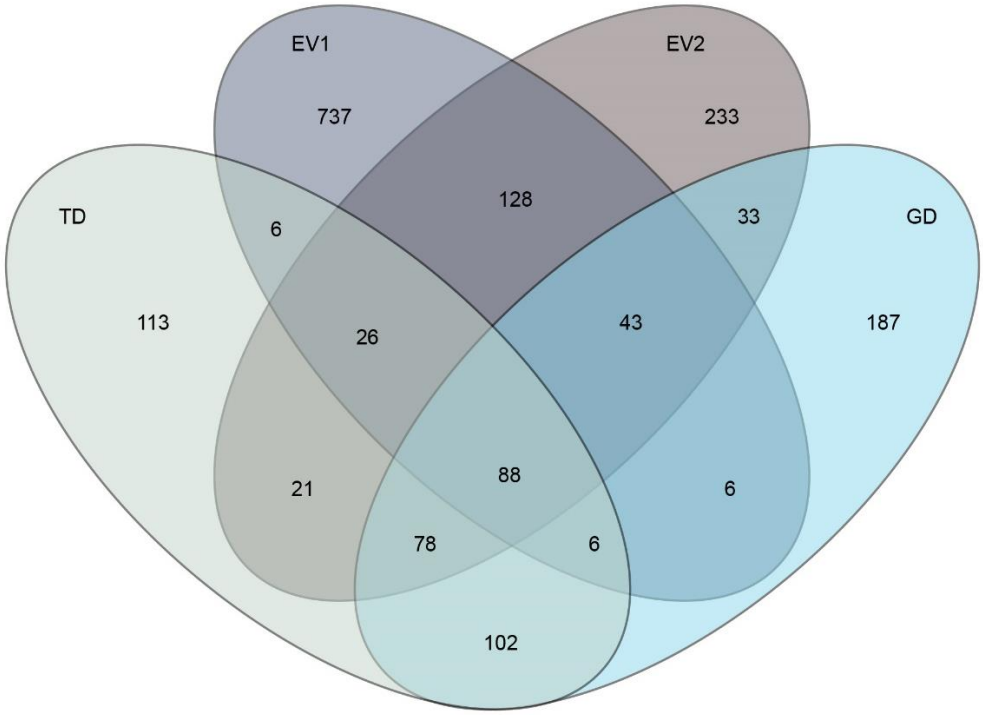

Figure 2.7: Venn diagram of OTUs (97% similar sequences) in EV-1, EV-2, GD, and TD. Samples were collected at a depth of 0.6 m in each deposit. Overall richness is 1807 OTUs.

2.5.3 Mineralogy

The PXRD patterns were generally consistent among all samples, including 12 from EV-2 and one each from EV-1, GD, and TD (Figure 2.8). All samples exhibited peaks for quartz [SiO_2] and various clay minerals, including kaolinite [$Al_2(Si_2O_5)(OH)_4$], illite [$K_{0.65}Al_{2.0}[Al_{0.65}Si_{3.35}O_{10}](OH)_2$], and chlorite [$A_{5\text{-}6}T_4Z_{18}$, where A = Al, Fe^{2+}, Fe^{3+}, Li, Mg, Mn, or Ni; T = Al, Fe^{3+}, Si, or a combination; Z = O and/or OH]. Geochemical modelling indicated the CFT pore water is consistently at saturation with respect to calcite in all deposits and either at or approaching saturation with respect to siderite in the full-scale deposits. These modelling results are consistent with mineral phases identified by PXRD. Similar to previous studies focused on FFT, quartz, kaolinite, illite, and chlorite generally dominated the CFT mineral assemblages (Bayliss and Levinson, 1976; Kaminsky, 2008; Kasperski and Mikula, 2011).

2.5.4 Solid-phase geochemistry

Whole rock elemental analysis

The elemental composition of the CFT samples (Figure 2.9) was dominated by Si ($\mu = 2.8 \cdot 10^5$ mg kg^{-1}, $\sigma = 2.1 \cdot 10^4$ mg kg^{-1}) and Al ($\mu = 9.1 \cdot 10^4$ mg kg^{-1}, $\sigma = 1.1 \cdot 10^4$ mg kg^{-1}). Elevated concentrations of C ($\mu = 7.6 \cdot 10^4$ mg kg^{-1}, $\sigma = 1.4 \cdot 10^4$ mg kg^{-1}), Fe ($\mu = 2.1 \cdot 10^4$ mg kg^{-1}, $\sigma = 2.3 \cdot 10^3$ mg kg^{-1}), K ($\mu = 1.7 \cdot 10^4$ mg kg^{-1}, $\sigma = 1.4 \cdot 10^3$ mg kg^{-1}), and titanium (Ti; $\mu = 5.1 \cdot 10^3$ mg kg^{-1}, $\sigma = 510$ mg kg^{-1}) were also observed. Remaining elements present at concentrations greater than 25 mg kg^{-1} as well as nickel (Ni), lead (Pb), arsenic (As), and molybdenum (Mo), which are elements of concern in the AOSR followed the general order Mg > S > Ca > Na > Mn > barium (Ba) > phosphorus (P) > vanadium (V) > chromium (Cr) > zinc (Zn) > Ni > Pb > As > Mo. The elevated concentrations of Si, Al, and K are attributed to high silicate and aluminosilicate (i.e. clay) mineral contents of these CFT samples. Carbon may be contributed by carbonate minerals or unrecovered bitumen or PHCs. Remaining elements are likely derived from minor and trace elements from association of clay minerals, with Fe, Mg, Na, Mn, Ba, P, V, Cr, Zn, Ni, and Pb all strongly correlated to Al ($0.592 < R < 0.972$; $P << 0.05$).

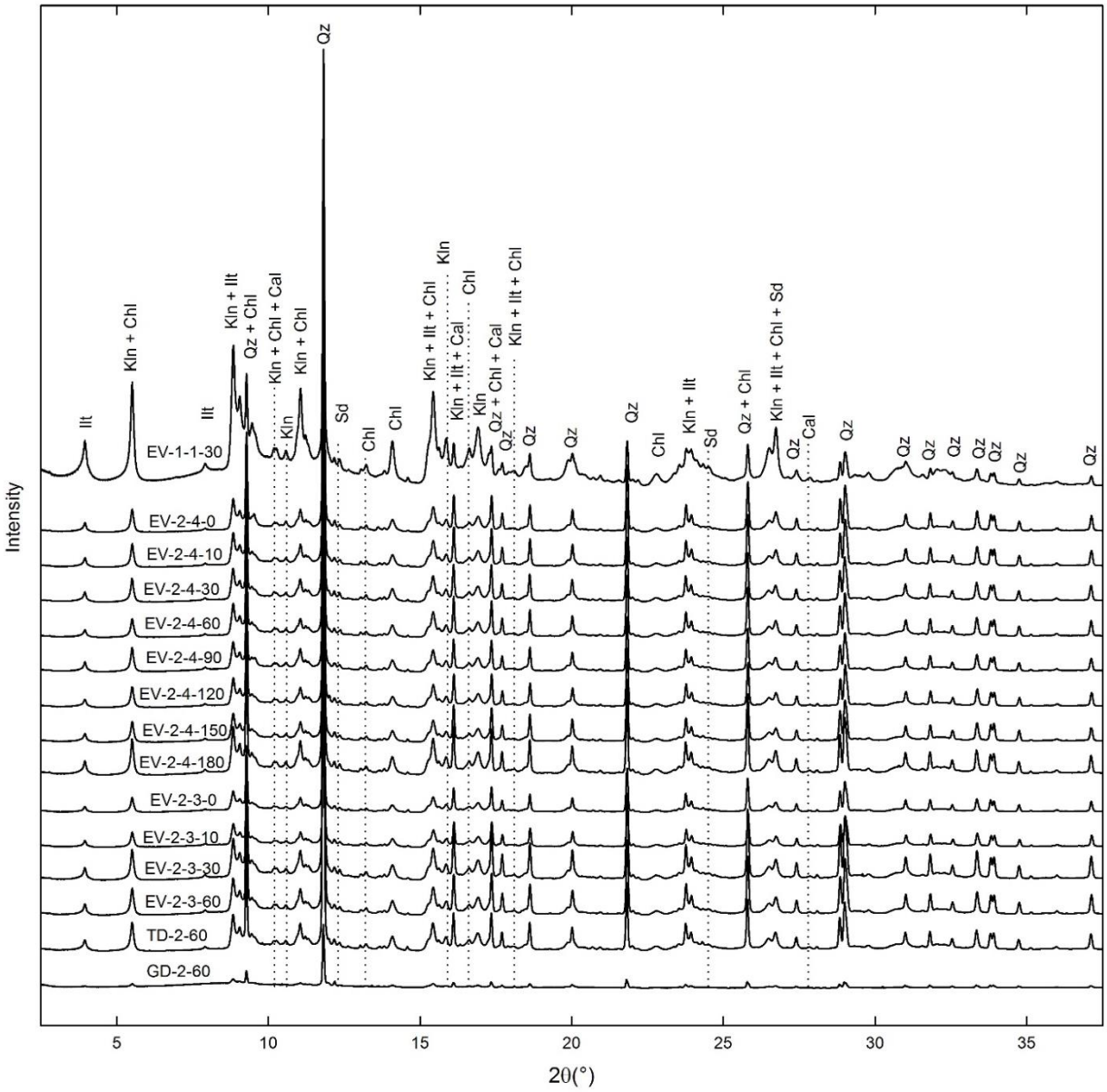

Figure 2.8: PXRD patterns for samples from EV-1, EV-2, GD, and TD.

X-Ray absorption near edge structure

The S K-edge XANES spectra varied slightly among deposits and with depth (Figure 2.10). Peaks positioned between 2473 and 2477 eV are characteristic of +0.5 to +2 oxidation states and are likely associated with organic S compounds (Zeng et al., 2013). A minor peak positioned at approximately 2482.7 eV corresponds to the +6 oxidation state, or SO_4. Peaks assigned to organic S compounds were generally consistent among all samples, whereas the SO_4 peak was more prominent for EV-2 than EV-1. This disparity may result from differences in gypsum amendment rates, as the samples from EV-1 were taken from Location 1, which has

notable geochemical differences. Minor SO_4 peaks were apparent in near-surface samples from GD and TD; similar peaks were not observed at greater depths.

The Fe XANES data was very consistent amongst the twelve samples (Figure 2.11). The main peak was very broad and represents a mixture of Fe(II) and Fe(III) components. The top sample from GD showed a minor shift in peak energy and did not exhibit the double hump feature of the other plots.

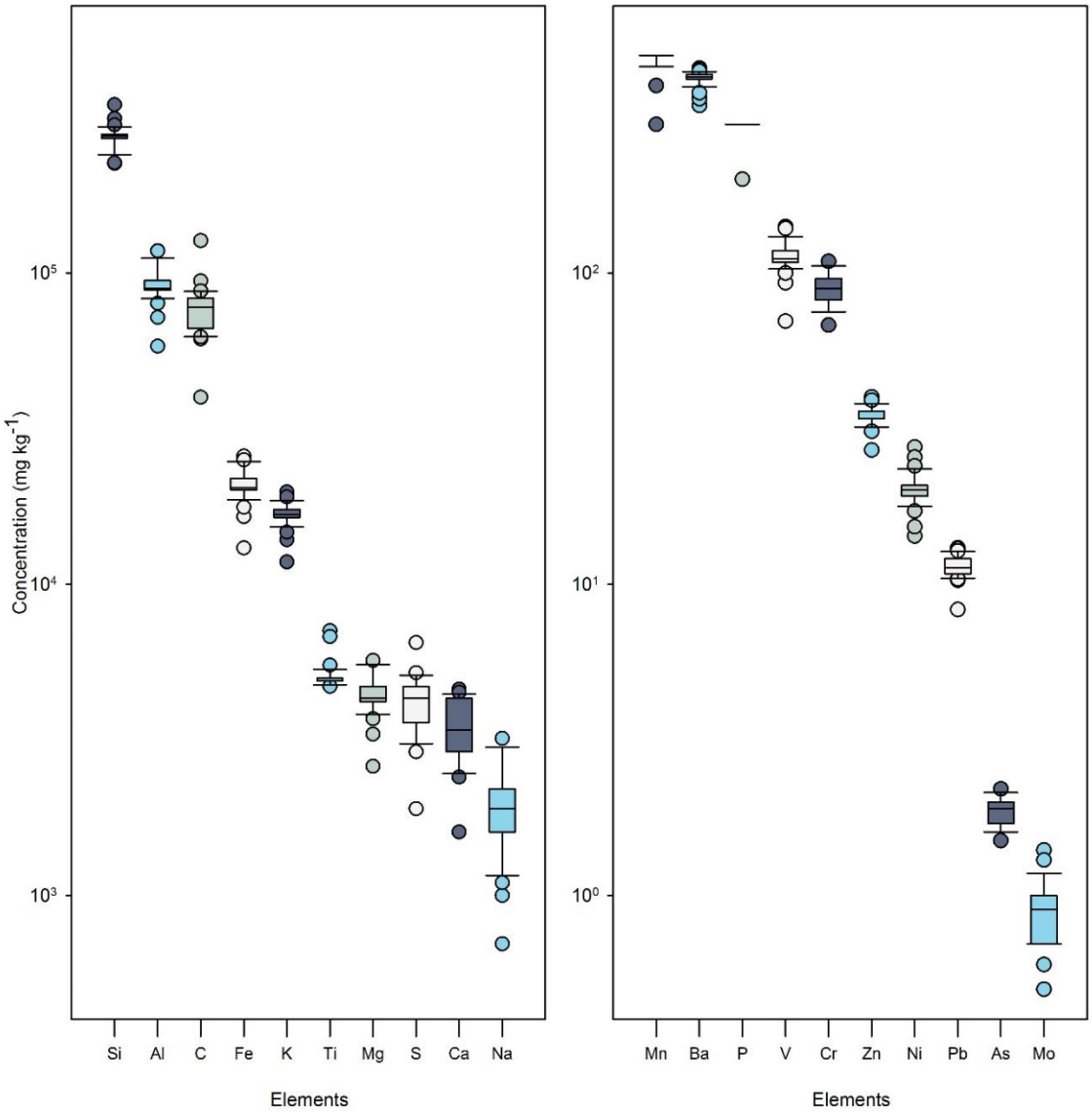

Figure 2.9: Whole rock elemental data for the CFT deposits. The midline of the box represents the median value, whereas the lower and upper boundaries of the box represent the first and third quartiles, respectively. The whiskers represent 10 and 90%.

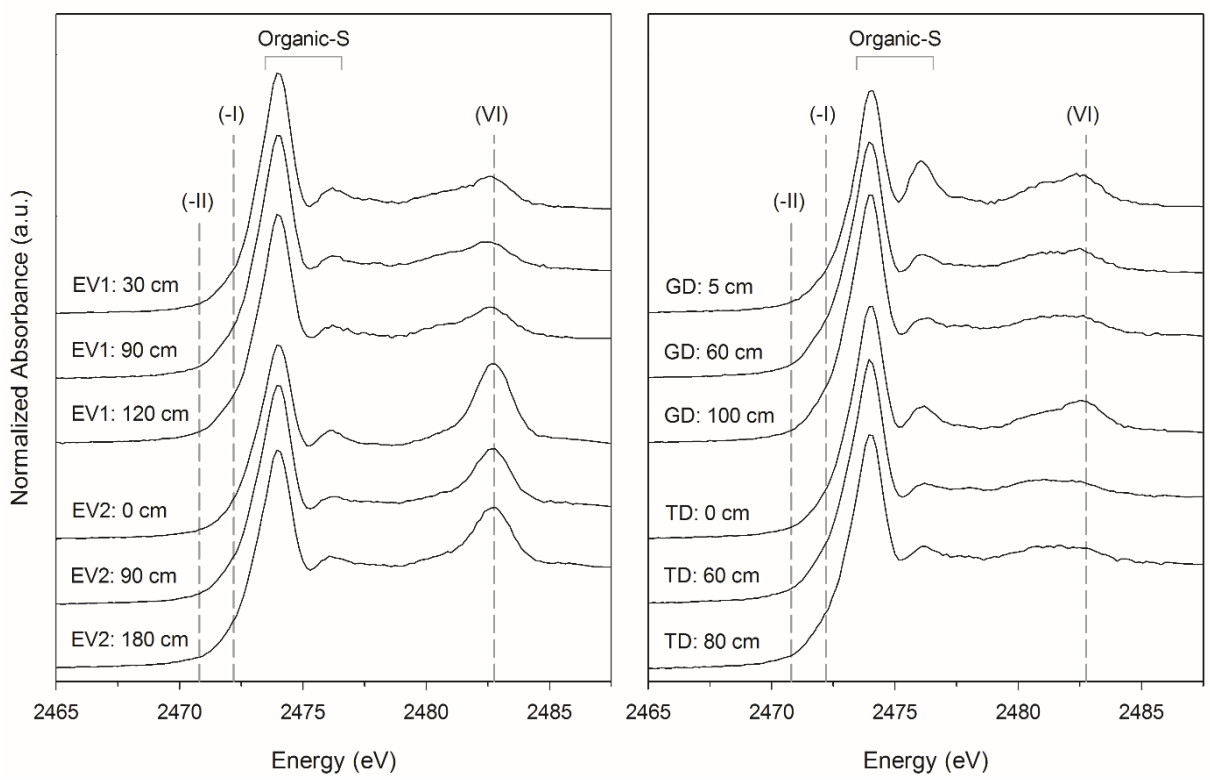

Figure 2.10: Sulfur K-edge XANES spectra for EV-1, EV-2, GD, and TD.

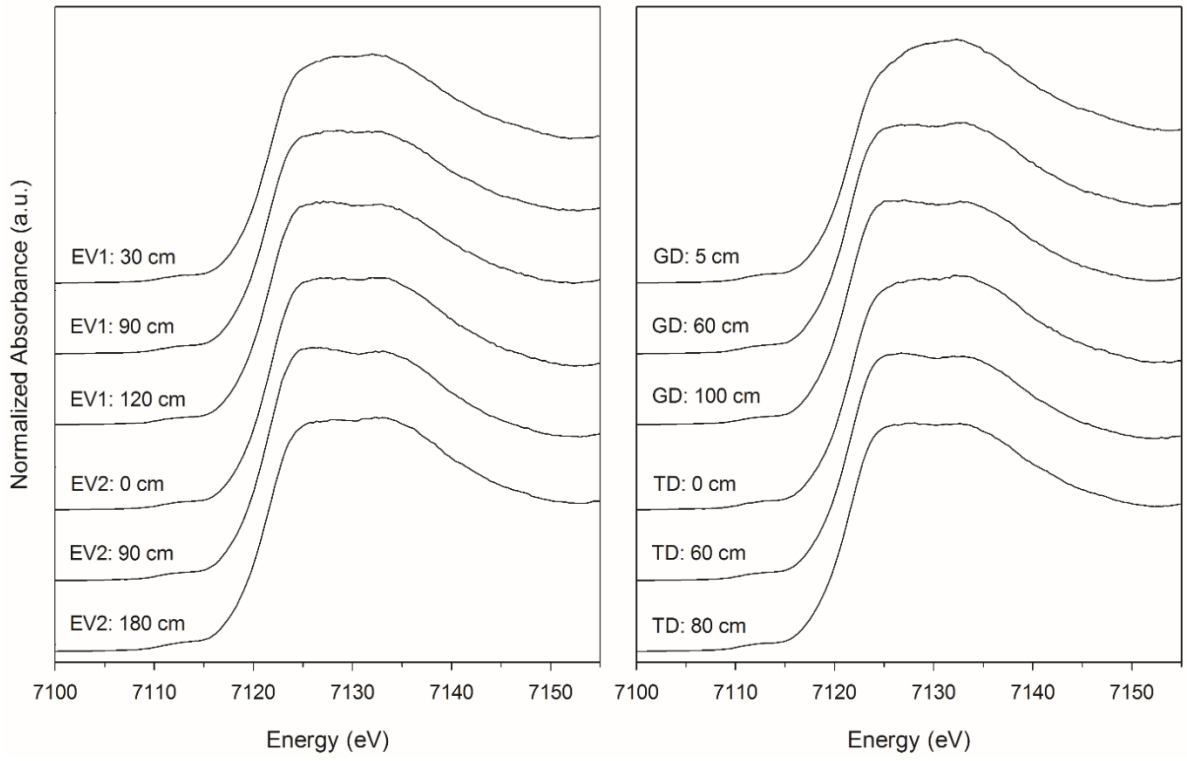

Figure 2.11: Iron K-edge XANES spectra for EV-1, EV-2, GD, and TD.

2.6 Discussion

2.6.1 Controls on pore-water chemistry

Biogeochemical redox processes

The biogeochemistry of CFT pore water is dominated by anaerobic processes including Fe reduction, SO_4 reduction, and methanogenesis. Although measured Eh values are likely not representative of the actual redox potential, the elevated concentrations of dissolved H_2S and the presence of relatives of known SRB and methanogens indicate that the system is anoxic and reducing (i.e., Eh < -200 mV), particularly at depths greater than 0.3 m.

Slight increases in total Fe concentrations with depth are attributed to Fe reduction. As Fe(III) exhibits low solubility at pH >5.5, it is assumed that the presence of dissolved Fe at pH conditions within the CFT deposits (i.e., pH 6 - 8) is largely due to Fe(II). Furthermore, pore-water concentrations of Fe are generally low, which is likely due to precipitation of secondary Fe(II) sulfides and a relatively low total Fe content. This interpretation is consistent with elevated dissolved H_2S concentrations and pore water at or near saturation with respect to $FeS_{(s)}$. Clay minerals are a potential source of reducible Fe(III) and may, therefore, contribute Fe(II) to solution under anaerobic conditions (Stucki, 2006). The Fe XANES data indicates the presence both Fe(II)- and Fe(III)-bearing phases, which could be used as an electron acceptor by FeOB (e.g., *Thiobacillus*) and FeRB (e.g., *Geobacteraceae*), relatives of which were identified in these deposits.

Although dissolved SO_4 was present in all deposits, the S K-edge XANES spectra indicate that solid phase SO_4 concentrations were low compared to other S compounds. Spectra obtained for EV-2 - the most recently formed deposit - exhibited prominent SO_4 peaks, whereas those measured for EV-1 exhibited less prominent SO_4 peaks. Sulfur K-edge XANES spectra collected for the test deposits (i.e., GD, TD), which were formed in 2010, exhibited only a minor SO_4 peak in near surface samples. This observed trend in the presence of solid-phase SO_4 among deposits may reflect SO_4 reduction in the deposits with time. In contrast, the presence of SO_4 near the surface of TD and GD may be indicative of evaporative gypsum precipitation. Concentrations of H_2S were inversely correlated to SO_4 concentrations ($-0.658 \leq R \leq -0.407$, $P < 0.05$ in EV-1, EV-2, and TD), which also suggests that SO_4 reduction is occurring in these

deposits. Additionally, the presence of relatives of known SRB including *Desulfurivibrio*, *Desulfocapsa*, and *Desulfuromonas*, also supports this interpretation.

The presence of relatives of known methanogens, including *Methanosaeta*, *Methanobacterium*, *Methanoregula*, and *Methanolinea*, is indicative of the potential for methanogenesis within these deposits. Elevated pCO_2 may result from acetoclastic methanogenesis, which is likely an important control on pore-water pH within all deposits. Measured pH values are fairly consistent with depth and similar among the deposits. Geochemical modeling and PXRD results suggest that equilibrium with carbonates (i.e., siderite, calcite, dolomite) may also be an important control on pore-water pH within the CFT deposits.

Pore water from one core in EV-1 (Location 1) exhibited apparent differences from the other locations in that deposit for a number of parameters, including pH, alkalinity, Ca, Mg, Na, K, SO_4, and H_2S. These dissimilarities may have resulted from a lower gypsum amendment rate at this location. The concentrations of the other cations – principally Na – would also have been affected due to less Ca being available for ion exchange reactions. The concentration of H_2S at this location were much greater than the concentrations in other locations of EV-1, indicating a more advanced SO_4-reduction reaction, which could also explain the high alkalinity values. Additionally, it was the only core with visible bitumen in the supernatant following centrifugation; perhaps, unrecovered bitumen from the tailings pond was dredged and processed, and, therefore, the resulting mineralogy and pore-water chemistry are different at that location.

Evaporative solute concentration

Increasing concentrations of dissolved ions near the surface of the CFT deposits are attributed to evaporative concentration. Pore-water Cl concentrations approximately double near the surface of the full-scale deposits compared to samples from greater depth at the same location. Assuming that Cl behaves conservatively within CFT deposits, approximately 30 to 40 % of pore water must be lost via evaporation to produce the observed increase in Cl concentrations at a depth of 0.1 m. The other major ions, Ca, Mg, Na, K, and SO_4 are all strongly or moderately correlated to one another and to Cl ($0.622 \leq R \leq 0.950$, $P << 0.05$ in all cases), which supports the evaporative concentration model. However, there are some differences among the ions. For example, the observed increase in dissolved Ca concentrations is greater than for Cl. This observation suggests that evaporative concentration of dissolved Na may promote ion exchange with Ca at clay mineral surfaces.

Ion exchange

The ion exchange reaction (Equation 2.1) is manipulated in both directions in the CFT system. Initially, Na ions are introduced via NaOH addition to enhance bitumen extraction from the ore. Exchange sites at clay mineral surfaces become dominated by Na, which increases the thickness of the EDLs. Gypsum addition introduces Ca ions to the CFT to exchange for Na, thereby reducing the thickness of the EDL and enhancing dewatering during centrifugation. This process leads to large increases in dissolved Na of up to 500 mg L^{-1} within CFT pore water. Over time, the effects of evaporative concentration cause the equilibrium between Ca and Na to shift, and Na exchanges back onto the clay particles, liberating some Ca back into the pore water. Concentrations of Mg and K in the pore water are affected in this process as Na will also exchange for these ions.

Assuming CFT pore-water SO_4 concentrations reflect FFT amendment rates for EV-1 and EV-2, the amount of Ca added to the system as gypsum, and therefore, how much Ca has exchanged onto the clay can be estimated (Table 2.4). This assumption is likely valid because CFT pore water is generally under-saturated with respect to gypsum and there has been limited time for SO_4 reduction to drastically affect SO_4 concentrations. The mass balance calculations suggest that 80 to 90 % of Ca added via gypsum amendment had exchanged onto the clay mineral surfaces. The ratio of Na to Ca also decreased by up to 82 % in the surface samples compared to the samples below 0.2 m depth, which suggests the equilibrium exchange between these cations shifted due to evaporative concentration.

The target gypsum amendment rate was 1.5 kg tonne dry FFT^{-1}; however short-term increases in this rate may have been implemented to achieve desired geotechnical characteristics. The initial rate of gypsum addition was calculated assuming that parent FFT had a solids content of 30 % (g g^{-1}), bulk density of 1.23 g cm^{-3}, and particle density of 2.70 g cm^{-3} (Table 2.4). These calculations indicated that the gypsum amendment rate was approximately 12.3 kg $tonne^{-1}$ in EV-2, and between 3.5 and 10.6 kg $tonne^{-1}$ in EV-1. These values are two to nine times higher than the target amendment rate of 1.5 kg $tonne^{-1}$. The lowest rate in EV-1 corresponds to Location 1, which had many geochemical dissimilarities compared to the other cores in that deposit. The results of this calculation for GD and TD, which exhibit values of 2.3 kg $tonne^{-1}$ and less than 1.6 kg $tonne^{-1}$, respectively, may not be valid as the characteristics of the parent FFT for those deposits cannot be verified. For example, if the bulk density and solids content of the

parent FFT were slightly higher due to using more consolidated FFT solids for the test deposits, than these values would be much lower and closer to the stated amendment rates of 0.8 kg tonne^{-1} in GD and zero in TD.

Table 2.4: Calculation of Ca added to CFT system, ratio of Na:Ca, and the estimated gypsum amendment rate. Unless otherwise specified, the values are averaged from sampling locations below 0.2 m depth. Location 3 from GD and Location 4 from TD were not included in these calculations as they did not have samples from locations below 0.2 m.

Location	SO_4 meas. meq L^{-1}	Ca added meq L^{-1}	Ca meas. meq L^{-1}	Ca exch. meq L^{-1}	Na:Ca at depth	Na:Ca at surface	Na:Ca change %	SO_4 meas. mmol L^{-1}	Amendment Rate kg tonne^{-1}
EV-1-1	14.8	14.8	0.5	14.3	180	66	63	7.4	3.5
EV-1-2	45.6	45.6	8.3	37.3	17	8	51	22.8	10.6
EV-1-3	38.2	38.2	4.7	33.5	27	11	60	19.1	8.9
EV-1-4	41.4	41.4	6.0	35.4	21	11	45	20.7	9.7
EV-2-1	53.2	53.2	15.8	37.4	10	8	21	26.6	12.4
EV-2-2	53.1	53.1	9.7	43.4	14	12	16	26.6	12.4
EV-2-3	50.2	50.2	6.1	44.0	24	22	7	25.1	11.7
EV-2-4	55.0	55.0	11.0	44.0	13	13	2	27.5	12.8
GD-1	10.1	10.1	1.5	8.7	42	15	64	5.0	2.4
GD-2	10.0	10.0	1.6	8.4	36	14	62	5.0	2.3
TD-1	0.6	0.6	0.5	0.1	139	112	20	0.3	0.1
TD-2	2.3	2.3	0.5	1.8	127	85	33	1.2	0.5
TD-3	6.7	6.7	0.6	6.2	129	23	82	3.4	1.6

2.6.2 Comparison with OSPW and FFT pore water

Pore-water chemistry in the CFT deposits was generally consistent with FFT and OSPW, in particular for values of pH, alkalinity, ammonia, Fe, and H_2S (Table 2.5). However, values of EC, total NA, Ca, Mg, Na, K, Cl, F, Mn, and SO_4 in the CFT deposits exceed previously reported values for FFT and OSPW. These differences may be attributed to (1) the evaporative concentration of solutes during *in situ* CFT dewatering, and (2) biogeochemical changes associated with gypsum and polyacrylamide addition.

Gypsum addition and ion exchange reactions are likely reasons for the elevated values of EC, Ca, Mg, Na, K, and SO_4, observed in the full-scale deposits (EV-1, and EV-2). Elevated dissolved SO_4 concentrations are directly attributed to gypsum, whereas elevated values of EC reflect the high concentrations of ions in the CFT pore water. Concentrations of Ca are elevated

due to gypsum addition; however, ion exchange substantially increased Na concentrations in CFT pore water. Other cations, including Mg and K, are impacted to a lesser extent by gypsum addition.

Table 2.5: Summary of FFT and OSPW pore-water chemistry values from literature and pore-water chemistry values from EV-1, EV-2, GD, and TD

Type	FFT	OSPW	EV-1	EV-2	GD	TD
pH	7.8-8.5[abcd]	7.0-8.4[cef]	7.8-8.7	7.4-8.3	7.6-8.2	7.6-8.3
Eh (mV)	-2- -220[acd]	250-400[c]	75-340	82-390	220-380	160-380
EC (mS cm^{-1})	3.2-3.5[ac]	0.3-3.4[ce]	4.1-10.9	6.7-13.5	1.3-3.1	2.9-4.6
Alkalinity (mg L^{-1} as $CaCO_3$)	780-1400[abd]	650-820[e]	130-820	230-560	230-750	390-1000
Ammonia (mg L^{-1} as NH_3-N)	2.3-13[abcgh]	BDL-14[ceg]	2-17	3-16	2-14	1-12
Total NA (mg L^{-1})	50-90[ab]	40-70[e]	45-260	39-110	45-140	36-100
Ca (mg L^{-1})	3-27[acdgh]	4-24[cg]	7.0-470	96-370	22-120	7.7-78
Mg (mg L^{-1})	3-17[acdgh]	4-24[cg]	7.3-130	34-150	13-42	9.4-43
Na (mg L^{-1})	530-1050[acdgh]	500-840[ceg]	910-2400	1300-3700	260-770	690-1020
K (mg L^{-1})	9-25[acdgh]	16-20[cg]	15-62	25-45	15-20	10-24
Cl (mg L^{-1})	130-630[acdgh]	75-700[ceg]	600-1300	670-2200	83-440	250-500
F (mg L^{-1})	BDL[c]	BDL[c]	0.96-5.5	1-2.8	0.9-2.0	1.0-2.9
Mn (mg L^{-1})	0.05-0.07[ch]	0.06-0.08[c]	0.02-0.85	0.05-1.3	0.02-0.21	0.02-0.25
Fe (mg L^{-1})	BDL-3.58[ch]	0.02-0.4[c]	BDL-2.1	BDL-1.8	0.01-0.14	0.004-0.73
SO_4 (mg L^{-1})	0-400[abcdghi]	0-530[cefg]	530-4700	1700-6400	330-1000	1-1400
H_2S (µg L^{-1})	0.3-340[hi]	0-90[f]	5-521	2-24	2-16	2-41

a (Salloum et al., 2002)
b (Fedorak et al., 2003)
c (Chen et al., 2013)
d (Siddique et al., 2014a)
e (Allen, 2008)
f (Ramos-Padrón et al., 2011)
g (Stasik et al., 2014)
h (Stasik and Wendt-Potthoff, 2014)
i (Chi Fru et al., 2013)

2.6.3 Implications for water quality

The pore water in the CFT deposits is generally characterized by a large increase in EC and dissolved ion concentrations relative to FFT pore water. This increase is especially large for pore water immediately below the surface of the CFT deposits, where evaporative concentration of solutes occurs. Water released as runoff due to dewatering within the CFT deposits may, therefore, be characterized by high concentrations of dissolved salts and NA. Salts may negatively impact flora and soil structure of the receiving landscape (Pouliot et al., 2012; Purdy et al., 2005), and elevated NA concentrations may be toxic and environmentally persistent (Clemente and Fedorak, 2005; Oiffer et al., 2009). However, the amount of water released from

the CFT deposits will be substantially less than the volumes of OSPW and FFT contained within tailings ponds. For example, 12 Mm^3 of CFT is produced per year; only a portion of the CFT pore water would be expelled within a given year (< 1 Mm^3). Additionally, there are other overburden materials in the AOSR, such as the saline-sodic Cretaceous Clearwater shale formation, that produce pore water with EC values as high as those values exhibited by the CFT deposits. Nevertheless, the release of pore water with diminished water quality needs to be considered in decisions of where to place CFT in the mine closure landscape. Furthermore, the supernatant from centrifugation of the CFT is recycled for processing along with OSPW. Continued gypsum addition to the CFT without freshwater addition will lead to large increases in EC over time. Increasing concentrations of Na and Cl are already a problem associated with recycling OSPW.

2.7 Conclusions

Development of CFT technology will aid oil sands mine operators in meeting Directive 074. However, evaporative concentration combined with *in situ* dewatering within the CFT deposits leads to elevated concentrations of salts and trace elements in the pore water near the surface of these deposits and in runoff generated during freeze-thaw cycling. Pore-water constituents are largely derived from parent FFT and associated OSPW, although the addition of gypsum also contributes Ca and SO_4 and alters the balance of cations through ion exchange Gypsum and polyacrylamide are added to enhance the geotechnical characteristics of CFT; however, these amendments also support the biogeochemical processes of Fe reduction, SO_4 reduction, and methanogenesis occurring within these deposits. The impact of the release of CFT pore water should be considered for mine closure planning.

CHAPTER 3 BIOGEOCHEMICAL REDOX PROCESSES IN CENTRIFUGED OIL SANDS FINE TAILINGS

3.1 Executive Summary

Centrifuged fine tailings (CFT) were developed to assist in reduction of fluid fine tailings (FFT) volumes stored in oil sands tailings ponds. Gypsum and polyacrylamide are added to the CFT to enhance dewatering, and both additives may influence microbial processes. Several studies have examined microbially-mediated Fe reduction, SO_4 reduction, and methanogenesis in FFT, which is the parent material of CFT. However, these important biogeochemical reduction-oxidation (redox) processes have not been studied in CFT. The motivation for this study was therefore to examine these processes in CFT deposits. Microbial communities were assessed with high-throughput (16S rRNA gene) sequencing and combined with hydrocarbon assessment data and geochemical data to constrain *in situ* biogeochemical redox processes and to evaluate the impact of chemical amendments on these processes. Microbes associated with Fe reduction, SO_4 reduction, and methanogenesis were identified as were hydrocarbon-degrading microbes. Most notably, gypsum addition appears to correlate with decreases in the F1 fraction hydrocarbons (i.e. BTEX) as the CFT deposits with gypsum addition exhibited much lower concentrations of BTEX compounds than the deposit without gypsum addition. Corresponding differences in abundances of *Desulfobacteraceae* and *Burkholderiales* were observed in the gypsum-amended (higher abundance) vs non-gypsum-amended (lower abundance) deposits.

3.2 Introduction

Surface mining operations in the Athabasca Oil Sands Region (AOSR) of Northern Alberta, Canada currently have a footprint of > 700 km^2, with tailings ponds alone covering approximately 200 km^2 (Kasperski and Mikula, 2011). Fluid tailings, which are a slurry of solids in oil sands process-affected water (OSPW), contain elevated concentrations of salts, naphthenic acids (NA), trace elements, and petroleum hydrocarbons (PHCs; Allen, 2008; Kavanagh et al., 2011). Tailings, both in terms of volume and composition, have been identified as a concern for the current and future environmental footprint of the AOSR (Council of Canadian Academies,

2015). The chemistry of fluid tailings is strongly influenced by OSPW, which is characterized by slightly alkaline pH and elevated electrical conductivity (EC; Allen, 2008; Chen et al., 2013; Ramos-Padrón et al., 2011). Sodium (Na) hydroxide added during processing improves bitumen recovery and contributes to these high EC values. Fluid fine tailings (FFT) are clay-rich and tend to resist settlement and dewatering due to their high Na concentrations. Directive 074 was issued by the Alberta Energy Regulator (AER) to mandate reductions in FFT inventories within tailings ponds and to promote progressive reclamation of oil sands mines (AER, 2009).

Centrifuged fine tailings (CFT) technology was developed in response to Directive 074 to reduce long term storage of FFT in tailings ponds. After a few years of settlement, FFT is dredged from the mudline of the tailings ponds, amended with polyacrylamide and gypsum [$CaSO_4 \cdot 2H_2O$], and decanter-centrifuged. Polyacrylamide and gypsum promote flocculation and coagulation, respectively, during the centrifugation process. The residual solids are truck end-dumped into a sub-aerial deposit. The resulting CFT exhibits an initial moisture content of 50 to 58 % (w/w). The moisture content decreases to less than 30 % (w/w) due to *in situ* dewatering and consolidation by freeze-thaw cycling and evaporation. These lower water contents provide increased geotechnical strength, which is an important characteristic and consideration to facilitate progressive reclamation of mines.

Although CFT is deposited sub-aerially, saturated or tension-saturated conditions are likely to persist in CFT deposits, and, therefore, microbially-mediated reduction-oxidation (redox) mechanisms are likely similar to those in FFT deposits. Important biogeochemical redox processes in FFT deposits include iron (Fe) reduction (Siddique et al., 2014b; Stasik and Wendt-Potthoff, 2014; Stasik et al., 2014), sulfate (SO_4) reduction (Chen et al., 2013; Ramos-Padrón et al., 2011; Stasik and Wendt-Potthoff, 2014; Stasik et al., 2014), and methanogenesis (Chen et al., 2013; Ramos-Padrón et al., 2011; Siddique et al., 2014b, 2012, 2011, 2008, 2007, 2006; Stasik and Wendt-Potthoff, 2014; Stasik et al., 2014). Polyacrylamide, a CFT additive, contains carbon (C) and nitrogen (N) (Kay-Shoemake et al., 1998), and may enhance anaerobic microbial growth (Haveroen et al., 2005). Studies have also shown that gypsum addition promotes SO_4 reduction in FFT (Ramos-Padrón et al., 2011; Salloum et al., 2002), potentially suppressing methanogenesis (Holowenko et al., 2000; Ramos-Padrón et al., 2011; Stumm and Morgan, 1996).

Iron reduction

Reduction of Fe(III) in goethite [αFeOOH], amorphous Fe(III) (hydr)oxides, Fe(III)-bearing clay minerals or other Fe(III)-bearing mineral phases produces Fe(II), bicarbonate (HCO_3^-), and water (H_2O):

$$4FeOOH + (CH_2O) + 7H^+ \leftrightarrow 4Fe^{2+} + HCO_3^- + 6H_2O, \quad 3.1$$

which has a Gibbs free energy value of -292 kJ mol^{-1}. Iron reduction is generally considered to be more thermodynamically favourable than SO_4 reduction and methanogenesis; however, under alkaline conditions (pH > 7), SO_4 reduction and methanogenesis are generally favoured (Bethke et al., 2011). The most commonly reported FeRB are in class *Deltaproteobacteria*, family *Geobacteraceae* (Achenbach et al., 2001; Coates et al., 2001; Lovley et al., 1993). Members of this family have been observed in petroleum-contaminated environments (Coates et al., 2001) and are capable of mineralizing PHCs (Lovley and Phillips, 1988; Lovley and Woodward, 1996). In the class *Betaproteobacteria*, the family *Comamonadaceae* has also been reported to include FeRB (Willems, 2014), and members of this family have previously been observed in FFT (Siddique et al., 2014b).

Sulfate reduction

Sulfate is chemically stable, and microbial catalysis is required to reduce SO_4 to sulfide S(-II), except in high temperature environments. Sulfate reduction accounts for approximately 97 % of the S(-II) present at Earth's surface (Rickard, 2012). Sulfate reduction is a dissimilatory metabolic process where SO_4 is used as an electron acceptor to drive cell metabolism. In this process, SO_4 and elemental sulfur (S) reduction are coupled with oxidation of organic carbon (CH_2O) to produce bisulfide (HS^-) at circumneutral pH:

$$\frac{1}{2}SO_4^{2-} + (CH_2O) + \frac{3}{2}H^+ \leftrightarrow \frac{1}{2}HS^- + HCO_3^- + H_2O, \quad 3.2$$

$$S^0 + (CH_2O) + H_2O \leftrightarrow 2HS^- + HCO_3^- + H^+ \quad 3.3$$

which have Gibbs free energy values of -343 kJ mol^{-1} (Equation 3.2) and -241 kJ mol^{-1} (Equation 3.3), respectively. Bisulfide readily reacts with Fe(II) and other metals in solution to form sparingly soluble sulfide phases:

$$HS^- + Fe^{2+} \leftrightarrow FeS_{(s)} + H^+ \quad 3.4$$

Widdel (1988) described two metabolic groups of SRB: one that performs incomplete oxidation of the substrates to acetate (CH_3COOH) and carbon dioxide (CO_2), and one that performs

complete oxidation of the substrates to CO_2. However, CO_2 readily hydrolyzes to form bicarbonate (HCO_3^-) at circumneutral pH.

$$CO_2 + OH^- \leftrightarrow HCO_3^- \quad 3.5$$

Many SRB are in class *Deltaproteobacteria* (Birkeland, 2005), including the genera *Desulfocapsa*, *Desulfurivibrio*, *Desulfobacterium*, and *Desulfuromonas*, which have been identified in gypsum-treated oil sands FFT (Ramos-Padrón et al., 2011). Relatives of the family *Desulfobulbaceae* have been also identified in FFT deposits (Siddique et al., 2014b).

Methanogenesis

Microbially-mediated hydrocarbon degradation may generate CO_2 or methane (CH_4) under anaerobic conditions. Hydrogenotrophic methanogens couple hydrogen (H_2) oxidation with organic carbon reduction to generate CH_4 (Equation 3.6), whereas acetoclastic methanogens produce CH_4 via acetate fermentation (Equation 3.7; Schlesinger and Bernhardt, 2013):

$$CO_2 + 4H_2 \leftrightarrow CH_4 + 2H_2O \quad 3.6$$

$$CH_3COOH \rightarrow CH_4 + CO_2 \quad 3.7$$

the Gibbs free energy value is -17.4 for Equation 3.6 and -28 kJ mol^{-1} for Equation 3.7 (Zehnder and Stumm, 1988). Although the energy yield from methanogenesis is relatively low, at circumneutral pH, methanogens are energetically competitive with FeRB and SRB (Bethke et al., 2011). Methanogenesis will dominate when other terminal electron acceptors (TEAs) are exhausted (Schlesinger and Bernhardt, 2013). Relatives of the methanogens, *Methanolinea*, *Methanoregula*, and *Methanosaeta* have previously been identified in FFT (Ramos-Padrón et al., 2011; Siddique et al., 2014b).

Objectives

The objective of this study was to constrain biogeochemical redox processes in the CFT deposits, and to assess impacts of gypsum amendment on microbial communities and PHC degradation. Core samples from multiple locations within four CFT deposits were examined as part of complementary geochemical and microbiological investigations. Results of this study provide insight on the redox processes active in the CFT deposits and of their evolution over time.

3.3 Site Description

Syncrude Canada Limited (Syncrude) operates the Mildred Lake mine, which is located approximately 35 km north of Fort McMurray, Alberta, where short cool summers and long cold winters are the norm (Hackbarth and Nastasa, 1979). Environment Canada's Mildred Lake weather station, which is located adjacent to the mine site, has recorded minimum and maximum mean monthly temperatures of -17.4°C (January) and 18.4°C (July), respectively, since 1994 (Environment Canada, 2015). Over the past 20 years, mean annual precipitation was 388 mm (σ = 95 mm), and average monthly rainfall for May through August was 51 mm over this period. Snow falls typically between September and May, when the average monthly temperatures are below 0°C, and accounts for approximately 30% of the annual precipitation (Environment Canada, 2015).

Four CFT deposits at the Mildred Lake mine were the focus of this study (Figure 3.1). The two test deposits (designated TD and GD, 57°05'N 111°37'W) and two full-scale production deposits (designated EV-1 and EV-2, 57°00'N 111°45'W) were produced by truck end-dumping of CFT materials. The test deposits were constructed in 2010 during development of CFT technologies. Polyacrylamide, added at 0.7 to 0.85 kg tonne^{-1} dry weight FFT, was the sole amendment in the TD deposit, whereas the GD deposit was amended with both polyacrylamide and gypsum at 0.7 to 0.85 kg tonne^{-1} dry weight FFT and ~0.8 kg tonne^{-1} dry weight FFT, respectively (Table 3.1). The GD deposit was 40 m in length and less than 1.1 m thick. The TD deposit was slightly larger, at approximately 100 m long and 1.0 m to 1.4 m in thickness. The test deposits underwent four freeze-thaw cycles before sample collection was performed in June 2014. Polyacrylamide and gypsum were added to CFT contained in the full-scale production deposits (EV-1, EV-2); however, the amendment rates were higher for EV-1 and EV-2 compared to the test deposits. The full-scale deposits were amended at a target rate of 1.5 kg tonne^{-1} dry weight FFT for both polyacrylamide and gypsum. Deposition of CFT within EV-1 occurred in August and September 2012 and completed from May to July 2013. Deposition of CFT within EV-2 occurred in a more compact time frame between May and July 2013. Each deposit covered an area of approximately 10^5 m^2. These deposits were roughly 1.7 m thick during sampling in December 2013 for EV-1 and June 2014 for EV-2. Consequently, only a portion of the CFT in EV-1 had undergone a freeze-thaw cycle, whereas all CFT in EV-2 had undergone a complete cycle prior to sample collection.

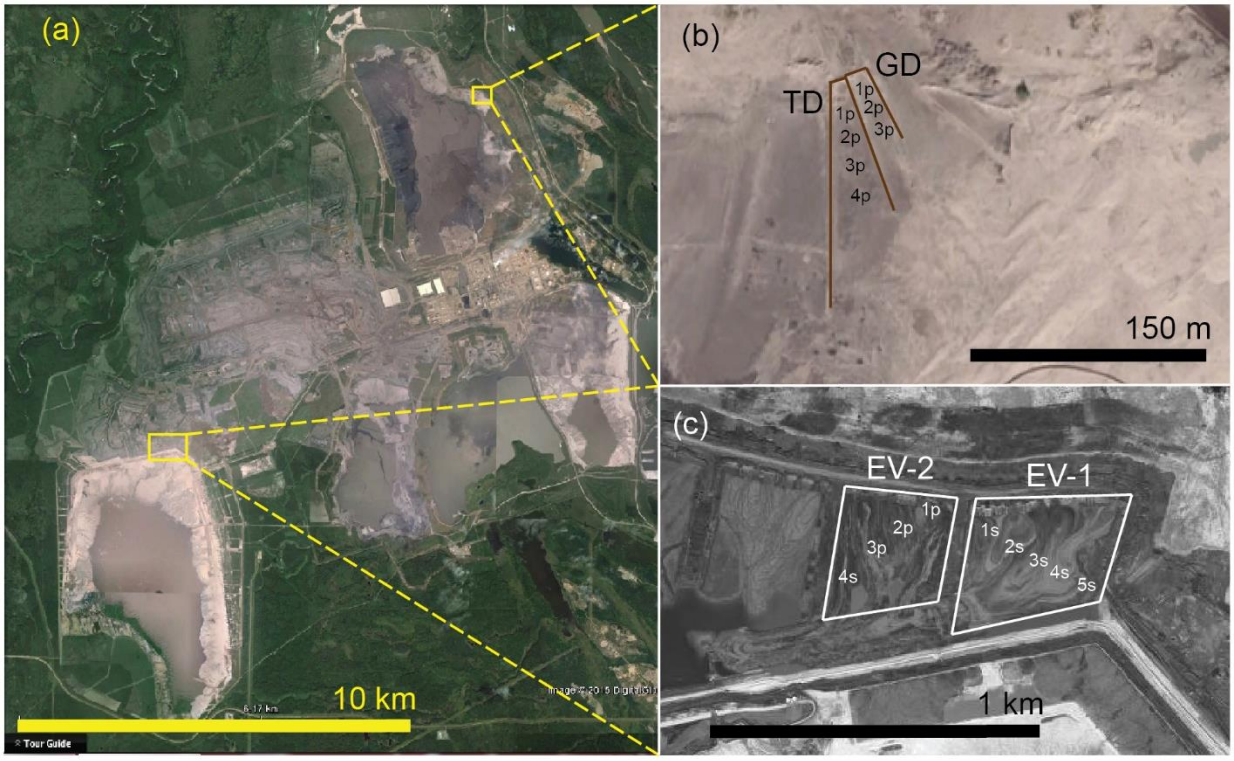

Figure 3.1: Plan view image of (a) the Mildred Lake mine site with enlarged images showing the (b) test deposits (i.e. GD, TD) and (c) full-scale deposits (i.e. EV-1, EV-2). Locations where paired and single cores were collected are noted by "p" and "s", respectively. (Images (a) and (b) © 2015 DigitalGlobe, Image (c) provided by Syncrude)

Table 3.1: Summary of amendments and boreholes per deposit

Deposit ID	Estimated Gypsum added (kg tonne^{-1} dry weight)	Estimated Polyacrylamide added (kg tonne^{-1} dry weight)	Number of core locations	Maximum core depth
EV-1	1.5	1.5	5	1.6
EV-2	1.5	1.5	4 (3 paired)	1.8
GD	0.8	0.7 to 0.85	3 (3 paired)	1.1
TD	none	0.7 to 0.85	4 (4 paired)	1.2

3.4 Materials and Methods

3.4.1 Sample collection

Core samples were collected along transects of the full-scale (EV-1, EV-2) and test (GD, TD) deposits to examine spatial variability of biogeochemical parameters and processes in the CFT deposits. In EV-2, GD, and TD, paired cores (i.e. two adjacent cores at a single location)

were collected to ensure sufficient sample was available for complementary pore-water and solid-phase analyses. Continuous core samples were obtained by using a piston-coring technique similar to that described by Starr and Ingleton (1992). Briefly, aluminum (Al) tubing with a 7.2 cm diameter was advanced at depth intervals of approximately 0.6 m to collect the cores. Compaction across the interval was assumed linear, and, scaling factors were therefore calculated as the recovered length divided by the pushed depth. Upon retrieval, the cores were immediately sealed with paraffin wax and polyethylene caps to minimize potential for oxygen exposure. The cores were shipped to the University of Saskatchewan on ice. Samples from EV-1 were collected in December 2013; consequently, samples were collected from the frozen upper 0.6 m using an auger. The frozen samples were transferred to polypropylene bags and shipped on ice to the University of Saskatchewan. One core from each paired set of cores was stored at +4°C until analysis, while the others, as well as all samples from EV-1, were stored at -20°C.

3.4.2 Petroleum hydrocarbons

Cores stored at +4°C were analyzed for PHCs and gravimetric moisture content. These cores were transferred to an anoxic chamber (< 5 vol% H_2, balance nitrogen gas [N_2]), and stainless steel spoons were used to transfer approximately 250 mL of CFT into glass jars with Teflon-lined lids. These samples were capped and sealed without a headspace using vinyl tape and were stored at +4°C until analysis. Gravimetric moisture contents were determined on sub-samples from these cores. A total of twenty-five samples plus five randomly-selected replicates from different depths in EV-2, GD, and TD were analyzed for PHCs by an external lab using the method described by the Canadian Council of Ministers of the Environment (CCME, 2001); EV-1 was not assessed because it was collected during a previous sampling trip and samples had not been preserved for these analyses. The CCME hydrocarbon method separates groups of PHCs based on number of carbon (C) atoms in a chain or ring. The F1 fraction is for hydrocarbons with 6 to 10 C atoms, and includes the BTEX compounds (benzene, toluene, ethylbenzene, and xylene). The other hydrocarbon fractions include F2 (10 to 16 C atoms), F3 (16 to 34 C atoms), and F4 (34 to 50 C atoms). High temperature gas chromatography (HTGC) was used to measure hydrocarbons with 34 C atoms and greater and captures compounds with greater than 50 C atoms. This fraction is labelled C34-C50+. Pearson correlations were calculated to examine statistical correlations between the hydrocarbon data and SO_4 concentrations.

3.4.3 Microbiology

Sub-sampling of the CFT core samples for DNA extraction was conducted in an anaerobic chamber (< 5 vol% H_2, balance N_2). Sub-samples were collected in sterile (free of deoxyribonucleic acid, DNA; ribonucleic acid, RNA; deoxyribonuclease, DNase; and ribonuclease, RNase) 15 mL conical polyethylene tubes that the bottoms had been cut off using ethanol- and flame-sterilized tubing snips. The tubes were transferred into the anaerobic chamber in an autoclaved aluminum foil-covered plastic beaker. The caps were loosened before pushing the tubes into the thawed CFT core samples. Once the sub-samples were collected, the caps were tightened and the cut ends were sealed with paraffin wax. The tubes were stored at -20°C until DNA extraction could be performed.

Trials of DNA extraction were performed with three commercially available soil DNA extraction kits (PowerSoil and PowerWater kits, Mo Bio Laboratories Inc., Carlsbad, USA; FastDNA Spin Kit for Soil, MP Biomedicals, Santa Ana, USA) to determine which kit was most effective for DNA extraction from the CFT materials. Samples from a single sub-sample were extracted in triplicate with each kit. The DNA extracts were quantified with a fluorometer (Qubit dsDNA HS Assay Kit, Qubit 2.0, Life Technologies), and their purity was assessed with a spectrophotometer (260/280 and 260/230 ratios; Nanodrop 2000, Thermo Scientific). The highest concentration and greatest purity of DNA was obtained from the FastDNA Spin kit for Soil DNA.

The manufacturer's protocol for the FastDNA kit was then optimized to maximize DNA concentrations and purity of the CFT sub-core samples. The procedure was modified by (1) repeating the extraction step and pooling supernatant before the addition of binding matrix, (2) performing the ethanol wash step three times, and (3) eluting twice with PCR grade water. The extracted samples were quantified on the Qubit 2.0 and a Take-3 plate with an Epoch spectrophotometer (BioTek, VT, USA). The extracted samples were stored at -20°C until required for further analyses.

Sample locations with a full suite of geochemical data were selected for DNA extraction. Extractions were performed on sub-core samples from EV-1 (n = 7), EV-2 (n = 17), TD (n = 10), and GD (n = 9). Extraction of DNA was not performed for EV-1 samples obtained by auguring due to the concern that cross-contamination of samples over the 0 to 0.6 m depth interval may have occurred at each location in that deposit. Triplicate DNA extractions were performed for

each of the selected sub-samples. Samples for sequencing technical replicates were also prepared. Nine individually-extracted DNA samples from a single sub-core were pooled and concentrated from both GD and TD at the 0.6 m depth to obtain a more concentrated genomic DNA extract that could be sent out with each sequencing batch.

High-throughput sequencing analyses were performed to assess spatial variability of microbial populations in each CFT deposit. Replicates from 30 locations with measurable DNA concentrations were sent for analysis, including samples of the two technical replicates (MiSeq, Illumina Inc., Sand Diego, USA). The sequencing primers (515F/806R) targeted the V4 variable region of the 16S rRNA gene for both Bacteria and Archaea (Research & Testing Laboratories, Lubbock, TX, USA). Approximately 20,000 sequencing reads were obtained per sample. Sequences from each sample were processed using the mothur software suite (Schloss et al., 2009). Sequences were trimmed to 300 base pairs (bp), and sequences with homopolymers greater than 8 bps in size or with any ambiguous bps were rejected. UCHIME (Edgar et al., 2011) was used to identify and remove chimeric sequences. The resulting set of sequences were aligned to the SILVA database (Pruesse et al., 2007) and randomly subsampled to 14,250 sequences to eliminate bias caused by differences in sequencing read numbers between samples. Abundances from sequenced replicates for a sample location were averaged. Beta dissimilarity was assessed with the Yue and Clayton theta calculation (Yue and Clayton, 2005) and the Jaccard calculation (Smith et al., 1996). Non-metric multidimensional scaling (NMDS) and principal component analysis (PCA) were used to determine potential groupings of the sequenced locations.

3.5 Results

3.5.1 Petroleum hydrocarbons

The mean gravimetric moisture content in EV-2 was 33 % (w/w; σ = 5 % (w/w); n = 10) and increased slightly with depth (Figure 3.2). The moisture content in TD was very consistent with depth (μ = 27 % (w/w); σ = 2 % (w/w); n = 10), as was the moisture content in GD (μ = 16 % (w/w); σ = 9 % (w/w); n = 10), except for three locations, which exhibited soil moisture contents of approximately 5 % (w/w). These lower water contents are likely due to the presence of tailings sand, which was used to construct the test deposit impoundments. Field observations indicated that some of this sand had blown on top of the CFT.

Concentrations of PHCs were determined for samples from EV-2, GD, and TD (n = 10 for each). Samples from EV-1 were not analyzed for PHCs due to inadequate sample preservation.

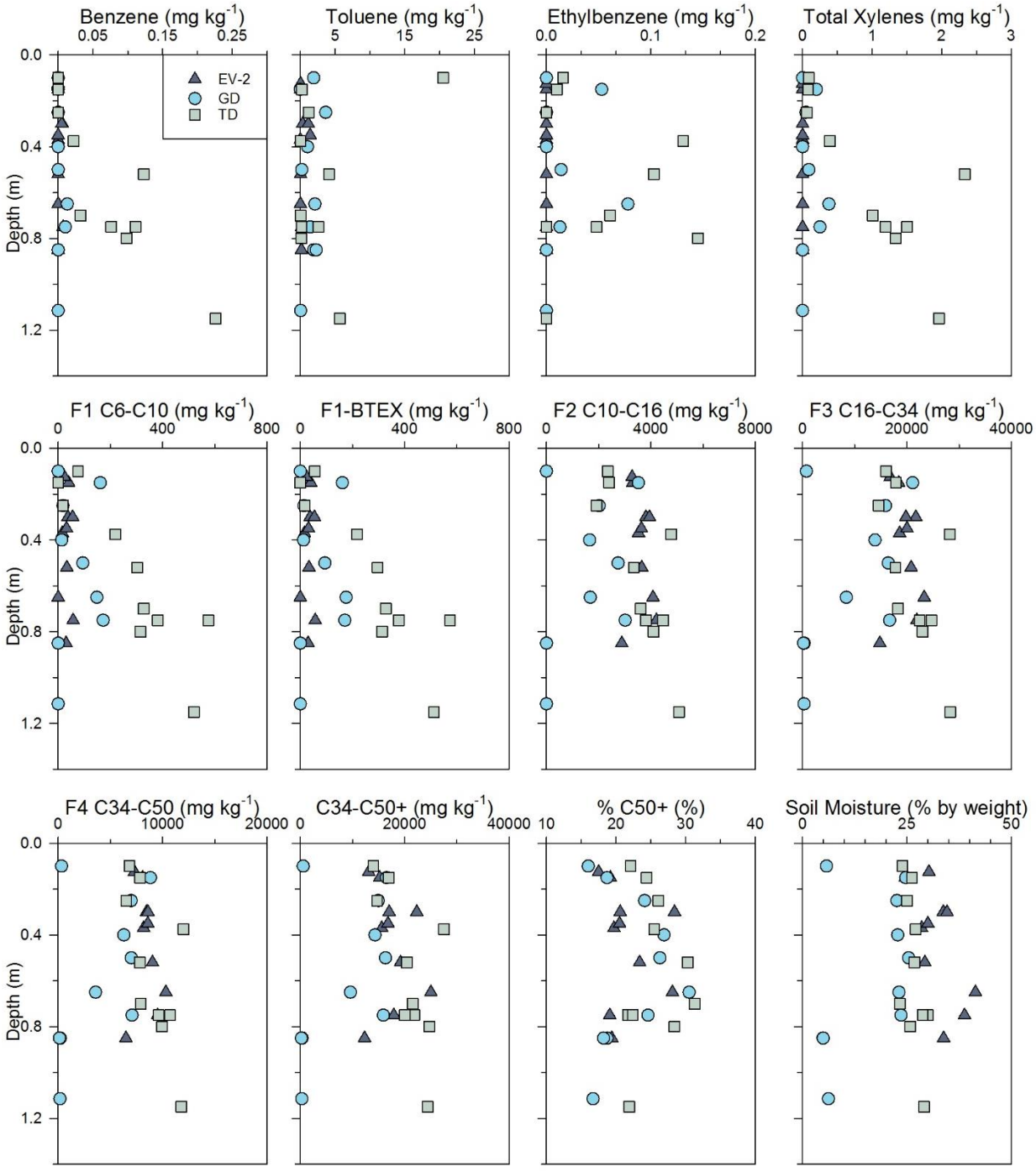

Figure 3.2: Concentrations of CCME hydrocarbon fractions with depth for EV-2, GD, and TD

F1 fraction hydrocarbons

The F1 and F1-BTEX concentrations were generally consistent, indicating that BTEX compounds make up the bulk of the F1 fraction PHCs (Figure 3.2). Generally, the F1 and F1-BTEX concentrations increased with depth in GD and TD, but remained consistent with depth in EV-2. Concentrations of F1 and F1-BTEX concentrations in TD consistently dominated concentrations exhibited by GD and EV-2. Generally, F1 concentrations in GD were between those of TD and EV-2. Benzene concentrations in EV-2 and GD were generally at or below the method detection limit (BDL; <0.005 mg kg^{-1}). In the TD deposit, benzene concentrations increased with depth - from BDL near the surface (< 0.3 m) to 0.25 mg kg^{-1} at 1.2 m depth (μ = 0.07 mg kg^{-1}; σ = 0.07 mg kg^{-1}). Typically, toluene was present the highest concentration among BTEX compounds. Toluene concentrations were generally consistent with depth, with mean concentrations of 0.3 mg kg^{-1} in EV-2 (σ = 0.5 mg kg^{-1}), 1.4 mg kg^{-1} in GD (σ = 1.2 mg kg^{-1}), and 3.5 mg kg^{-1} in TD (σ = 6.3 mg kg^{-1}). The method detection limit is 0.02 mg kg^{-1} for toluene. Concentrations of ethylbenzene were below detection in EV-2 (<0.010 mg kg^{-1}), and near or below detection in GD (μ = 0.02 mg kg^{-1}; σ = 0.03 mg kg^{-1}). Ethylbenzene concentrations generally increased with depth in TD, with a mean concentration of 0.05 mg kg^{-1} (σ = 0.06 mg kg^{-1}). Total xylene concentrations also increased with depth in TD (μ = 1.0 mg kg^{-1}; σ = 0.8 mg kg^{-1}), whereas they were below detection in EV-2 (<0.03 mg kg^{-1}), and near the detection limit in GD (μ = 0.1 mg kg^{-1}; σ = 0.1 mg kg^{-1}).

F2 to F4+ fraction hydrocarbons

Concentrations of PHCs in the F2 to F4+ fractions were generally more consistent among the deposits than for the F1 fraction. Generally, EV-2 and TD exhibited very similar concentrations that were slightly higher than those observed for GD (Figure 3.2). There was a very slight increase in concentrations with depth for the F2 to F4+ PHCs. In GD, each of these fractions exhibited three outlying values; they corresponded to the samples with low soil moisture content and were likely comprised of tailings sand rather than CFT. The F4+ PHC fraction measured by HTGC were typically 1.5 to 3 times higher in concentration than the F4 extractable fraction measured by GC, indicating that PHCs with more than 50 C atoms were present in the samples. Unlike the other fractions of PHCs, the percentage of C50+ increased with depth from 15 to 25% near the surface of each deposit to 25 to 35% in each deposit at 0.7 m and then decreased slightly with depth to 15 to 25% at 1.2 m.

The F2 fraction concentrations generally increased with depth and ranged from 2900 to 4200 mg kg^{-1} (μ = 3600 mg kg^{-1}; σ = 400 mg kg^{-1}) for EV-2, from BDL to 3500 mg kg^{-1} (μ = 1500 mg kg^{-1}; σ = 1400 mg kg^{-1}) in GD, and from 1900 to 5100 mg kg^{-1} (μ = 3600 mg kg^{-1}; σ = 1100 mg kg^{-1}) for TD (Figure 3.2). Mean concentrations in the F3 PHC fraction were similar in EV-2 and TD at 20,000 mg kg^{-1} (σ = 2500 mg kg^{-1}) and 21,000 mg kg^{-1} (σ = 4900 mg kg^{-1}), respectively, whereas mean concentrations in GD were much lower (9,400 mg kg^{-1}; σ = 8300 mg kg^{-1}). Concentrations of the F4 PHC fraction generally increased with depth and ranged from 6500 to 10,300 mg kg^{-1} (μ = 8500 mg kg^{-1}; σ = 1100 mg kg^{-1}) for EV-2, 100 to 8800 mg kg^{-1} (μ = 4100 mg kg^{-1}; σ = 3600 mg kg^{-1}) for GD, and 6500 to 12,000 mg kg^{-1} (μ = 9100 mg kg^{-1}; σ = 2000 mg kg^{-1}) for TD. The TD deposit exhibited the greatest average concentration of the F4+ fraction with a mean value of 21,000 mg kg^{-1} (σ = 4400 mg kg^{-1}), EV-2 exhibited a mean concentration of 17,000 mg kg^{-1} (σ = 3900 mg kg^{-1}), and GD exhibited a mean concentration of 8900 mg kg^{-1} (σ = 7600 mg kg^{-1}). However, the percent of hydrocarbons exceeding 50 C atoms never exceeded 32 %, with TD exhibiting the highest mean percent of 25 % (σ = 4 %), EV-2 exhibited a mean percent of 22 % (σ = 4 %), and GD exhibited a mean percent of 22 % (σ = 5 %). All values over 30% were found in the test deposits.

3.5.2 Microbiology

The microbial communities varied between deposits and both horizontally and vertically within each deposit (Figure 3.3). Generally, similar taxa were observed at the same depth in other locations within a given deposit, although percentage abundances of those taxa varied.

The dominant microbial taxa across all deposits were the bacterial phyla *Proteobacteria*, *Chloroflexi*, *Bacteroidetes*, and *Firmicutes* (Figure 3.3). *Proteobacteria* comprised nearly 60 % of the total reads summed for all samples, and *Chloroflexi*, *Bacteroidetes*, and *Firmicutes* comprised 18, 6, and 4 % of total reads, respectively. Other phyla included *Actinobacteria* (3.5 %), *Acidobacteria* (2.5 %), *Nitrospirae* (1.4 %), and *Deinococcus-Thermus* (1.0 %). All other phyla, including Archaeal phyla, comprised less than 1.0 % of the total reads.

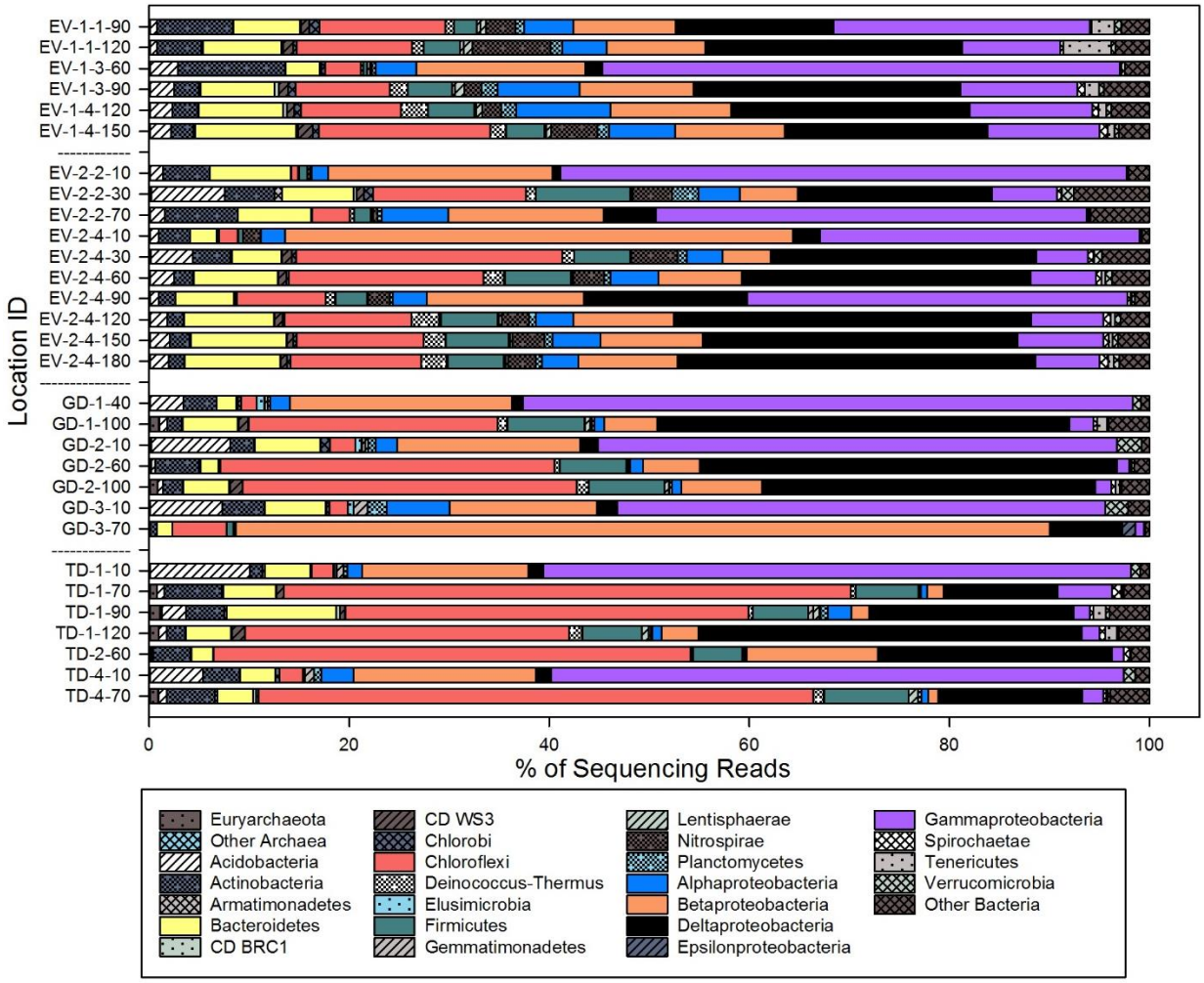

Figure 3.3: Summary bar plot of all subsampled sequencing reads for EV-1, EV-2, GD, and TD. The number following the deposit ID represents the core location, and the final number represents the sampling depth in cm.

Archaea

Although the sequencing data from all samples consisted primarily of Bacterial reads, Archaea were also identified in the sequencing data from all but the near surface samples (< 0.1 m) in EV-2 (Figure 3.4). The TD deposit exhibited the highest percent reads of Archaeal taxa (up to 1.3 % of reads in an individual sample), followed closely by the GD deposit (up to 1.0 % reads), whereas the full-scale deposits exhibited Archaeal reads of one tenth the test deposit values or less (maximum reads were 0.12 % in EV-1 and 0.24 % in EV-2). Samples from below 0.1 m in the test deposits were characterized by higher Archaeal reads than the full-scale deposits, specifically of the class *Methanomicrobia*. Archaeal reads included relatives of known methanogens (e.g., *Methanobacterium*, *Methanolinea*, *Methanoregula*, and *Methanosaeta*) and

other uncultured putative methanogenic archaeal clones (Brauer et al., 2010; Imachi et al., 2008; Mori and Harayama, 2011; Saito et al., 2015; Smith and Ingram-Smith, 2007). Maximum *Thaumarchaeota* reads were obtained in EV-2 and TD, whereas GD and TD contained maximum *Thermoplasmata* reads. Relatives of *Halobacteria* were not a major contributor to Archaeal reads, except for in GD Location 2 (0.1 m). Relatives of phylum *Crenarchaeota* were only detected in three samples: EV-2 Location 4 (1.2 m), GD Location 2 (1.0 m), and TD Location 4 (0.7 m).

Bacteria

Samples collected from near the surface (i.e. 0.1 m) in EV-2, GD, and TD were high in *Gammaproteobacteria* and *Betaproteobacteria* reads with low or no *Deltaproteobacteria* identified (Figures Figure 3.3 and Figure 3.5). The maximum *Acidobacteria* reads in each deposit were from the near surface samples except in EV-2 (0.3 m) and included relatives of *Blastocatella*, *Geothrix*, and *Thermoanaerobaculum*, as well as many reads for an unclassified species in subdivision 7 (Coates et al., 1999; Foesel et al., 2013; Kielak et al., 2009; Losey et al., 2013). Generally, there were more *Bacteroidetes* and *Firmicutes* reads in samples from below 0.3 m depth in all deposits. These classes are functionally diverse, and the sequences included halotolerant Bacteria and relatives of Bacteria capable of methanogenic organic matter degradation, and syntrophic benzene degradation under Fe-reducing conditions (Abram et al., 2011; Baldwin et al., 2015; Choi and Cho, 2006; Kunapuli et al., 2007). Samples from TD exhibited higher *Chloroflexi* reads than the deposits containing gypsum-amended CFT (i.e. EV-1, EV-2, GD). In contrast, the gypsum and polyacrylamide-amended deposits exhibited higher *Deltaproteobacteria* reads than TD (it was amended with only polyacrylamide). The full-scale deposits exhibited a larger number of *Alphaproteobacteria*, *Deinococcus-Thermus*, and *Nitrospirae* reads compared to the test deposits. Additionally, EV-1 contained more *Actinobacteria* reads than the other deposits.

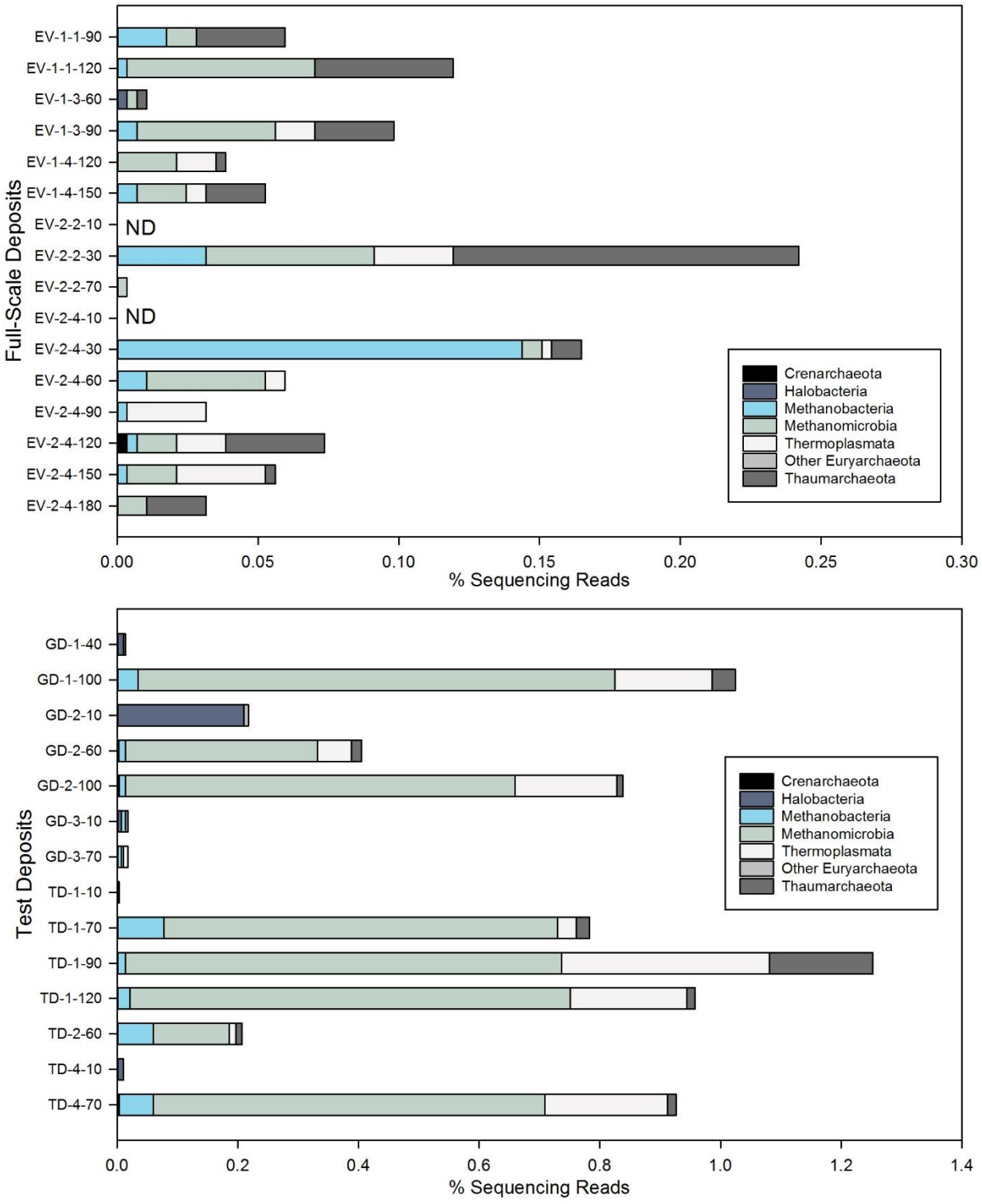

Figure 3.4: Summary bar plot of Archaeal reads as a portion of total sequencing reads for EV-1, EV-2, GD, and TD. The number following the deposit name represents the borehole number, and the final number represents the sampling depth in cm. “ND” stands for not detected.

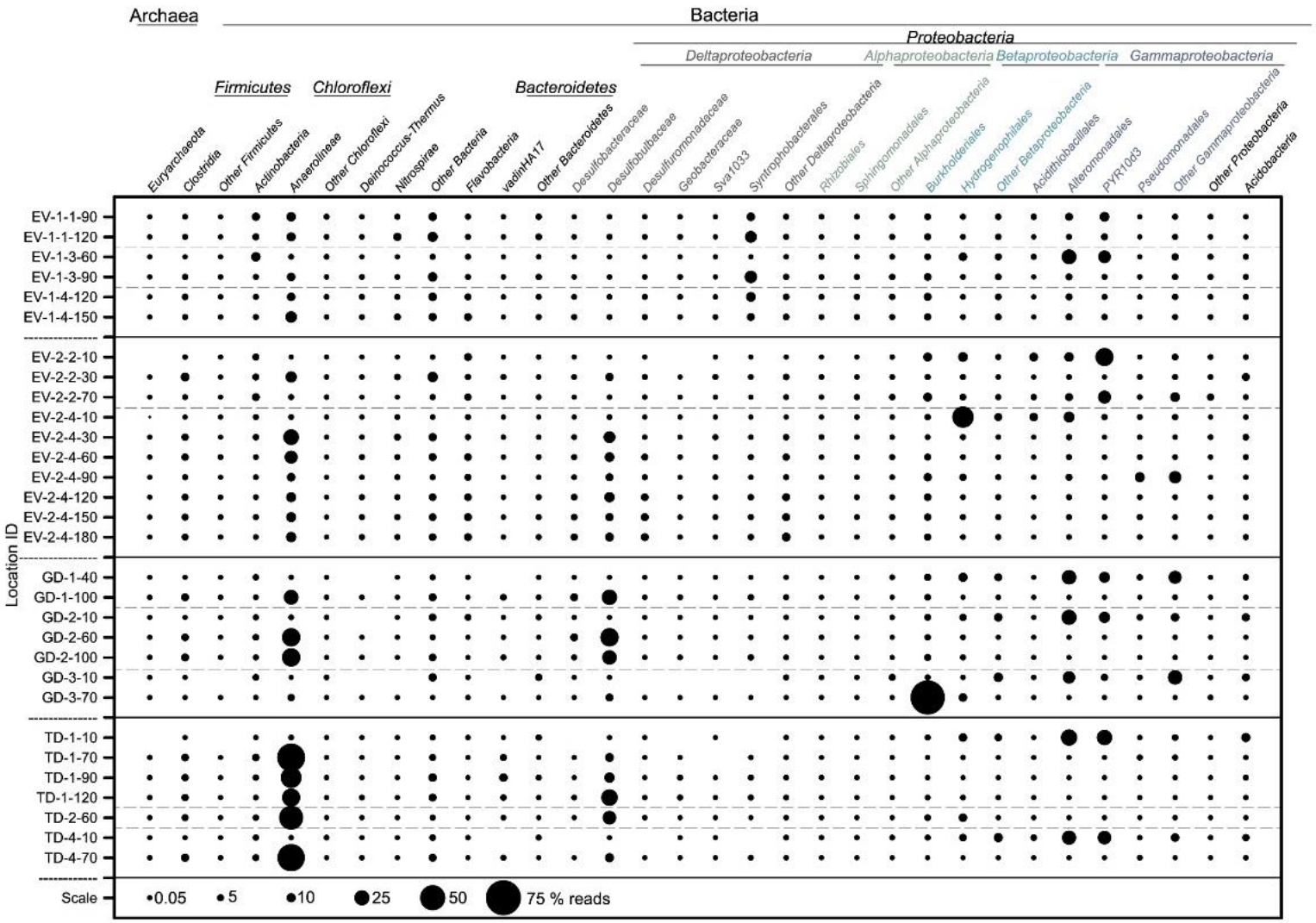

Figure 3.5: Bubble chart showing relative abundance of dominant/important taxa in the CFT deposits. All sample replicates were subsampled to 14,250 reads, and sequenced reads from sample replicates were averaged and divided by 14,250 to obtain the percent read for each sample. Bubbles represent % reads for relatives of taxa of interest for EV-1, EV-2, GD, and TD. The number following the deposit ID represents the core location, and the final number represents the sampling depth in cm.

Proteobacteria

Gammaproteobacteria comprised 1 to 75 % of the *Proteobacterial* reads for each sample (Figures Figure 3.5 and Figure 3.5), and dominated communities near the surface of the CFT deposits. Orders *Acidithiobacillales*, *Alteromonadales*, and *Pseudomonadales*, and reads classified as relatives of the uncultured clone *PYR10d3* were dominant within *Gammaproteobacteria* reads. These orders include relatives of known FeRB, SRB, nitrite dissimilators, and polycyclic aromatic hydrocarbon (PAH)-degraders (Kersters et al., 2006; Semple and Westlake, 1987; Vangnai and Klein, 1974). Reads classified as uncultured soil bacterium clone *PYR10d3* made up a large portion of the *Gammaproteobacteria* reads in numerous samples at shallow depths. This organism is uncultured but has been observed in PAH-contaminated soil and is putatively a pyrene-degrading bacterium (Singleton et al., 2006).

Deltaproteobacteria were 1 to 86 % of the *Proteobacterial* reads for each sample, and a major proportion of these reads consisted of the orders *Desulfobacterales*, *Desulfuromonadales*, and *Syntrophobacterales* (Figures Figure 3.5 and Figure 3.5). These orders contain known FeRB and SRB that have been found in a variety of hydrocarbon-contaminated environments (Cheng et al., 2014; Fowler et al., 2014; Kuever, 2014; Kunapuli et al., 2007). Reads for this phylum were low in near-surface samples but were much higher in samples below 0.1 m. Samples contained the families *Desulfobacteraceae* and *Desulfobulbaceae* from the order *Desulfobacterales*, and *Desulfobulbaceae* was more prevalent than *Desulfobacteraceae* in EV-2, GD, and TD. Relatives of the genera *Desulfocapsa* and *Desulfurivibrio* were both present in all samples. The order *Desulfobacterales* dominated *Deltaptroteobacteria* reads in EV-2, GD, and TD. We observed the families *Desulfuromonadaceae*, *Geobacteraceae*, and *Sva1033* from the order *Desulfuromononadales*. Reads for this order were generally less than those for *Desulfobacterales* and were typically more abundant in the full-scale deposits (EV-1 and EV-2) than the test deposits (GD and TD). *Geobacteraceae*, a known FeRB (Lovley et al., 1993; Röling, 2014), were most abundant at depths greater than 1 m. The order *Syntrophobacterales* comprised up to 17.7 % of reads in individual samples and dominated *Deltaproteobacteria* reads in EV-1.

The *Betaproteobacteria* class typically comprised 6 to 30 % of *Proteobacterial* reads in the samples (Figures Figure 3.5 and Figure 3.5). Near-surface samples exhibited more reads for this class than samples below 0.1 m. This class contains the orders of *Burkholderiales* and *Hydrogenophilales*. The order *Burkholderiales*, which contains the family *Comamondaceae*,

includes species that are capable of degrading a variety of aromatic compounds, such as BTEX (Pérez-Pantoja et al., 2012). Reads for *Burkholderiales* were generally higher than reads for *Hydrogenophilales*. The order *Hydrogenophilales*, which contains the genus *Thiobacillus*, includes species which are capable of oxidizing sulfur compounds by reducing nitrate or nitrite (Kelly and Wood, 2000).

The *Alphaproteobacteria* class comprised up to 16 % of the reads for the *Proteobacteria* phylum in the samples (Figures Figure 3.5 and Figure 3.5). Reads for this phylum were low in near-surface samples from EV-2 and in samples from GD and TD. This class contains the orders *Rhizobiales* and *Sphingomonadales* that are known to contain nitrogen-fixing and pyrene-degrading microbes (Carvalho et al., 2010; Singleton et al., 2006).

Other bacterial phyla

The *Anaerolineae* class of the *Chloroflexi* phylum was one of the dominant classes of bacteria observed (Figures Figure 3.5 and Figure 3.5). Reads for this class were in low abundance in near-surface samples of all CFT deposits but increased to high read numbers in samples below 0.3 m. The test deposits exhibited higher percentage abundances for this class than the full-scale deposits, and abundances in the TD deposit were particularly high. *Anaerolineae* has been linked to syntrophic methanogenic *n*-alkane degradation, and *Chloroflexi* has been identified as a toluene degrader under methanogenic conditions (Fowler et al., 2014; Liang et al., 2015).

The phylum *Bacteroidetes* contains the orders *Flavobacteria* and *vadinHA17*, a bacterium identified in anaerobic organic carbon-laden wastewaters (Abram et al., 2011; Baldwin et al., 2015). This phylum was present in all samples, but the full-scale deposits generally exhibited slightly more reads than the test deposits (Figures Figure 3.3 and Figure 3.5). The full-scale deposits contained more reads for *Flavobacteria* compared to the test deposits, whereas these deposits contained fewer reads for *vadinHA17* than the test deposits. *Flavobacteria* was dominated by the genus *Lutibacter*, which contains species that have been identified from marine settings (Choi and Cho, 2006; Park et al., 2010, 2013).

The *Clostridia* class of the *Firmicutes* phylum exhibited low reads in near-surface samples, and reads for this class increased with depth (Figures Figure 3.3 and Figure 3.5). This class has been linked to hydrocarbon degradation under both methanogenic and Fe-reducing conditions (Kunapuli et al., 2007; Siddique et al., 2012)

Representatives of other phyla, including *Actinobacteria*, *Deinococcus-Thermus*, *Nitrospirae*, and *Acidobacteria*, were also present (Figures Figure 3.3 and Figure 3.5). *Actinobacteria* reads were consistent with depth and similar among the deposits although the full-scale deposits exhibited higher maximum reads. The phylum was dominated by reads from the family *Microbacteriaceae*, which contain facultative anaerobic mesophilic and psychrophilic microbes (Evtushenko and Takeuchi, 2006). The highest reads for this phylum were found at the 0.6 m or 0.7 m depth in all deposits. *Deinococcus-Thermus* reads were either not detected or only detected in very low abundance in near surface samples, but more reads from this phylum were detected in deeper samples, including relatives of the genus *Thermus*, which contains thermophilic microbes (Brock and Freeze, 1969). *Nitrospirae*, a phylum containing nitrite-oxidizing bacteria (Daims, 2014), was in very low abundance in the test deposits. Reads for this phylum were low in near-surface samples and increased with depth in the full-scale deposits. In the test deposits, *Acidobacteria* exhibited highest percent reads in the near surface samples, but samples below 0.1 m exhibited very low abundances for this phylum. Reads were consistent with depth in EV-1. In EV-2, reads were low near the surface, highest at the 0.3 m depth, and consistent with depth for the rest of the sample locations.

Beta Diversity

Based on the Yue and Clayton theta coefficient of dissimilarity in community structure (Yue and Clayton, 2005), sequencing replicates clustered together tightly with few exceptions (Figure 3.6). The samples that did not cluster were: GD Location 3 (0.1 m), TD Location 2 (0.6 m), and TD Location 4 (0.7 m); however, the replicates of these three samples were within three branches or less. Generally speaking, there were two broad clusters of sample types: samples from the upper 0.4 m of the CFT deposits (the upper branch of the tree in Figure 3.6), and samples from depths greater than 0.4 m (the lower branch of the tree in Figure 3.6).

Community richness was assessed by the Jaccard coefficient of dissimilarity; the difference between this calculation and the Yue Clayton calculation is that the Jaccard coefficient does not include non-shared OTUs in the calculations. Sequenced replicates were also typically clustered together, except for samples: EV-2 Location 2 (0.3 m), EV-2 Location 4 (0.9 and 1.5 m), TD Location 4 (0.7 m), and GD Location 2 (0.6 m; Figure 3.7). The upper branch consisted of samples from near the surface of the test deposits (GD and TD). The middle branch consisted of samples from the full scale deposits (EV-1 and EV-2). In these branches, samples

from each deposit generally clustered together. The bottom branch consisted of samples from the depths of GD and TD. These samples did not cluster by deposit or by depth.

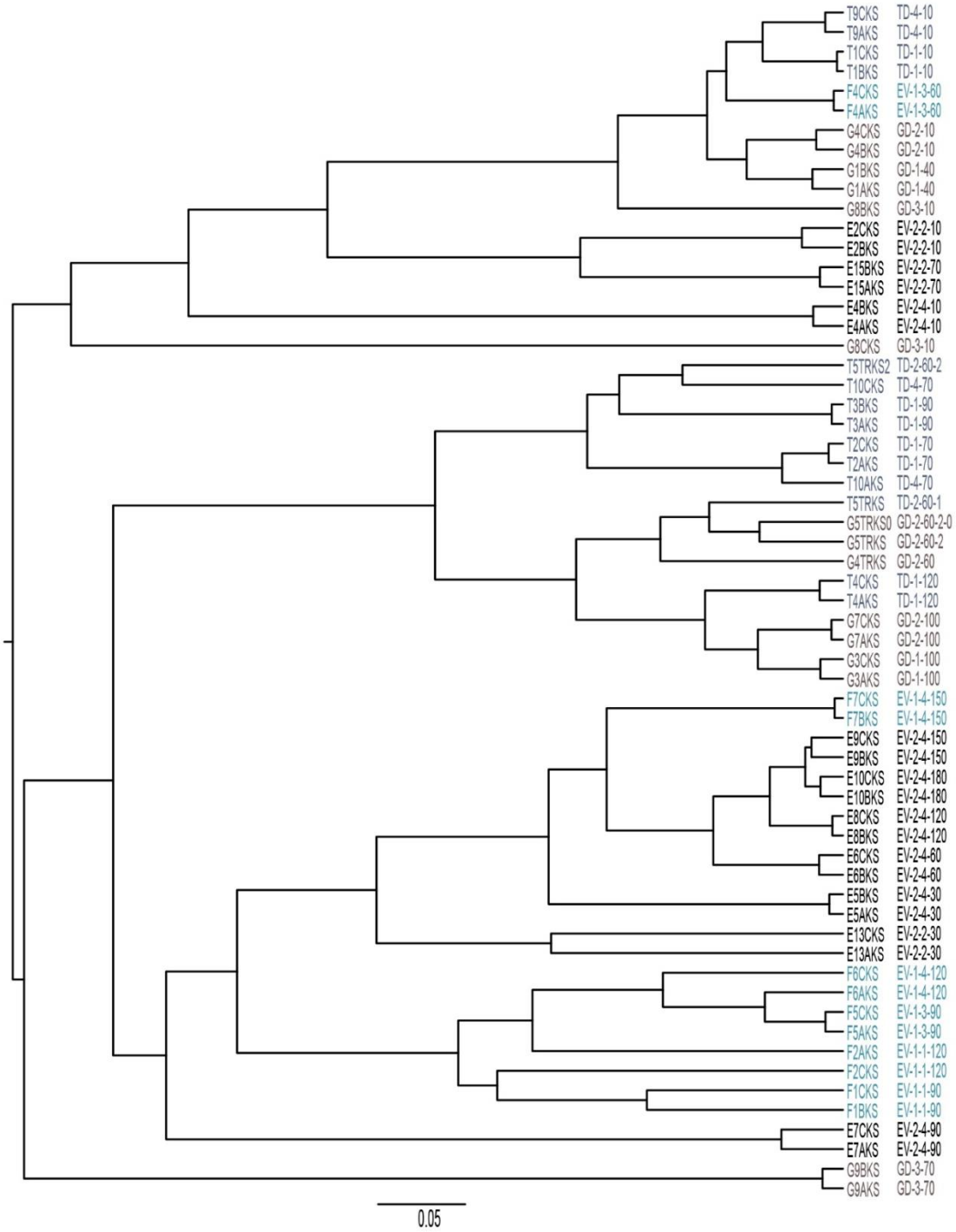

Figure 3.6: Beta diversity dendrogram by Yue and Clayton theta calculation for community structures/diversity (Yue and Clayton, 2005) for EV-1, EV-2, GD, and TD. First column is the sequencing replicate names. Second column is the deposit name, borehole number, and depth (in cm).

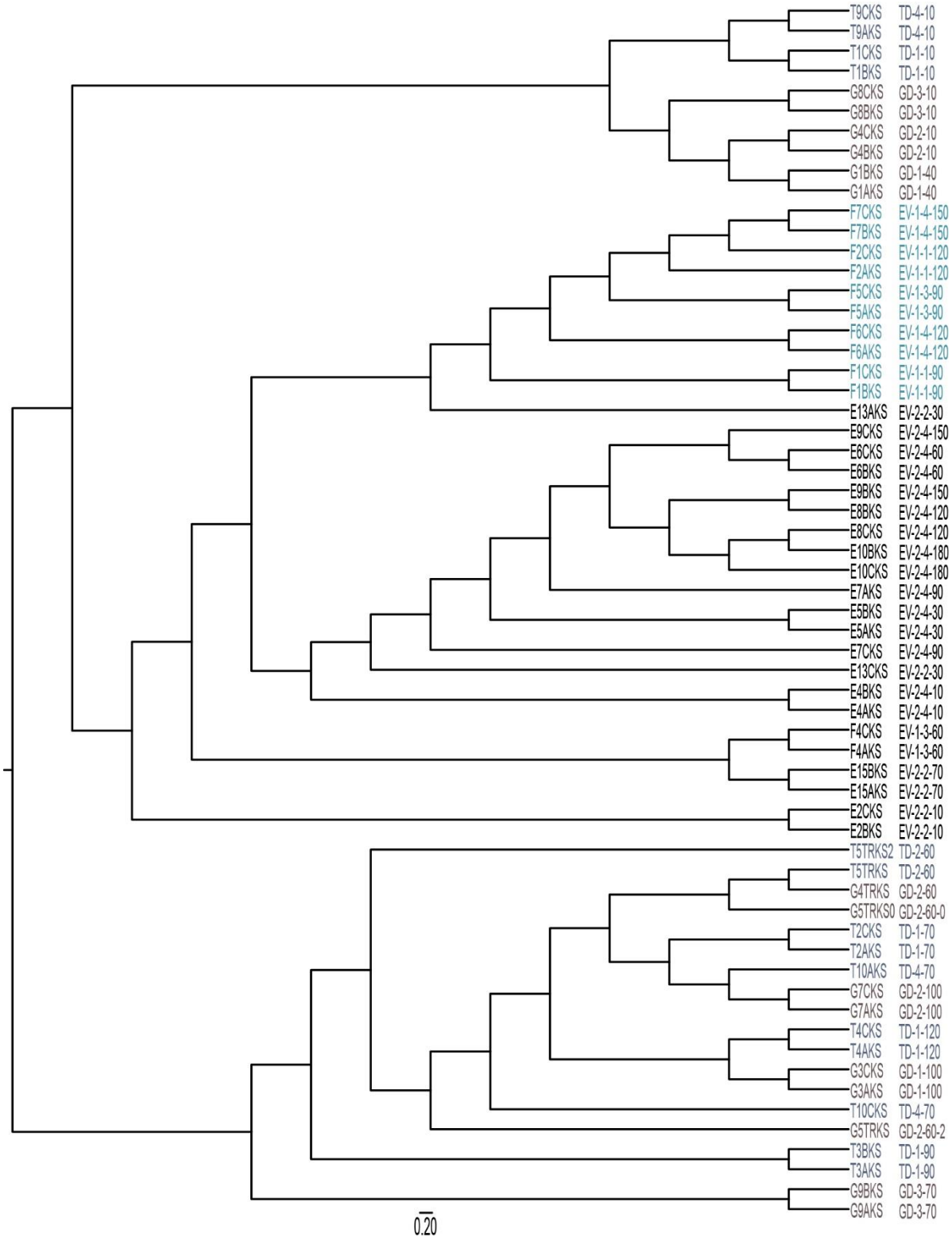

Figure 3.7: Beta diversity dendrogram for community membership/richness by Jaccard coefficient of dissimilarity (Smith et al., 1996) for EV-1, EV-2, GD, and TD. First column is the sequencing replicate names. Second column is the deposit name, borehole number, and depth (in cm).

Calculations for NMDS indicated that three dimensions provided an R^2 value of 89 % and a stress of 0.14 (Figure 3.8). Four groups appeared to be clustered within space. Group A was comprised of test deposit samples from depths greater than 0.4 m in GD and greater than 0.3 m in TD. Many samples from below 0.3 m in EV-2 were clustered in Group B. Group C contained many of the samples from EV-1. The surface samples from EV-2 (< 0.3 m), GD (< 0.4 m), and TD (< 0.3m) were generally clustered in group D.

The PCA exhibited an R^2 value of 84% in two dimensions (Figure 3.9). Only three groupings were obvious. Group A consisted of the test deposit samples from greater than 0.3 m. Group B consisted of samples from EV-1 and samples from below 0.3 m in EV-2. Group C consisted generally of the surface samples from EV-2, GD, and TD. A linear trend was also apparent and may potentially be related to increasing concentrations of dissolved ions as depth decreases.

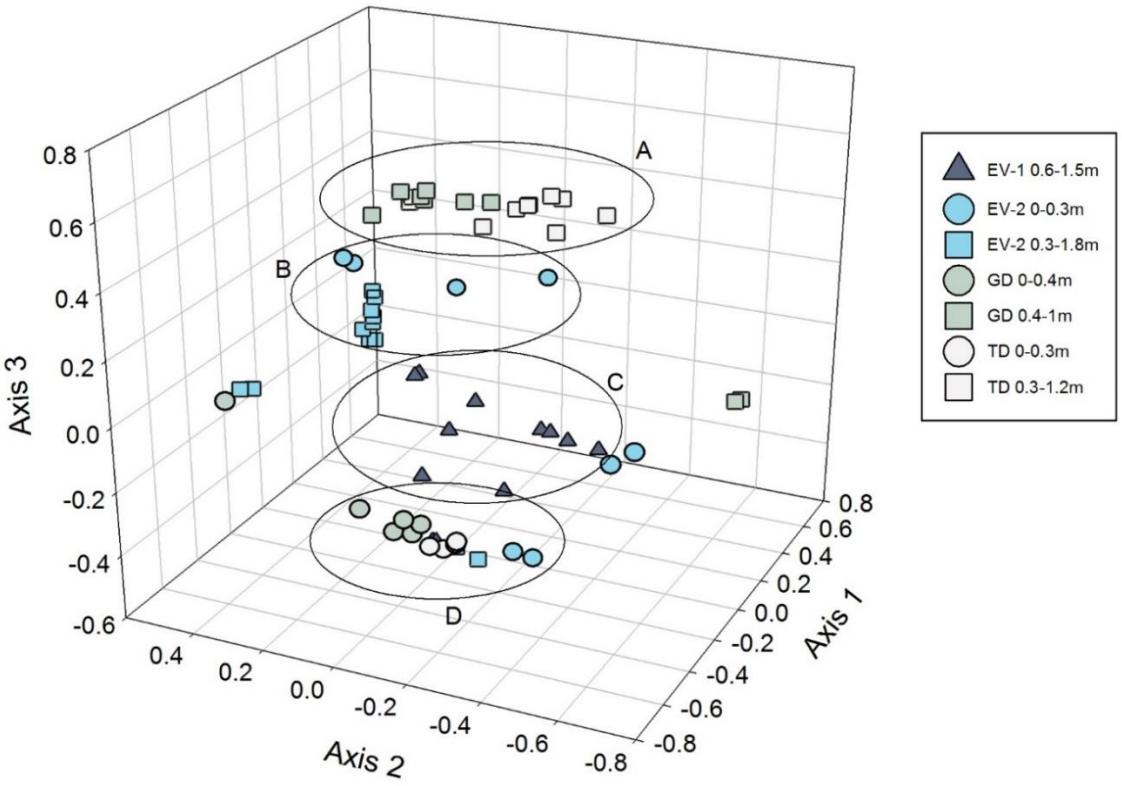

Figure 3.8: Beta diversity analysis by NMDS for EV-1, EV-2, GD, and TD

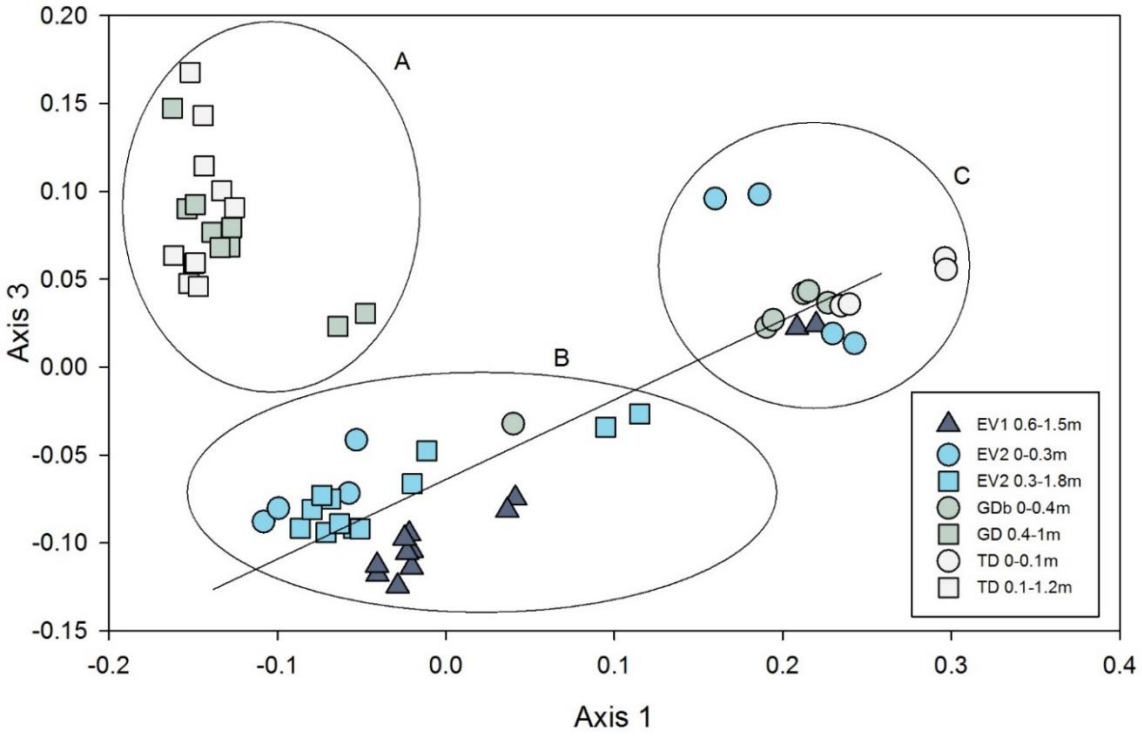

Figure 3.9: Beta diversity analysis by PCA for EV-1, EV-2, GD, and TD.

3.6 Discussion

3.6.1 Summary of CFT pore-water chemistry

Pore-water chemistry within EV-1, EV-2, GD, and TD was described in detail in Chapter 2 of this thesis. Briefly, pore-water pH was mildly alkaline (7.5-8.7; $\mu = 7.9$; $\sigma = 0.3$) and was generally consistent with depth among the four CFT deposits (Figure 2.2). Measured values of Eh in the CFT deposits ranged from +80 to +400 mV (Figure 2.2). These values were higher than expected for an anaerobic reducing system, which may be due to low concentrations of active redox couples, the presence of zero-valent S (Couture and Van Cappellen, 2011), or alteration through inadvertent exposure of the CFT samples to air due to diffusion through the polyethylene storage bags. Due to the presence of dissolved H_2S and relatives of known SRB and methanogens, the actual Eh is expected to be -200 mV or lower. Elevated values of EC were found, with higher values exhibited by the full-scale deposits ($\mu = 7.6$ mS cm^{-1}; $\sigma = 2.0$ mS cm^{-1}) than the test deposits ($\mu = 3.1$ mS cm^{-1}; $\sigma = 0.8$ mS cm^{-1}; Figure 2.2). Values of EC increased near the surface of each deposit. Alkalinity increased slightly with depth in all deposits and had a mean value of 470 mg L^{-1} as $CaCO_3$ (Figure 2.2). Ammonia concentrations generally increased with depth and ranged from 1 to 17 mg L^{-1} as NH_3-N (Figure 2.5). Total NA concentrations

exhibited a mean value of 74 mg L^{-1} across all deposits and increased near the surface of each deposit (Figure 2.5). Many ions, including Ca, Na, Mg, K, Cl, Mn, and SO_4 increased near surface (Figures Figure 2.3, Figure 2.5, and Figure 2.6), which suggests evaporative concentration. The dominant ions include Ca (10 – 470 mg L^{-1}), Na (260 – 3700 mg L^{-1}), Cl (80 - 2200 mg L^{-1}), and SO_4 (1 – 6400 mg L^{-1}). Conversely, both Fe and hydrogen sulfide (H_2S) increased with depth (Figure 2.6). The mean H_2S concentration was 28 µg L^{-1}, and H_2S was inversely correlated with SO_4.

3.6.2 Microbial processes

Denitrification and nitrite oxidation

Aerobic redox processes such as denitrification and nitrite oxidation were not expected to be dominant microbial processes in the CFT deposits due to tension-saturation; however, these processes may be occurring. Pore-water nitrate and nitrite concentrations were consistently below detection limits (BDL); however, because relatives of denitrifying and nitrite oxidizing bacteria were identified in the sequencing data there may be a cryptic nitrogen cycle occurring in these deposits. The order *Rhodocyclales* (*Betaproteobacteria*), which contains known denitrifiers *Thauera* and *Azoarcus* (Oren, 2014), exhibited more sequence reads in the full-scale deposits than the test deposits. *Pseudomonadales*, which contains nitrite-oxidizing bacteria (Vangnai and Klein, 1974), was identified in higher abundance near the surface of GD as well as at the 0.9 m depth of EV-2. Very few sequencing reads in GD and TD were obtained for *Nitrospirae*, a phylum containing nitrite-oxidizing bacteria (Daims, 2014), whereas this phylum was observed greater abundance in EV-1 at 1.2 and 1.5 m depth and in EV-2 at 0.3 m depth.

Iron reduction

Total dissolved Fe concentrations increased slightly with depth in EV-1 and EV-2, but generally remained consistent with depth in the test deposits. At the pH values observed in the CFT deposits, Fe(II) is expected to dominate total Fe in pore water. Sources of Fe(III) for microbial Fe reduction may include Fe(III) (hydr)oxide minerals or structural Fe(III) associated with the clay minerals present in the CFT deposits (Stucki, 2006). Microbial Fe reduction is not limited to FeRB – such as members of the family *Geobacteraceae*, which was observed to increase with depth – but may also be mediated by *Clostridia* (Kunapuli et al., 2007), *Desulfobulbaceae* (Kunapuli et al., 2007; Lovley et al., 1993), methanogens (Bond and Lovley,

2002), and *Synergistia* (Siddique et al., 2014b). Sequences assigned to these taxa were observed in all CFT deposits, and, in combination with the iron data, this suggests that Fe reduction is likely occurring.

Sulfate reduction

Elevated HS^- concentrations and the presence of many relatives of known SRB are indicative of SO_4 reduction within the CFT deposits. Our sequencing data shows evidence for the presence of organisms that may be able to reduce SO_4 or other sulfur compounds, such as *Desulfurivibrio* and *Desulfocapsa* (Kuever, 2014; Sorokin et al., 2008). These organisms were also identified in a gypsum-amended oil sands tailings pond at abundances of up to 15% (Ramos-Padrón et al., 2011). Increases in dissolved HS^- with depth are indicative of anoxic conditions and SO_4 reduction, and also supports the conclusion that these microbes are present and active in all CFT deposits, particularly those amended with gypsum (EV-1, EV-2, GD).

Increased pore-water SO_4 concentrations in gypsum-amended CFT deposits generally corresponded to decreases in concentrations of the F1 fraction PHCs including BTEX compounds ($-0.447 < R < -0.557$; $P < 0.05$ between SO_4 and benzene, ethylbenzene, total xylenes, F1, and F1-BTEX. No statistical correlation between SO_4 and toluene). The TD deposit, which was not amended with gypsum, exhibited consistently higher concentrations of these hydrocarbons than EV-2 and GD, which were amended with gypsum. Gypsum-amendment has been shown to enhance PHC degradation in both aerobic and anaerobic environments (Penn et al., 2014; Rothermich et al., 2002). *Desulfobacteraceae*, which is reported to be involved in crude oil *n*-alkane degradation (Cheng et al., 2014), were abundant taxa in gypsum-amended CFT deposits, whereas the TD deposit contained very little abundance of this taxa. Additionally, the order *Burkholderiales*, although not an SRB, was more abundant in gypsum-amended deposits than in TD. This order is capable of degrading many aromatic compounds such as BTEX (Pérez-Pantoja et al., 2012). Likely, the excess SO_4 would not be a limiting nutrient in the gypsum-amended system, and may allow them to rapidly degrade these F1 PHCs.

Methanogenesis

Microbial and geochemical data supports the hypothesis that methanogenesis is occurring in all four deposits. Archaea were present at larger percentages of sequencing reads as depth increased, however, never exceeded 1.3 % of sequencing reads in a sample. Known methanogens

identified in CFT sequencing data were previously identified as dominant taxa (~65%) in FFT (Siddique et al., 2014b), and in a gypsum-amended oil sands tailings pond they represented approximately 15% of the community (Ramos-Padrón et al., 2011). A higher proportion of sequencing reads from individual samples were identified as Archaea in TD compared to the gypsum-amended deposits, which may suggest that gypsum amendment shifts the microbial community towards SO_4 reduction and away from methanogenesis. Relatives of known methanotrophs, *Methylobacterium*, *Methylocystis*, and *Methylosinus* (Hanson and Hanson, 1996), were identified in the sequencing data; however their abundance was very low.

Hydrocarbon degradation

As CFT is homogeneous when it is deposited, concentrations of PHCs are expected to be initially consistent with depth. Concentrations of the various measured PHCs increased with depth in the measured deposits. This indicates that biotic or abiotic PHC degradation may be occurring. Diverse microbial taxa identified in the CFT sequencing reads are capable of directly or indirectly affecting PHC degradation. Under methanogenic conditions, toluene degradation occurs with the assistance of syntrophic partners *Syntrophaceae*, *Desulfovibrionales*, and *Chloroflexi* (Fowler et al., 2014). *Methanosaeta*, hydrogenotrophic methanogens, *Desulfobacteraceae*, and *Syntrophaceae* were involved in crude oil *n*-alkane degradation (Cheng et al., 2014). *Desulfobulbaceae* and *Clostridiales* were reported to be involved in Fe-reduction during benzene degradation (Kunapuli et al., 2007). *PYR10d3* was first identified in PAH-contaminated soil and appears to be a pyrene degrader (Singleton et al., 2006). Other PAH-degraders include *Pseudomonadales* and *Alteromonadales* (Kersters et al., 2006), and various members of the order *Burkholderiales* are capable of degrading a variety of aromatic compounds (Pérez-Pantoja et al., 2012).

3.6.3 Comparison to other oil sands-related environments

Generally, the CFT deposits contain similar microbial taxa as FFT, however the proportions were different. In CFT, methanogens constituted less than 1 % of the microbial community, but FFT and a gypsum-treated oil sands tailings pond had an abundance of ~65 % and <15 %, respectively (Ramos-Padrón et al., 2011; Siddique et al., 2014b). Likely the addition of gypsum has shifted the metabolic capability of the microbial community towards SO_4 reduction and away from methanogenesis. *Proteobacteria* was approximately 60 % of sequenced

reads in CFT, which could be due to the high proportion of reads for SRB. In contrast, *Proteobacteria* was the dominant phylum in the tailings pond (~40 %; Ramos-Padrón et al., 2011), but was less than 20% of sequenced reads in FFT (Siddique et al., 2014b). *Comamonadaceae* dominated non-Archaeal reads in FFT (~10 %; Siddique et al., 2014b), but showed slightly lower abundance in CFT (~6 %). Sequenced reads for *Chloroflexi* were in general agreement for both CFT and in the gypsum-treated tailings pond (~20 %; Ramos-Padrón et al., 2011). Conversely, reads for *Firmicutes* were three times less abundant in CFT than the tailings ponds (~5 % and ~15 %, respectively; Ramos-Padrón et al., 2011). *Firmicutes* have been commonly detected in methanogenic petroleum-contaminated environments (Liang et al., 2015), and, since reads for methanogens were a low proportion of microbial reads in the CFT, *Firmicutes* may also have lost their competitive advantage to the SRB. Taxa observed in all samples of CFT and also in FFT include *Desulfobulbaceae* (i.e., *Desulfocapsa* and *Desulfurivibrio*), *Syntrophobacterales, Hydrogenophilales*, and *Comamonadaceae*.

Samples of OSPW also exhibited 60% of sequenced reads for *Proteobacteria*; however, *Alphaproteobacteria* were much more dominant than in CFT (30 % in OSPW vs < 10 % in CFT; Islam et al., 2015). Many *Alphaproteobacteria* are capable of photosynthesis and are therefore found in water columns and near-surface soil samples (Madigan and Martinko, 2006). Neither light nor oxygen penetrates very far into the profile of CFT; therefore, a lower abundance of these microbes was expected. *Deltaproteobacteria* dominated CFT *Proteobacterial* sequences, particularly in non-surface samples, whereas *Deltaproteobacteria* were less than 10 % of *Proteobacterial* sequences in OSPW (Islam et al., 2015). The dominance of *Deltaproteobacteria* in CFT is largely due to the presence of SRB. Nitrogen-cycling bacteria, such as *Rhodocyclales* and *Pseudomonadales* (Oren, 2014; Vangnai and Klein, 1974), were more prevalent in OSPW than in CFT at 12 % vs <2 % and 15 % vs <3 %, respectively (Islam et al., 2015). These differences may be due to low concentrations of nitrite and nitrate in CFT. *Nitrospirae* comprised approximately 10 % of the sequenced reads in OSPW (Islam et al., 2015), but was less than 2 % of total sequences in CFT, perhaps because it is a mostly aerobic family (Daims, 2014). *Chloroflexi* was approximately four times more abundant in CFT than in OSPW (18 % vs 5 %, respectively; (Islam et al., 2015). In CFT, *Chloroflexi* was predominately represented by *Anaerolineaceae*, which is a syntrophic partner of *Methanosaeta* – relatives of this methanogen dominated Archaeal reads in this study, whereas this methanogen comprised a small amount of

Archaeal reads (< 10 %) in OSPW (Islam et al., 2015). *Acidobactiera*, *Bacteroidetes*, and *Verrucomicrobia* had similar abundances in both CFT and OSPW.

Sediment in the Athabasca River north of Fort McMurray was also dominated by *Proteobacteria* (~40 % of bacterial sequences); however, *Alphaproteobacteria* and *Betaproteobacteria* generally dominated (Yergeau et al., 2012), whereas *Gammaproteobacteria* and *Deltaproteobacteria* were the dominant class in CFT; likely more oxygen, nitrogen, and light would be available in the river sediment. *Bacteroidetes*, *Firmicutes*, and *Chloroflexi* were also abundant in these samples (approximately 10 %, 10 %, 5 %, respectively; (Yergeau et al., 2012), and these values are in general agreement with those from CFT. Archaeal taxa in these sediments was also dominated by *Euryarchaeota*, however *Methanospirillum* and *Methanosarcina* dominated these taxa, and *Methanosaeta*, *Methanobacterium*, and *Methanolinea* made generally smaller contributions than in CFT (Yergeau et al., 2012). Clay and NA were found to influence microbial community structure in the samples as well as proximity to the oil sands tailings ponds (Yergeau et al., 2012).

3.7 Conclusions

In combination with geochemical analyses, the DNA sequencing data suggests that Fe reduction, SO_4 reduction, and methanogenesis are on-going within the CFT deposits. Known relatives of FeRB (i.e. *Geobacteraceae*), SRB (i.e. *Desulfurivibrio*, *Desulfocapsa*), and methanogens (i.e. *Methanolinea*, *Methanoregula*, *Methanosaeta*, *Methanobacterium*) were detected. The distribution patterns of these microbes also correspond to geochemical changes that we expect to result from their activity (e.g. increasing H_2S and Fe(II) concentrations with depth in each deposit). Many of the microbes detected in CFT were also identified in FFT, OSPW, and river sediment sites near oil sands mines. Geochemistry in the CFT also supports these observations of on-going redox processes. These redox processes could be quantified by performing most probable numbers experiments, rate reactions, and quantitative polymerase chain reactions (qPCR) targeting functional genes related to these processes. Additionally, numerous microbes with known PHC degradation potential (i.e. *Methanosaeta*, *Burkholderiales*, *Desulfobulbaceae*) were detected. Gypsum addition seems to inversely correlate with PHC degradation of the F1 fraction (i.e. BTEX); further studies could be done to elucidate the mechanism and products of this degradation and determine whether any microbial species are involved.

CHAPTER 4 CONCLUSIONS

4.1 Summary of Findings

Centrifuged fine tailings (CFT) were deposited in field-scale test deposits prior to deposition in full-scale production deposits. Both full-scale production deposits (EV-1, EV-2) and one of the test deposits (GD) were amended with both polyacrylamide and gypsum. The other test deposit (TD) was amended with only polyacrylamide.

Pore-water chemistry of the full-scale deposits was characterized by higher concentrations of calcium (Ca), magnesium (Mg), sodium (Na), potassium (K), chloride (Cl), fluoride (F), manganese (Mn), iron (Fe), sulfate (SO_4), hydrogen sulfide (H_2S), and total naphthenic acid (NA) than the test deposits (Figures Figure 2.3, Figure 2.5, and Figure 2.6). This observation is consistent with the larger quantities of gypsum that are added to the full-scale deposits (approximately double amendment rate of the test deposits; however, in the production deposits, gypsum amendment has varied up to six times higher than the target amendment rate). Electrical conductivity (EC) in the CFT deposits generally reflect these trends in concentrations of dissolved ions (Figure 2.2). The test deposits were characterized by higher redox potential (Eh) and alkalinity than the full-scale deposits, whereas ammonia concentration and pH were similar among all deposits (Figures Figure 2.2 and Figure 2.5).

Evaporative concentration results in higher concentrations of dissolved ions near the surface of the CFT deposits than at depth. These increases are particularly apparent in the full-scale deposits, and include: Ca, Na, Cl, SO_4, and total NAs. Dissolved Ca concentrations were up to 500 mg L^{-1} near surface of the full-scale deposits, but decreased to approximately 150 mg L^{-1} at depths below 0.3 m (Figure 2.3). In contrast, pore-water Ca concentrations were generally less than 100 mg L^{-1} in the test deposits. Dissolved Na concentrations in EV-1 and EV-2 exceeded 2000 mg L^{-1} near the surface but decreased to approximately 1500 mg L^{-1} below 0.3 m (Figure 2.3). Sodium concentrations in the test deposits generally did not exceed 1000 mg L^{-1}. Dissolved Cl concentrations exceed 1000 mg L^{-1} near the surface of the full-scale deposits (Figure 2.5). At depths greater than 0.3 m, Cl concentrations were approximately 800 mg L^{-1} in the full-scale

deposits. In contrast, pore-water Cl concentrations in the test deposits were consistently less than 500 mg L^{-1}. Dissolved SO_4 concentrations were approximately 2000 mg L^{-1} at depths below 0.3 m in the full-scale deposit but increased up to 6400 mg L^{-1} near surface (Figure 2.6). Pore-water SO_4 concentrations in the test deposits were generally less than 1400 mg L^{-1}. Total NA reached concentrations up to 250 mg L^{-1} near the surface of EV-1 but was typically less than 100 mg L^{-1} at depths greater than 0.3 m in all CFT deposits.

In contrast to Ca, Na, Cl, SO_4, and total NAs, concentrations of dissolved ammonia, Fe, H_2S generally increased with depth. Ammonia concentrations increased from approximately 5 mg L^{-1} near surface to 15 mg L^{-1} at depth (Figure 2.5). Dissolved Fe was below detection near surface and increased to approximately 2 mg L^{-1} at depth (Figure 2.6). This observation is generally consistent with increasing abundances of Fe-reducing bacteria (FeRB) observed with depth in the CFT deposits (Figure 3.5). Similarly, dissolved H_2S and SO_4 concentrations were inversely correlated and the highest H_2S concentrations were generally observed 0.5 m below the surface of CFT (Figure 2.6).

Betaproteobacteria and *Gammaproteobacteria* and *Acidobacteria* were most abundant near surface (Figures Figure 3.3 and Figure 3.5). These taxa generally decreased in abundance below 0.3 m, whereas *Chloroflexi* (i.e. *Anaerolineaceae*), *Deltaproteobacteria* (i.e. *Desulfurivibrio*, *Desulfocapsa*, *Geobacteraceae*), Archaea (i.e. *Methanosaeta*, *Methanolinea*, *Methanoregula*, *Methanomicrobia*), *Bacteroidetes*, and *Firmicutes* exhibited higher abundance at this depth compared to the surface of the CFT deposits (Figures Figure 3.3 to Figure 3.5). The test deposits (i.e. GD, TD) generally contained more Archaea than the full-scale deposits. This disparity is attributed to greater abundance of *Deinococcus-Thermus*, *Nitrospirae*, *Bacteroidetes*, *Syntrophobacterales*, and *Alphaproteobacteria* in EV-1 and EV-2 which likely results from the higher rates of gypsum and polyacrylamide amendment during production of CFT contained in the full-scale deposits. The gypsum-amended deposits generally contained more *Deltaproteobacteria* (i.e. SRB) than TD, whereas TD generally contained more *Chloroflexi* than the gypsum-amended deposits. Gene sequences reads of relatives of FeRB (i.e. *Geobacteraceae*), SRB (i.e. *Desulfurivibrio*, *Desulfocapsa*), methanogens (i.e. *Methanosaeta*, *Methanolinea*), and hydrocarbon degraders (i.e. *PYR10d3*, *Burkholderiales*, *Syntrophaceae*) were identified in all CFT deposits.

The chemistry of CFT solids was dominated by silicon (Si) and aluminum (Al), which is consistent with the high clay content of CFT (Figure 2.9). Synchrotron-based Fe K-edge X-ray adsorption near edge structure (XANES) spectroscopy suggested that both Fe(II) and Fe(III) were present in CFT solids (Figure 2.11). Sulfur (S) K-edge XANES spectra revealed the presence of SO_4 in EV-1 and EV-2, and in near surface samples from GD and TD (Figure 2.10). Organic S compounds also comprised a major component of these S K-edge XANES spectra. Mineralogical characterization revealed the presence of quartz, various clay minerals, calcite, and siderite, which is consistent with previous results for FFT (Figure 2.8).

Petroleum hydrocarbon (PHC) concentrations were generally similar between the gypsum-amended deposits (EV-2 and GD) for all fractions of hydrocarbons (Figure 3.2). Although TD exhibited similar concentrations for the F2, F3, and F4 fractions and higher concentrations for the F1 fraction, this deposit exhibited consistently higher concentrations of all PHC fractions than the gypsum-amended deposits (i.e. EV-2, GD). This observation suggests that SO_4 reduction may play an important role in degradation of these light PHCs in CFT deposits.

A conceptual model of the processes occurring in CFT includes both physical and biogeochemical processes (Figure 4.1). Freeze-thaw cycling, a process to increase the geotechnical strength, dewaters the CFT and decreases the moisture content from the production value of 50 to 58 % to less than 30 %. Evaporative flux from the surface of the CFT deposits leads to concentration of dissolved ions. Thus, high concentrations of dissolved Na, Ca, Cl, and SO_4 can be observed near the surface of the deposits. Concentrations of Ca increased at a rate greater than that of Cl. The likely mechanism behind this observation is ion exchange of Na for Ca as Na concentrations increase near the surface. The redox processes of Fe reduction, SO_4 reduction, and methanogenesis are on-going in the CFT deposits. Iron reduction likely occurs in the upper portions of the CFT deposits, whereas methanogenesis likely occurs towards the bottom of the deposit. Sulfate reduction appears to occur throughout the much of the deposit profile.

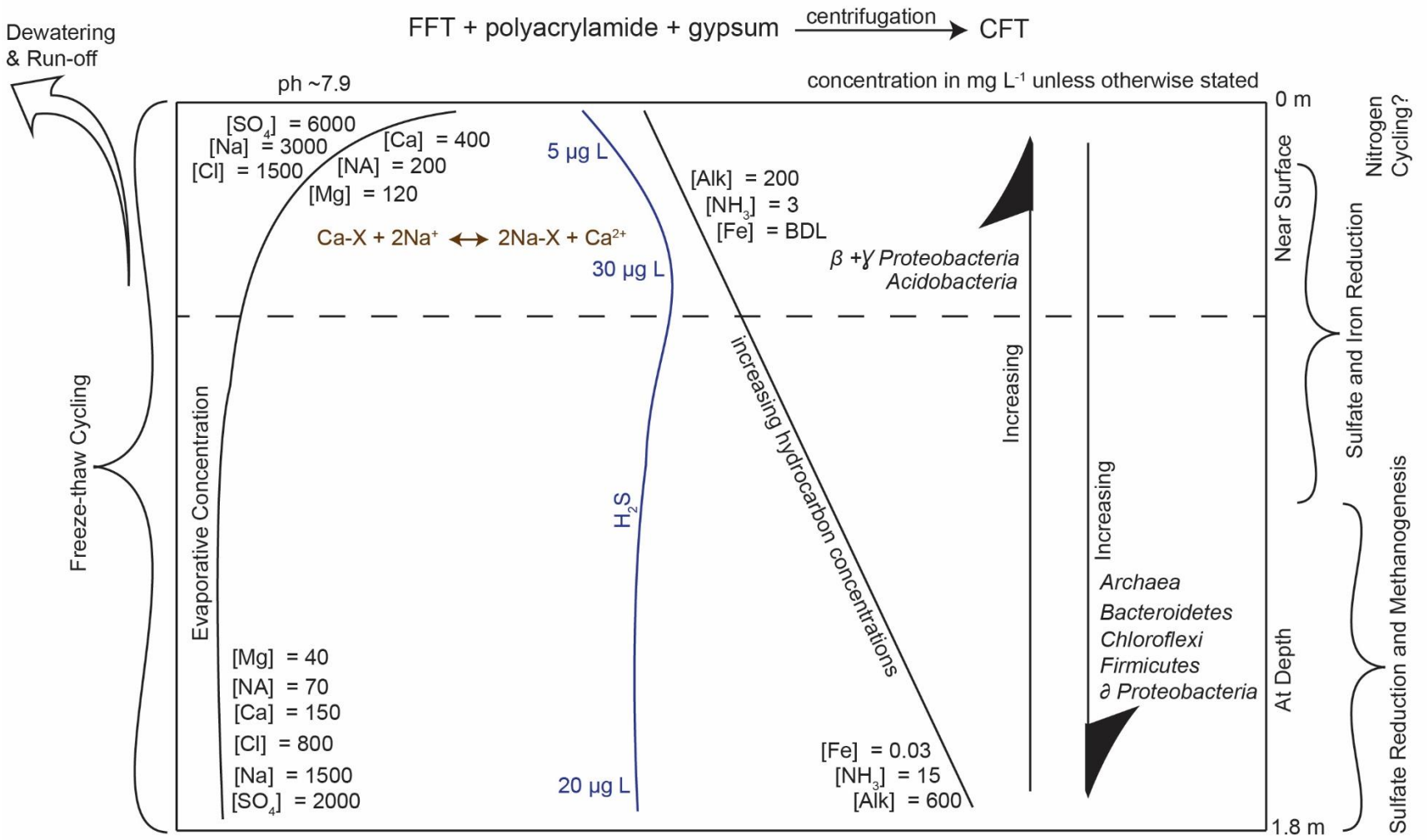

Figure 4.1: Conceptual model of biogeochemical processes for full-scale production CFT deposits

4.2 Recommendations

Pore water near the surface of the CFT deposits contained high concentrations of salts and NAs, and so further work could quantify rates of evaporative flux. The pore-water quality near the surface of the CFT deposits would not generally be suitable for revegetation; however, mine closure plans do not currently anticipate revegetating CFT directly. Likely CFT will be placed in deposits that may or may not also contain coke, another waste product of site that may assist in adsorbing NAs (Zubot et al., 2012), which will then be covered with topsoil. In the meantime, evaluating the quality and quantity of run-off water produced by the CFT deposits would determine if catchment and treatment systems should be considered. Further microbial characterization, including culture-based assessment of FeRB, SRB, and methanogens, could help examine rates of redox reactions and determine if any of these reactions are closely linked to PHC degradation. Additionally, CFT deposits will be constructed in a series of lifts with new layers of CFT placed atop layers that have undergone at least one freeze-thaw cycle. It would be beneficial to determine the effects of new layers on *in situ* physical and biogeochemical processes in a few years' time after each layer is able to undergo at least one freeze-thaw cycle. Microbial assessment at this time would provide information on the length of time that the added gypsum is able to promote sulfate reduction and if the microbial community shifts towards methanogenesis as the CFT ages. These pieces of information would help inform mine closure planning.

REFERENCES

Abram, F., Enright, A.-M., O'Reilly, J., Botting, C.H., Collins, G., O'Flaherty, V., 2011. A metaproteomic approach gives functional insights into anaerobic digestion. J. Appl. Microbiol. 110, 1550–60. doi:10.1111/j.1365-2672.2011.05011.x

Achenbach, L.A., Bender, K.S., Chakraborty, R., Coates, J.D., Cole, K.A., Lack, J.G., O'Connor, S.M., 2001. Anaerobic benzene oxidation coupled to nitrate reduction in pure culture by two strains of Dechloromonas. Nature 411, 1039+.

AER, 2009. Directive 074: Tailings Performance Criteria and Requirements for Oil Sands Mining Schemes. Calgary.

AER, 2015. Bulletin 2015-11: Directive 074: Tailings Performance Criteria and Requirements for Oil Sands Mining Schemes Suspended. Edmonton.

Allen, E.W., 2008. Process water treatment in Canada's oil sands industry: 1. target pollutants and treatment objectives. J. Environ. Eng. Sci. 7, 123–138.

Baldwin, S.A., Khoshnoodi, M., Rezadehbashi, M., Taupp, M., Hallam, S., Mattes, A., Sanei, H., 2015. The microbial community of a passive biochemical reactor treating arsenic, zinc, and sulfate-rich seepage. Front. Bioeng. Biotechnol. 3, 27. doi:10.3389/fbioe.2015.00027

Ball, J.W., Nordstrom, D.K., 1991. User's Manual for WATEQ4F, with revised thermodynamic database and test cases for calculating speciation of major, trace, redox elements in natural waters. Menlo Park.

Banerjee, D.K., 2012. Oil Sands, Heavy Oil & Bitumen: From Recovery to Refinery. PennWell Corporation, Tulsa.

Bayliss, P., Levinson, A.A., 1976. Mineralogical review of the Alberta oil sand deposits (Lower Cretaceous, Mannville Group). Bull. Can. Pet. Geol. 24, 211–224.

Bethke, C.M., Sanford, R.A., Kirk, M.F., Jin, Q., Flynn, T.M., 2011. The thermodynamic ladder in geomicrobiology. Am. J. Sci. 311, 183–210. doi:10.2475/03.2011.01

Birkeland, N.-K., 2005. Sulfate-reducing bacteria and archaea, in: Olivier, B., Magot, M. (Eds.), Petroleum Microbiology. ASM Press, Washington, pp. 34–54.

Bond, D.R., Lovley, D.R., 2002. Reduction of Fe(III) oxide by methanogens in the presence and absence of extracellular quinones. Environ. Microbiol. 4, 115–124. doi:10.1046/j.1462-2920.2002.00279.x

Boulding, J.R., Ginn, J.S., 2003. Practical Handbook of Soil, Vadose Zone, and Ground-Water Contamination: Assessment, Prevention, and Remediation, 2nd ed. CRC Press, Boca Raton.

Brauer, S.L., Cadillo-Quiroz, H., Ward, R.J., Yavitt, J.B., Zinder, S.H., 2010. Methanoregula boonei gen. nov., sp. nov., an acidiphilic methanogen isolated from an acidic peat bog. Int. J. Syst. Evol. Microbiol. 61, 45–52. doi:10.1099/ijs.0.021782-0

Brock, T.D., Freeze, H., 1969. Thermus aquaticus gen. n. and sp. n., a nonsporulating extreme thermophile. J. Bacteriol. 98, 289–97.

CAPP, 2012. Land Use in Canada's Oil Sands.

Carvalho, F.M., Souza, R.C., Barcellos, F.G., Hungria, M., Vasconcelos, A.T.R., 2010. Genomic and evolutionary comparisons of diazotrophic and pathogenic bacteria of the order Rhizobiales. BMC Microbiol. 10, 37. doi:10.1186/1471-2180-10-37

CCME, 2001. Reference Method for the Canada-Wide Standard for Petroleum Hydrocarbons in Soil - Tier 1 Method. Winnipeg.

Chen, M., Walshe, G., Chi Fru, E., Ciborowski, J.J.H., Weisener, C.G., 2013. Microcosm assessment of the biogeochemical development of sulfur and oxygen in oil sands fluid fine tailings. Appl. Geochemistry 37, 1–11. doi:10.1016/j.apgeochem.2013.06.007

Cheng, L., Shi, S., Li, Q., Chen, J., Zhang, H., Lu, Y., 2014. Progressive degradation of crude oil n-alkanes coupled to methane production under mesophilic and thermophilic conditions. PLoS One 9, e113253. doi:10.1371/journal.pone.0113253

Chi Fru, E., Chen, M., Walshe, G., Penner, T., Weisener, C., 2013. Bioreactor studies predict whole microbial population dynamics in oil sands tailings ponds. Appl. Microbiol. Biotechnol. 97, 3215–24. doi:10.1007/s00253-012-4137-6

Choi, D.H., Cho, B.C., 2006. Lutibacter litoralis gen. nov., sp. nov., a marine bacterium of the family Flavobacteriaceae isolated from tidal flat sediment. Int. J. Syst. Evol. Microbiol. 56, 771–6. doi:10.1099/ijs.0.64146-0

Clemente, J.S., Fedorak, P.M., 2005. A review of the occurrence, analyses, toxicity, and biodegradation of naphthenic acids. Chemosphere 60, 585–600. doi:10.1016/j.chemosphere.2005.02.065

Coates, J.D., Bhupathiraju, V.K., Achenbach, L.A., Mclnerney, M.J., Lovley, D.R., 2001. Geobacter hydrogenophilus, Geobacter chapellei and Geobacter grbiciae, three new, strictly anaerobic, dissimilatory Fe(III)-reducers. Int. J. Syst. Evol. Microbiol. 51, 581–588. doi:10.1099/00207713-51-2-581

Coates, J.D., Ellis, D.J., Gaw, C. V, Lovley, D.R., 1999. Geothrix fermentans gen. nov., sp. nov., a novel Fe(III)-reducing bacterium from a hydrocarbon-contaminated aquifer. Int. J. Syst. Evol. Microbiol. 49, 1615–22. doi:10.1099/00207713-49-4-1615

Council of Canadian Academies, 2015. Technological Prospects for Reducing the Environmental Footprint of Canadian Oil Sands: The expert panel on the potential for new and emerging technologies to reduce the environmental impacts of oil sands development. Ottawa.

Couture, R.-M., Van Cappellen, P., 2011. Reassessing the role of sulfur geochemistry on arsenic speciation in reducing environments. J. Hazard. Mater. 189, 647–52. doi:10.1016/j.jhazmat.2011.02.029

Cunningham, J.A., Rahme, H., Hopkins, G.D., Lebron, C., Reinhard, M., 2001. Enhanced in situ bioremediation of BTEX-contaminated groundwater by combined injection of nitrate and sulfate. Environ. Sci. Technol. 35, 1663–1670. doi:10.1021/es001722t

Daims, H., 2014. The Family Nitrospiraceae, in: Rosenberg, E., DeLong, E.F., Lory, S., Stackebrandt, E., Thompson, F. (Eds.), The Prokaryotes: Other Major Lineages of Bacteria

and The Archaea. Springer Berlin Heidelberg, Berlin, Heidelberg, pp. 733–749. doi:10.1007/978-3-642-38954-2

Edgar, R.C., Haas, B.J., Clemente, J.C., Quince, C., Knight, R., 2011. UCHIME improves sensitivity and speed of chimera detection. Bioinformatics 27, 2194–200. doi:10.1093/bioinformatics/btr381

Edwards, E.A., Wills, L.E., Reinhard, M., Grbić-Galić, D., 1992. Anaerobic degradation of toluene and xylene by aquifer microorganisms under sulfate-reducing conditions. Appl. Environ. Microbiol. 58, 794–800.

Environment Canada, 2015. Canadian Climate Data [Online] [WWW Document]. URL http://climate.weather.gc.ca (accessed 5.20.15).

Evtushenko, L.I., Takeuchi, M., 2006. The Family Microbacteriaceae, in: The Prokaryotes: Other Major Lineages of Bacteria and The Archaea. Springer, New York, pp. 1020–1098.

Fedorak, P.M., Coy, D.L., Dudas, M.J., Simpson, M.J., Renneberg, A.J., MacKinnon, M.D., 2003. Microbially-mediated fugitive gas production from oil sands tailings and increased tailings densification rates. J. Environ. Eng. Sci. 2, 199–211.

Foesel, B.U., Rohde, M., Overmann, J., 2013. Blastocatella fastidiosa gen. nov., sp. nov., isolated from semiarid savanna soil - the first described species of Acidobacteria subdivision 4. Syst. Appl. Microbiol. 36, 82–9. doi:10.1016/j.syapm.2012.11.002

Fowler, S.J., Gutierrez-Zamora, M.-L., Manefield, M., Gieg, L.M., 2014. Identification of toluene degraders in a methanogenic enrichment culture. FEMS Microbiol. Ecol. 89, 625–36. doi:10.1111/1574-6941.12364

Government of Alberta, 2015. Tailings Management Framework for the Mineable Athabasca Oil Sands. Edmonton.

Grewer, D.M., Young, R.F., Whittal, R.M., Fedorak, P.M., 2010. Naphthenic acids and other acid-extractables in water samples from Alberta: what is being measured? Sci. Total Environ. 408, 5997–6010. doi:10.1016/j.scitotenv.2010.08.013

Hach Company, 2007. Nitrogen , Ammonia - Salicylate Method 10205, in: Hach Water Analysis Handbook. Hach Company, pp. 1–6.

Hackbarth, D.A., Nastasa, N., 1979. The Hydrogeology of the Athabasca Oil Sands Area, Alberta.

Hanson, R.S., Hanson, T.E., 1996. Methanotrophic bacteria. Microbiol. Rev. 60, 439–71.

Haveroen, M.E., MacKinnon, M.D., Fedorak, P.M., 2005. Polyacrylamide added as a nitrogen source stimulates methanogenesis in consortia from various wastewaters. Water Res. 39, 3333–41. doi:10.1016/j.watres.2005.05.042

Holowenko, F.M., MacKinnon, M.D., Fedorak, P.M., 2000. Methanogens and sulfate-reducing bacteria in oil sands fine tailings waste. Can. J. Microbiol. 46, 927–937.

Ignasiak, T.M., Kotlyar, L., Longstaffe, F.J., Strausz, O.P., Montgomery, D.S., 1983. Separation and characterization of clay from Athabasca asphaltene. Fuel 62, 353–362. doi:10.1016/0016-2361(83)90096-0

Imachi, H., Sakai, S., Sekiguchi, Y., Hanada, S., Kamagata, Y., Ohashi, A., Harada, H., 2008. Methanolinea tarda gen. nov., sp. nov., a methane-producing archaeon isolated from a

methanogenic digester sludge. Int. J. Syst. Evol. Microbiol. 58, 294–301. doi:10.1099/ijs.0.65394-0

Islam, M.S., Zhang, Y., McPhedran, K.N., Liu, Y., Gamal El-Din, M., 2015. Next-generation pyrosequencing analysis of microbial biofilm communities on granular activated carbon in treatment of oil sands process-affected water. Appl. Environ. Microbiol. 81, 4037–48. doi:10.1128/AEM.04258-14

Ivanova, E.P., Mikhailov, V. V., 2001. A new family, Alteromonadaceae fam. nov., including marine Proteobacteria of the genera Alteromonas, Pseudoalteromonas, Idiomarina, and Colwellia. Microbiology 70, 10–17. doi:10.1023/A:1004876301036

Kaminsky, H.A.W., 2008. Characterization of an Athabasca oil sand ore and process streams. University of Alberta.

Kasperski, K.L., Mikula, R.J., 2011. Waste streams of mined oil sands: characteristics and remediation. Elements 7, 387–392. doi:10.2113/gselements.7.6.387

Kavanagh, R.J., Frank, R.A., Oakes, K.D., Servos, M.R., Young, R.F., Fedorak, P.M., MacKinnon, M.D., Solomon, K.R., Dixon, D.G., Van Der Kraak, G., 2011. Fathead minnow (Pimephales promelas) reproduction is impaired in aged oil sands process-affected waters. Aquat. Toxicol. 101, 214–20. doi:10.1016/j.aquatox.2010.09.021

Kay-Shoemake, J.L., Watwood, M.E., Lentz, R.D., Sojka, R.E., 1998. Polyacrylamide as an organic nitrogen source for soil microorganisms with potential effects on inorganic soil nitrogen in agricultural soil. Soil Biol. Biochem. 30, 1045–1052. doi:10.1016/S0038-0717(97)00250-2

Kelly, D.P., Wood, A.P., 2000. Confirmation of Thiobacillus denitrificans as a species of the genus Thiobacillus, in the beta-subclass of the Proteobacteria, with strain NCIMB 9548 as the type strain. Int. J. Syst. Evol. Microbiol. 50, 547–50. doi:10.1099/00207713-50-2-547

Kersters, K., Vos, P. De, Gillis, M., Swings, J., Vandamme, P., Stackebrandt, E., 2006. Introduction to the Proteobacteria, in: Dworkin, M., Falkow, S., Rosenberg, E., Schleifer, K.-H., Stackebrandt, E. (Eds.), The Prokaryotes: A Handbook on the Biology of Bacteria. Springer New York, New York, NY, pp. 3–37. doi:10.1007/0-387-30745-1

Kielak, A., Pijl, A.S., van Veen, J.A., Kowalchuk, G.A., 2009. Phylogenetic diversity of Acidobacteria in a former agricultural soil. ISME J. 3, 378–82. doi:10.1038/ismej.2008.113

Kijjanapanich, P., Annachhatre, A.P., Lens, P.N.L., 2014. Biological sulfate reduction for treatment of gypsum contaminated soils, sediments, and solid wastes. Crit. Rev. Environ. Sci. Technol. 44, 1037–1070. doi:10.1080/10643389.2012.743270

Kuever, J., 2014. The Family Desulfobulbaceae, The Prokaryotes: Deltaproteobacteria and Epsilonproteobacteria. Springer Berlin Heidelberg, Berlin, Heidelberg. doi:10.1007/978-3-642-39044-9

Kunapuli, U., Lueders, T., Meckenstock, R.U., 2007. The use of stable isotope probing to identify key iron-reducing microorganisms involved in anaerobic benzene degradation. ISME J. 1, 643–53. doi:10.1038/ismej.2007.73

Liang, B., Wang, L.-Y., Mbadinga, S.M., Liu, J.-F., Yang, S.-Z., Gu, J.-D., Mu, B.-Z., 2015. Anaerolineaceae and Methanosaeta turned to be the dominant microorganisms in alkanes-dependent methanogenic culture after long-term of incubation. AMB Express 5, 117.

doi:10.1186/s13568-015-0117-4

Light, T.S., 1972. Standard solution for redox potential measurements. Anal. Chem. 44, 1038–1039. doi:10.1021/ac60314a021

Lindsay, S.S., Baedeker, M.J., 1988. Determination of aqueous sulfide in contaminated and natural water using the methylene blue method, in: Collins, A.G., Johnson, A.I. (Eds.), Ground-Water Contamination: Field Methods : A Symposium, Issue 963. ASTM International, Philadelphia, pp. 349–357.

Losey, N.A., Stevenson, B.S., Busse, H.-J., Sinninghe Damsté, J.S., Rijpstra, W.I.C., Rudd, S., Lawson, P.A., 2013. Thermoanaerobaculum aquaticum gen. nov., sp. nov., the first cultivated member of Acidobacteria subdivision 23, isolated from a hot spring. Int. J. Syst. Evol. Microbiol. 63, 4149–57. doi:10.1099/ijs.0.051425-0

Lovley, D.R., Giovannoni, S.J., White, D.C., Champine, J.E., Phillips, E.J.P., Gorby, Y.A., Goodwin, S., 1993. Geobacter metallireducens gen. nov. sp. nov., a microorganism capable of coupling the complete oxidation of organic compounds to the reduction of iron and other metals. Arch. Microbiol. 159, 336–344. doi:10.1007/BF00290916

Lovley, D.R., Phillips, E.J.P., 1988. Novel mode of microbial energy metabolism: organic carbon oxidation coupled to dissimilatory reduction of iron or manganese. Appl. Environ. Microbiol. 54, 1472–1480.

Lovley, D.R., Roden, E.E., Phillips, E.J.P., Woodward, J.C., 1993. Enzymatic iron and uranium reduction by sulfate-reducing bacteria. Mar. Geol. 113, 41–53. doi:10.1016/0025-3227(93)90148-O

Lovley, D.R., Woodward, J.C., 1996. Mechanisms for chelator stimulation of microbial Fe(III)-oxide reduction. Chem. Geol., Chemical And Biological Control On Mineral Growth And Dissolution Kinetics, American Chemical Society Meeting 132, 19–24. doi:10.1016/S0009-2541(96)00037-X

Madigan, M.T., Martinko, J.M., 2006. Brock Biology of Microorganisms, Eleventh. ed. Pearson Prentice Hall, Upper Saddle River, NJ.

Mitchell, J.K., Soga, K., 2005. Fundamentals of Soil Behavior, 3rd ed. John Wiley & Sons, Inc., Hoboken, NJ.

Mori, K., Harayama, S., 2011. Methanobacterium petrolearium sp. nov. and Methanobacterium ferruginis sp. nov., mesophilic methanogens isolated from salty environments. Int. J. Syst. Evol. Microbiol. 61, 138–43. doi:10.1099/ijs.0.022723-0

Nordstrom, D.K., 1977. Thermochemical redox equilibria of ZoBell's solution. Geochim. Cosmochim. Acta 41, 1835–1841. doi:10.1016/0016-7037(77)90215-0

Oiffer, A.A.L., Barker, J.F., Gervais, F.M., Mayer, K.U., Ptacek, C.J., Rudolph, D.L., 2009. A detailed field-based evaluation of naphthenic acid mobility in groundwater. J. Contam. Hydrol. 108, 89–106. doi:10.1016/j.jconhyd.2009.06.003

Oren, A., 2014. The Family Rhodocyclaceae, in: Rosenberg, E., DeLong, E.F., Lory, S., Stackebrandt, E., Thompson, F. (Eds.), The Prokaryotes: Alphaproteobacteria and Betaproteobacteria. Springer Berlin Heidelberg, Berlin, Heidelberg, pp. 975–998. doi:10.1007/978-3-642-30197-1

Park, S., Kang, S.-J., Oh, T.-K., Yoon, J.-H., 2010. Lutibacter maritimus sp. nov., isolated from a tidal flat sediment. Int. J. Syst. Evol. Microbiol. 60, 610–4. doi:10.1099/ijs.0.012401-0

Park, S.C., Choe, H.N., Hwang, Y.M., Baik, K.S., Seong, C.N., 2013. Lutibacter agarilyticus sp. nov., a marine bacterium isolated from shallow coastal seawater. Int. J. Syst. Evol. Microbiol. 63, 2678–83. doi:10.1099/ijs.0.047670-0

Parkhurst, D.L., Appelo, C.A.J., 2013. Description of Input and Examples for PHREEQC - A Computer Program for Speciation, Batch-Reaction, One-Dimensional Transport, and Inverse Geochemical Calculations, in: U.S. Geological Survey Techniques and Methods, Book 6. USGS, p. 497.

Penn, C.J., Whitaker, A.H., Warren, J.G., 2014. Surface Application of Oil-Base Drilling Mud Mixed with Gypsum, Limestone, and Caliche. Agron. J. 106, 1859. doi:10.2134/agronj14.0184

Pérez-Pantoja, D., Donoso, R., Agulló, L., Córdova, M., Seeger, M., Pieper, D.H., González, B., 2012. Genomic analysis of the potential for aromatic compounds biodegradation in Burkholderiales. Environ. Microbiol. 14, 1091–117. doi:10.1111/j.1462-2920.2011.02613.x

Pouliot, R., Rochefort, L., Graf, M.D., 2012. Impacts of oil sands process water on fen plants: implications for plant selection in required reclamation projects. Environ. Pollut. 167, 132–7. doi:10.1016/j.envpol.2012.03.050

Pruesse, E., Quast, C., Knittel, K., Fuchs, B.M., Ludwig, W., Peplies, J., Glöckner, F.O., 2007. SILVA: a comprehensive online resource for quality checked and aligned ribosomal RNA sequence data compatible with ARB. Nucleic Acids Res. 35, 7188–96. doi:10.1093/nar/gkm864

Purdy, B.G., Ellen Macdonald, S., Lieffers, V.J., 2005. Naturally saline boreal communities as models for reclamation of saline oil sand tailings. Restor. Ecol. 13, 667–677. doi:10.1111/j.1526-100X.2005.00085.x

Ramos-Padrón, E., Bordenave, S., Lin, S., Bhaskar, I.M., Dong, X., Sensen, C.W., Fournier, J., Voordouw, G., Gieg, L.M., 2011. Carbon and sulfur cycling by microbial communities in a gypsum-treated oil sands tailings pond. Environ. Sci. Technol. 45, 439–46. doi:10.1021/es1028487

Ravel, B., Newville, M., 2005. ATHENA, ARTEMIS, HEPHAESTUS: data analysis for X-ray absorption spectroscopy using IFEFFIT. J. Synchrotron Radiat. 12, 537–41. doi:10.1107/S0909049505012719

Rickard, D., 2012. Sulfidic Sediments and Sedimentary Rocks, Developments in Sedimentology. Elsevier, Amsterdam.

Röling, W.F.M., 2014. The Family Geobaccteraceae, The Prokaryotes: Deltaproteobacteria and Epsilonproteobacteria. Springer Berlin Heidelberg, Berlin, Heidelberg. doi:10.1007/978-3-642-39044-9

Rothermich, M.M., Hayes, L.A., Lovley, D.R., 2002. Anaerobic, sulfate-dependent degradation of polycyclic aromatic hydrocarbons in petroleum-contaminated harbor sediment. Environ. Sci. Technol. 36, 4811–4817. doi:10.1021/es0200241

Saito, Y., Aoki, M., Hatamoto, M., Yamaguchi, T., Takai, K., Imachi, H., 2015. Presence of a novel methanogenic archaeal lineage in anaerobic digesters inferred from mcrA and 16S

rRNA gene phylogenetic analyses. J. Water Environ. Technol. 13, 279–289. doi:10.2965/jwet.2015.279

Salloum, M.J., Dudas, M.J., Fedorak, P.M., 2002. Microbial reduction of amended sulfate in anaerobic mature fine tailings from oil sand. Waste Manag. Res. 20, 162–171. doi:10.1177/0734242X0202000208

Schlesinger, W.H., Bernhardt, E.S., 2013. Biogeochemistry: An analysis of global change. Academic Press, Oxford.

Schloss, P.D., Westcott, S.L., Ryabin, T., Hall, J.R., Hartmann, M., Hollister, E.B., Lesniewski, R.A., Oakley, B.B., Parks, D.H., Robinson, C.J., Sahl, J.W., Stres, B., Thallinger, G.G., Van Horn, D.J., Weber, C.F., 2009. Introducing mothur: open-source, platform-independent, community-supported software for describing and comparing microbial communities. Appl. Environ. Microbiol. 75, 7537–41. doi:10.1128/AEM.01541-09

Scott, A.C., Young, R.F., Fedorak, P.M., 2008. Comparison of GC-MS and FTIR methods for quantifying naphthenic acids in water samples. Chemosphere 73, 1258–64. doi:10.1016/j.chemosphere.2008.07.024

Semple, K.M., Westlake, D.W.S., 1987. Characterization of iron-reducing Alteromonas putrefaciens strains from oil field fluids. Can. J. Microbiol. 33, 366–371. doi:10.1139/m87-064

Siddique, T., Fedorak, P.M., Foght, J.M., 2006. Biodegradation of short-chain n-alkanes in oil sands tailings under methanogenic conditions. Environ. Sci. Technol. 40, 5459–5464. doi:10.1021/es060993m

Siddique, T., Fedorak, P.M., MacKinnon, M.D., Foght, J.M., 2007. Metabolism of BTEX and naphtha compounds to methane in oil sands tailings. Environ. Sci. Technol. 41, 2350–2356. doi:10.1021/es062852q

Siddique, T., Gupta, R., Fedorak, P.M., MacKinnon, M.D., Foght, J.M., 2008. A first approximation kinetic model to predict methane generation from an oil sands tailings settling basin. Chemosphere 72, 1573–80. doi:10.1016/j.chemosphere.2008.04.036

Siddique, T., Kuznetsov, P., Kuznetsova, A., Arkell, N., Young, R., Li, C., Guigard, S., Underwood, E., Foght, J.M., 2014a. Microbially-accelerated consolidation of oil sands tailings. Pathway I: changes in porewater chemistry. Front. Microbiol. 5, 11. doi:10.3389/fmicb.2014.00106

Siddique, T., Kuznetsov, P., Kuznetsova, A., Li, C., Young, R., Arocena, J.M., Foght, J.M., 2014b. Microbially-accelerated consolidation of oil sands tailings. Pathway II: solid phase biogeochemistry. Front. Microbiol. 5, 15. doi:10.3389/fmicb.2014.00107

Siddique, T., Penner, T., Klassen, J., Nesbø, C., Foght, J.M., 2012. Microbial communities involved in methane production from hydrocarbons in oil sands tailings. Environ. Sci. Technol. 46, 9802–10. doi:10.1021/es302202c

Siddique, T., Penner, T., Semple, K., Foght, J.M., 2011. Anaerobic biodegradation of longer-chain n-alkanes coupled to methane production in oil sands tailings. Environ. Sci. Technol. 45, 5892–9. doi:10.1021/es200649t

Singleton, D.R., Sangaiah, R., Gold, A., Ball, L.M., Aitken, M.D., 2006. Identification and quantification of uncultivated Proteobacteria associated with pyrene degradation in a

bioreactor treating PAH-contaminated soil. Environ. Microbiol. 8, 1736–45. doi:10.1111/j.1462-2920.2006.01112.x

Smith, K.S., Ingram-Smith, C., 2007. Methanosaeta, the forgotten methanogen? Trends Microbiol. 15, 150–5. doi:10.1016/j.tim.2007.02.002

Smith, R.G., Ng, S., 1993. Towards a model for the prediction of fine tails volume, in: Oil Sands: Our Petroleum Future. Edmonton, p. 33.

Smith, W., Solow, A.R., Preston, P.E., 1996. An Estimator of Species Overlap Using a Modified Beta-Binomial Model. Biometrics 52, 1472. doi:10.2307/2532861

Sorokin, D.Y., Tourova, T.P., Mussmann, M., Muyzer, G., 2008. Dethiobacter alkaliphilus gen. nov. sp. nov., and Desulfurivibrio alkaliphilus gen. nov. sp. nov.: two novel representatives of reductive sulfur cycle from soda lakes. Extremophiles 12, 431–9. doi:10.1007/s00792-008-0148-8

Starr, R.C., Ingleton, R.A., 1992. A new method for collecting core samples without a drilling rig. Ground Water Monit. Remediat. 12, 91–95. doi:10.1111/j.1745-6592.1992.tb00413.x

Stasik, S., Loick, N., Knöller, K., Weisener, C., Wendt-Potthoff, K., 2014. Understanding biogeochemical gradients of sulfur, iron and carbon in an oil sands tailings pond. Chem. Geol. 382, 44–53. doi:10.1016/j.chemgeo.2014.05.026

Stasik, S., Wendt-Potthoff, K., 2014. Interaction of microbial sulphate reduction and methanogenesis in oil sands tailings ponds. Chemosphere 103, 59–66. doi:10.1016/j.chemosphere.2013.11.025

Stucki, J.W., 2006. Properties and Behavior of Iron in Clay Minerals, in: Bergaya, F.., Theng, B.K.G.., Lagaly, G.. (Eds.), Handbook of Clay Science, Developments in Clay Science. Elsevier, Amsterdam, pp. 423–475. doi:10.1016/S1572-4352(05)01013-5

Stumm, W., Morgan, J.J., 1996. Aquatic Chemistry: Chemical equilibria and rates in natural waters, 3rd ed. John Wiley & Sons, Inc., New York.

Toby, B.H., Von Dreele, R.B., 2013. GSAS-II : the genesis of a modern open-source all purpose crystallography software package. J. Appl. Crystallogr. 46, 544–549. doi:10.1107/S0021889813003531

Vangnai, S., Klein, D.A., 1974. A study of nitrite-dependent dissimilatory micro-organisms isolated from oregon soils. Soil Biol. Biochem. 6, 335–339. doi:10.1016/0038-0717(74)90040-6

Widdel, F., 1988. Microbiology and ecology of sulfate- and sulfur-reducing bacteria, in: Zehnder, A.J.B. (Ed.), Biology of Anaerobic Microorganisms, Ecological and Applied Microbiology. John Wiley & Sons, Inc., New York, pp. 469–585.

Willems, A., 2014. The Family Comamonadaceae, in: Rosenberg, E., DeLong, E.F., Lory, S., Stackebrandt, E., Thompson, F. (Eds.), The Prokaryotes - Alphaproteobacteria and Betaproteobacteria. Springer Berlin Heidelberg, Berlin, Heidelberg, pp. 777–851. doi:10.1007/978-3-642-30197-1

Yergeau, E., Lawrence, J.R., Sanschagrin, S., Waiser, M.J., Korber, D.R., Greer, C.W., 2012. Next-generation sequencing of microbial communities in the Athabasca River and its tributaries in relation to oil sands mining activities. Appl. Environ. Microbiol. 78, 7626–37.

doi:10.1128/AEM.02036-12

Yue, J.C., Clayton, M.K., 2005. A similarity measure based on species proportions. Commun. Stat. - Theory Methods 34, 2123–2131. doi:10.1080/STA-200066418

Zehnder, A.J.B., Stumm, W., 1988. Geochemistry and biogeochemistry of anaerobic habitats, in: Zehnder, A.J.B. (Ed.), Biology of Anaerobic Microorganisms, Ecological and Applied Microbiology. John Wiley & Sons, Inc., New York, pp. 1–38.

Zeng, T., Arnold, W.A., Toner, B.M., 2013. Microscale characterization of sulfur speciation in lake sediments. Environ. Sci. Technol. 47, 1287–96. doi:10.1021/es303914q

Zubot, W., MacKinnon, M.D., Chelme-Ayala, P., Smith, D.W., Gamal El-Din, M., 2012. Petroleum coke adsorption as a water management option for oil sands process-affected water. Sci. Total Environ. 427-428, 364–72. doi:10.1016/j.scitotenv.2012.04.024

APPENDIX A: SCALING FACTORS, PRESELECTED SAMPLING LOCATIONS, AND ACTUAL SAMPLING LOCATIONS

Table A-1) Depth of sampling for each borehole, recovery per push, and scaling factors for EV-1

Sampling Location		EV-1-1	EV-1-2.5	EV-1-2	EV-1-3	EV-1-4	EV-1-5
Depth of sample	1	60		60	60	60	60
	2	120	120	120	120	120	120
	3	150	130	140	140	170	180
Pushed length	1	60		60	60	60	60
	2	60	60	60	60	60	60
	3	30	10	20	20	50	60
Recovery	1	bagged		bagged	bagged	bagged	bagged
	2	57	15	55	60	56	66
	3	32	10	18	19	47	61
Scale Factor	1	n/a		n/a	n/a	n/a	n/a
	2	0.95	0.25	0.92	1.00	0.93	1.10
	3	1.07	1.00	0.90	0.95	0.94	1.02

Table A-2) Depth of sampling for each borehole, recovery per push, and scaling factors for EV-2

Sampling Location		EV-2-1A	EV-2-1B	EV-2-2A	EV-2-2B	EV-2-3A	EV-2-3B	EV-2-4A
Depth of sample	1	60	60	60	60	60	60	60
	2	90	88	90	92	86	84	120
	3							180
Pushed length	1	60	60	60	60	60	60	60
	2	30	28	30	32	26	24	60
	3							60
Recovery	1	37	30	37	37	37	37	42
	2	34	15	33	30	26	29	42
	3							41
Scale Factor	1	0.62	0.50	0.62	0.62	0.62	0.62	0.70
	2	1.13	0.54	1.10	0.94	1.00	1.21	0.70
	3							0.68

Table A-3) Depth of sampling for each borehole, recovery per push, and scaling factors for GD

Sampling Location		GD-1A	GD-1B	GD-2A	GD-2B	GD-3A	GD-3B
Depth of sample	1	60	60	60	60	60	60
	2	113	113	104	103	95	100
Pushed length	1	60	60	60	60	60	60
	2	53	53	44	43	35	40
Recovery	1	47	23	41	40	42	36
	2	50	52	44	43	32	33
Scale Factor	1	0.78	0.38	0.68	0.67	0.70	0.60
	2	0.94	0.98	1.00	1.00	0.91	0.83

Table A-4) Depth of sampling for each borehole, recovery per push, and scaling factors for TD

Sampling Location		TD-1A	TD-1B	TD-2A	TD-2B	TD-2C	TD-3A	TD-3B	TD-4A	TD-4B
Depth of sample	1	60	60	60	60	60	60	60	60	75
	2	120	120		85	90	105	90	72	
Pushed length	1	60	60	60	60	60	60	60	60	75
	2	60	60		25	30	45	30	12	
Recovery	1	27	22	35	30	37	33	43	42	45
	2	53	50		24	29	23	30	12	
Scale Factor	1	0.45	0.37	0.58	0.50	0.62	0.55	0.72	0.70	0.60
	2	0.88	0.83		0.96	0.97	0.51	1.00	1.00	

Table A-5) Preselected locations for analyses for EV-1. GE means pH, Eh, EC, alkalinity, NH_3, H_2S, total NA, ICP-OES, ICP-MS, and IC. DNA means DNA extraction location. HC means hydrocarbon analysis. Gas means sample collected for measuring CO_2 and CH_4 on GC.

	Borehole	EV-1-1	EV-1-2.5	EV-1-2	EV-1-3	EV-1-4	EV-1-5
	Depth 1	60	60	60	60	60	60
	2	120	120	120	120	120	120
True Depth	3	150	130	140	140	170	180
0							
10		DNA, GE		DNA, GE	DNA, GE	DNA, GE	-
20		DNA, GE		DNA, GE	DNA, GE	DNA, GE	-
30		-					-
40		DNA, GE		DNA, GE	DNA, GE	DNA, GE	-
50		-					-
60		DNA, GE		DNA, GE	DNA, GE	DNA, GE	-
70		-					-
80		-					-
90		DNA, GE		DNA, GE	DNA, GE	DNA, GE	-
100		-					-
110		-					-
120		DNA, GE		DNA, GE	DNA, GE	DNA, GE	-
130		-					-
140		-		DNA, GE	DNA, GE		-
150		DNA, GE				DNA, GE	-
160							-
170						DNA, GE	-
180							-

Table A-6) Preselected locations for analyses for EV-2. GE means pH, Eh, EC, alkalinity, NH_3, H_2S, total NA, ICP-OES, ICP-MS, and IC. DNA means DNA extraction location. HC means hydrocarbon analysis. Gas means sample collected for measuring CO_2 and CH_4 on GC.

	Borehole	EV-2-1A	EV-2-1B	EV-2-2A	EV-2-2B	EV-2-3A	EV-2-3B	EV-2-4A
	Depth 1	60	60	60	60	60	60	60
True	2	90	88	90	92	86	84	120
Depth	3							180
0								
10		HC, Gas	DNA, GE	Gas	DNA, GE		DNA, GE	DNA, GE
20		HC, Gas	DNA, GE	Gas	DNA, GE	Gas	DNA, GE	DNA, GE
30		Gas	DNA, GE		DNA, GE	HC	DNA, GE	
40		Gas	DNA, GE	HC, Gas	DNA, GE	Gas	DNA, GE	DNA, GE
50		HC						
60		HC, Gas	DNA, GE	Gas	DNA, GE	Gas	DNA, GE	DNA, GE
70		Gas	DNA, GE			HC, Gas	DNA, GE	
80				HC, Gas	DNA, GE			
90		HC, Gas	DNA, GE	Gas		HC, Gas	DNA, GE	DNA, GE
100			**		DNA, GE	**	**	
110					**			
120								DNA, GE
130								
140								
150								DNA, GE
160								
170								
180								DNA, GE

Table A-7) Preselected locations for analyses for GD GE means pH, Eh, EC, alkalinity, NH_3, H_2S, total NA, ICP-OES, ICP-MS, and IC. DNA means DNA extraction location. HC means hydrocarbon analysis. Gas means sample collected for measuring CO_2 and CH_4 on GC.

	Borehole	GD-1A	GD-1B	GD-2A	GD-2B	GD-3A	GD-3B
True Depth	Depth 1	60	60	60	60	60	60
	2	113	113	104	103	95	100
10		HC, Gas	DNA, GE		DNA, GE		DNA, GE
20		Gas	DNA, GE	HC, Gas	DNA, GE	Gas	DNA, GE
30						HC	
40		HC, Gas	DNA, GE	Gas	DNA, GE	Gas	DNA, GE
50							
60		Gas	DNA, GE	HC, Gas	DNA, GE	Gas	DNA, GE
70						HC	
80		HC, Gas	DNA, GE	Gas	DNA, GE	Gas	DNA, GE
90				Gas	DNA, GE		
100		Gas	DNA, GE			HC, Gas	DNA, GE
110				Gas	DNA, GE	**	
120		HC, Gas	DNA, GE	**	**		

Table A-8) Preselected locations for analyses for TD. GE means pH, Eh, EC, alkalinity, NH_3, H_2S, total NA, ICP-OES, ICP-MS, and IC. DNA means DNA extraction location. HC means hydrocarbon analysis. Gas means sample collected for measuring CO_2 and CH_4 on GC.

	Borehole	TD-1A	TD-1B	TD-2A	TD-2B	TD-2C	TD-3A	TD-3B	TD-4A	TD-4B
True Depth	Depth 1	60	60		60	60	60	60	60	75
	2	120	120		85	90	105	90	72	
10		HC, Gas	DNA, GE			DNA, GE		DNA, GE		
20		Gas	DNA, GE		HC, Gas	DNA, GE	Gas	DNA, GE	Gas	DNA, GE
30							HC			
40		HC, Gas	DNA, GE		Gas	DNA, GE	Gas	DNA, GE	Gas	DNA, GE
50										
60		Gas	DNA, GE		HC, Gas	DNA, GE	Gas	DNA, GE	Gas	DNA, GE
70							HC, Gas	DNA, GE		
80		HC, Gas	DNA, GE		Gas	DNA, GE			-	-
90					HC	DNA, GE	Gas	DNA, GE	**	**
100		Gas	DNA, GE		**					
110							-			
120		HC, Gas	DNA, GE				**			

Table A-9) Actual analytical locations for EV-1

	HC	Gas	pH	Eh	EC	Alk	HS-	NH3	IC	ICP-OES	ICP-MS	NA	DNA E	qPCR	sequencing	PXRD	XANES	Whole Rock
Depth									EV-1-1									
10			Y	Y	Y	Y	Y	Y	Y	Y	x2	Y						
20																		
30			Y	Y	Y	Y	Y	Y	Y	Y	Y	Y				Y	Y	
40																		
50			Y	Y	Y	Y	Y	Y	Y	Y	Y	Y						
60																		
70																		
80																		
90			Y	Y	Y	Y	Y	Y	Y	Y	Y	Y	Y		Y		Y	
100																		
110																		
120			Y	Y	Y	Y	Y	Y	Y	Y	Y	Y	Y		Y		Y	Y
Depth									EV-1-2									
10			Y	Y	Y	Y	Y	Y	Y	Y	Y	Y						x2
20																		
30			Y	Y	Y	Y	Y	Y	Y	Y	Y	Y						
40																		
50			Y	Y	Y	Y	Y	Y	Y	Y	Y	Y						
60																		Y
70																		
80																		Y
90			Y	Y	Y	Y	Y	Y	Y	Y	Y	Y						
100																		
110																		
120			Y	Y	Y	Y	Y	Y	Y	Y	Y	Y	Y					
Depth									EV-1-3									
10			Y	Y	Y	Y	Y	Y	Y	Y	Y	Y						
20																		
30			Y	Y	Y	Y	Y	Y	Y	Y	x2	Y						
40																		
50			Y	Y	Y	Y	Y	Y	Y	Y	Y	Y						
60													Y		Y			
70																		Y
80																		
90			Y	Y	Y	Y	Y	Y	Y	Y	Y	Y	Y		Y			
100																		
110																		
120			Y	Y	Y	Y	Y	Y	Y	Y	Y	Y						

Table A-9) continued: Actual analytical locations for EV-1

	HC	Gas	pH	Eh	EC	Alk	HS-	NH3	IC	ICP-OES	ICP-MS	NA	DNA E	qPCR	sequencing	PXRD	XANES	Whole Rock
Depth									EV-1-4									
10			Y	Y	Y	Y	Y	Y	x2	Y	Y	Y						Y
20																		
30			Y	Y	Y	Y	Y	Y	Y	Y	x2	Y						
40																		
50			Y	Y	Y	Y	Y	Y	Y	Y	Y	Y						
60																		
70																		
80																		
90			Y	Y	Y	Y	Y	Y	x2	Y	Y	Y						
100																		
110																		
120			Y	Y	Y	Y	Y	Y	Y	Y	Y	Y	Y		Y			
130																		
140																		
150			Y	Y	Y	Y	Y	Y	Y	Y	Y	Y	Y		Y			

Table A-10) Actual analytical locations for EV-2

	HC	Gas	pH	Eh	EC	Alk	HS-	NH3	IC	ICP-OES	ICP-MS	NA	DNA E	qPCR	sequencing	PXRD	XANES	Whole Rock
Depth									EV-2-1									
10			Y	Y	Y	Y	Y	Y	x2	x2	Y	Y	Y					
20		Y																
30	Y	Y																
40		Y																
50	Y																	
60	Y	Y	Y	Y	Y	Y	Y	Y	Y	Y	Y	Y	Y					
70		x2																
80																		
90	Y	Y	Y	Y	Y	Y		Y	Y		Y		Y					
Depth									EV-2-2									
10		Y	Y	Y	Y	Y	Y	Y	x2	x2	Y	Y	Y		Y			
20	Y	Y																
30			Y	Y	Y	Y	Y	Y	Y	Y	Y	Y	Y		Y			
40	Y	Y																
50																		
60		Y	Y	Y	Y	Y	Y	Y	Y	Y	Y	Y	Y		Y			
70			Y	Y	Y	Y	Y	Y	Y	Y	Y	Y	Y					
80	Y	Y																
90		x2	Y	Y	Y	Y	Y	Y	Y	Y	Y	Y						
Depth									EV-2-3									
10			Y	Y	Y	Y	Y	Y	x2	x2	Y	Y	Y			x2		
20		Y																
30			Y	Y	Y	Y	Y	Y	Y	Y	Y	Y	Y			Y		
40	x2																	
50		Y																
60		x2	Y	Y	Y	Y	Y	Y	Y	Y	Y	Y	Y			Y		
70		Y	Y	Y	Y	Y	Y	Y	Y	Y	x2	Y						
80	Y																	
90		Y	Y	Y	Y	Y	Y	Y	x2	Y	Y	Y						
Depth									EV-2-4									
10			Y	Y	Y	Y	Y	Y	x2	x2	Y	Y	Y		Y	x2	Y	x2
20																		
30			Y	Y	Y	Y	Y	Y	Y	Y	Y	Y	Y		Y	Y		Y
40																		
50																		
60			Y	Y	Y	Y	Y	Y	Y	Y	Y	Y	Y		Y	Y		Y
70																		
80																		
90			Y	Y	Y	Y	Y	Y	Y	Y	x2	Y	Y		Y	Y	Y	x2
100																		
110																		
120			Y	Y	Y	Y	Y	Y	Y	Y	Y	Y	Y		Y	Y		Y
130																		
140																		
150			Y	Y	Y	Y	Y	Y	Y	Y	Y	Y	Y		Y	Y		Y
160																		
170																		
180			Y	Y	Y	Y	Y	Y	Y	x2	Y	Y	Y		Y	Y	Y	Y

Table A-11) Actual analytical locations for GD

Depth	HC	Gas	pH	Eh	EC	Alk	HS-	NH3	IC	ICP-OES	ICP-MS	NA	DNA E	qPCR	sequencing	PXRD	XANES	Whole Rock
									GD-1									
10		Y																
20	Y	Y																
30																		
40		Y							Y	Y			Y		Y			Y
50	Y																	
60		x2	Y	Y	Y	Y	Y	Y	Y	Y	Y	Y	Y					
70																		
80	Y	Y	Y	Y	Y	Y		Y	Y	Y	Y							
90																		
100		Y	Y	Y	Y	Y	Y	Y	Y	Y	Y	Y	Y		Y			
110		Y																
120	Y																	
									GD-2									
10			Y	Y	Y	Y	Y	Y	x2	x2	Y	Y	Y		Y		Y	x3
20	Y	Y																
30																		
40		Y																
50																		
60	Y	Y	Y	Y	Y	Y	Y	Y	Y	Y	Y	Y	Y		Y	Y	Y	Y
70			Y	Y	Y	Y	Y	Y	Y	Y	Y	Y	Y					
80		Y																
90		x2																
100			Y	Y	Y	Y	Y	Y	x2	Y	Y	Y	Y		Y		Y	x2
110		Y																
									GD-3									
10			Y	Y	Y	Y	Y	Y	x2	x2	Y	Y	Y		Y			
20		Y																
30	Y																	
40		Y																
50																		
60		Y																
70	Y		Y	Y	Y	Y	Y	Y	Y				Y		Y			Y
80																		
90																		
100	x2	Y																

Table A-12) Actual analytical locations for TD

	HC	Gas	pH	Eh	EC	Alk	HS-	NH3	IC	ICP-OES	ICP-MS	NA	DNA E	qPCR	sequencing	PXRD	XANES	Whole Rock
Depth									TD-1									
10			Y	Y	Y	Y	Y	Y	x2	x2	Y	Y	Y		Y			
20	Y																	
30		x2																
40																		
50	Y																	
60		x2																
70			Y	Y	Y	Y	Y	Y	Y	Y	Y	Y	Y		Y			
80	x2	Y																
90			Y	Y	Y	Y	Y	Y	x2	x2	x2	Y	Y		Y			
100		Y																
110																		
120	Y	Y	Y	Y	Y	Y	Y	Y	Y	Y	Y	Y	Y		Y			Y
Depth									TD-2									
10		Y	Y	Y	Y	Y	Y	Y	x2	x2	Y	Y					Y	x2
20	Y																	
30		Y																
40		Y																
50																		
60	Y		Y	Y	Y	Y	Y	Y	Y				Y		Y	Y	Y	Y
70		X2	Y	Y	Y	Y	Y	Y	Y	Y	Y	Y						
80			Y	Y	Y	Y		Y					Y				Y	Y
90	Y																	
Depth									TD-3									
10			Y	Y	Y	Y	Y	Y	x2	x2	Y	Y	Y					
20		Y																
30	Y																	
40		Y																
50																		
60		Y							Y	Y	Y							
70		Y	Y	Y	Y	Y	Y	Y			Y		Y					Y
80	Y																	
90		Y																
Depth									TD-4									
10			Y	Y	Y	Y	Y	Y	x2	x2	Y	Y	Y		Y			Y
20		x2																
30																		
40		Y																
50																		
60		Y																
70			Y	Y	Y	Y	Y	Y	Y				Y		Y			

APPENDIX B: RAW LAB RESULTS

Table B-1) Summary of pore-water data from EV-1, EV-2, GD, and TD

Deposit ID	Core ID	Depth (cm)	Sample Date	Temp (°C)	pH	Eh (mV)	EC (mS cm^{-1})	Alk. (mg L^{-1})	H_2S (µg L^{-1})	NH_3-N (mg L^{-1})
EV-1	1	90	2-Sep-14	21.9	8.13	75	4.07	820	78.9	4.1
EV-1	1	120	2-Sep-14	21.9	7.76	109	5.70	810	28.5	7.2
EV-1	1	20-40	8-Sep-14	22.3	8.61	329	4.43	450	100.9	6.1
EV-1	1	40-60	8-Sep-14	22.2	8.67	258	4.33	570	521.8	8.0
EV-1	1	0-20	8-Sep-14	22.1	8.15	318	6.97	500	52.6	BDL
EV-1	2	90	11-Sep-14	22.3	7.94	104	6.22	500	17.5	9.0
EV-1	2	120	11-Sep-14	22.1	7.79	75	8.37	670	29.6	9.0
EV-1	2	20-40	16-Sep-14	22.6	7.89	184	7.94	150	11.0	17.4
EV-1	2	40-60	19-Sep-14	22.1	7.96	158	7.20	170	13.2	16.4
EV-1	2	0-20	19-Sep-14	22.1	7.83	184	10.40	130	5.5	4.7
EV-1	3	40-60	20-Sep-14	22.5	8.27	286	5.22	290	37.3	10.4
EV-1	3	20-40	20-Sep-14	22.4	7.94	232	6.59	240	24.1	9.6
EV-1	3	0-20	20-Sep-14	22.4	7.91	223	9.73	210	9.9	2.0
EV-1	4	20-40	25-Sep-14	22.2	8.18	256	6.44	170	26.3	14.3
EV-1	4	40-60	25-Sep-14	22.3	8.07	250	6.89	180	31.8	15.6
EV-1	4	0-20	25-Sep-14	22.3	7.82	272	10.90	200	8.8	3.1
EV-1	3	120	29-Sep-14	22.5	8.09	341	6.24	700	60.3	8.6
EV-1	3	90	29-Sep-14	22.5	8.05	195	7.59	310	16.4	8.9
EV-1	4	120	30-Sep-14	22.1	7.76	114	6.16	450	23.0	12.5
EV-1	4	90	30-Sep-14	22.1	7.79	81	6.22	440	28.5	10.4
EV-1	4	150	2-Oct-14	22.4	7.86	153	5.96	540	29.6	12.4
EV-2	1	85	6-Oct-14	22.2	8.34	391	7.48	530		8.0
EV-2	2	70	8-Oct-14	22.9	7.83	145	7.81	290	9.9	15.5
EV-2	2	90	8-Oct-14	22.6	7.82	82	7.02	360	21.9	13.7
EV-2	1	60	9-Oct-14	22.7	7.87	194	10.00	448	24.1	12.1
EV-2	1	10	9-Oct-14	22.9	7.74	288	9.44	290	9.9	3.4
EV-2	3	70	14-Oct-14	22.7	7.82	368	7.62	360	12.1	10.8
EV-2	3	90	14-Oct-14	23.1	7.79	309	7.63	380	9.9	13.3
EV-2	2	60	15-Oct-14	23.2	7.61	89	7.51	370	15.3	14.5
EV-2	2	10	15-Oct-14	22.9	7.52	234	11.15	270	4.4	10.1
EV-2	2	30	15-Oct-14	22.5	7.74	85	8.36	230	16.4	15.9

Table B-1) Continued

Deposit ID	Core ID	Depth (cm)	Sample Date	Temp (°C)	pH	Eh (mV)	EC (mS cm^{-1})	Alk. (mg L^{-1})	H_2S (µg L^{-1})	NH_3-N (mg L^{-1})
EV-2	3	60	16-Oct-14	22.9	7.74	165	6.70	410	21.9	13.7
EV-2	3	10	16-Oct-14	23.0	7.74	266	13.53	370	9.9	11.1
EV-2	3	30	16-Oct-14	22.3	7.80	194	6.79	370	17.5	13.0
EV-2	4	150	17-Oct-14	22.9	7.47	163	7.45	400	8.8	15.0
EV-2	4	180	17-Oct-14	22.7	7.52	192	7.48	560	7.7	14.8
EV-2	4	60	20-Oct-14	23.3	7.60	138	7.25	340	13.2	14.4
EV-2	4	10	20-Oct-14	23.8	7.50	182	12.78	400	2.2	11.9
EV-2	4	30	20-Oct-14	24.3	7.46	109	8.22	320	11.0	16.4
EV-2	4	90	22-Oct-14	22.5	7.45	169	7.45	390	7.7	14.3
EV-2	4	120	22-Oct-14	22.5	7.52	115	7.31	410	12.1	15.0
TD	1	10	24-Oct-14	22.8	7.77	281	4.58	460	2.2	1.2
TD	2	60	27-Oct-14	23.0	8.17	234	3.07	880	25.2	10.7
TD	2	10	27-Oct-14	22.7	7.57	164	4.46	450	3.3	2.3
TD	2	70	28-Oct-14	22.4	8.14	236	2.96	870	20.8	10.0
TD	2	80	28-Oct-14	22.3	8.08	379	3.03	854		9.3
TD	3	70	29-Oct-14	22.2	8.33	328	3.59	750	9.9	11.9
TD	1	70	30-Oct-14	22.1	8.20	291	2.90	900	28.5	11.1
TD	1	120	30-Oct-14	22.3	7.89	269	3.21	1000	12.1	5.6
TD	1	90	30-Oct-14	22.7	8.15	345	3.01	940	40.6	9.7
TD	3	10	3-Nov-14	22.8	7.68	350	3.80	390	5.5	1.9
TD	4	10	4-Nov-14	22.8	7.81	218	4.36	710	15.3	3.8
TD	4	65	5-Nov-14	22.6	7.94	271	3.82		12.1	12.3
GD	1	60	5-Nov-14	22.2	7.57	223	2.72	340	2.2	8.1
GD	1	100	6-Nov-14	22.7	8.12	336	3.13	640	11.0	10.6
GD	1	80	6-Nov-14	22.4	7.89	308	3.05	520		14.2
GD	2	10	7-Nov-14	22.8	7.71	300	1.32	340	4.4	2.4
GD	2	60	8-Nov-14	22.8	7.78	340	2.67	440	8.8	11.7
GD	2	70	10-Nov-14	22.8	7.87	384	2.88	630	8.8	13.1
GD	2	100	10-Nov-14	22.5	8.17	346	2.85	750	16.4	14.7
GD	3	10	11-Nov-14	22.4	7.84	345	1.51	230	7.7	BDL
GD	3	70	12-Nov-14	22.5	7.97	370	2.87	340	9.9	10.4

Table B-2) CCME 2001 Hydrocarbons for EV-2, GD, TD (values in mg kg^{-1} unless otherwise noted)

Deposit ID	Core ID	Depth (cm)	Benzene	Toluene	Ethylbenzene	Total Xylenes	F1 C6-C10	F1-BTEX
EV-2	1	0-30	<0.005	<0.02	<0.010	<0.03	40	40
EV-2	1	30-45	<0.005	<0.02	<0.010	<0.03	16	16
EV-2	1	45-60	<0.005	0.03	<0.010	<0.03	33	33
EV-2	1	80-90	<0.005	0.14	<0.010	<0.03	30	30
EV-2	2	0-25	<0.005	0.03	<0.010	<0.03	23	23
EV-2	2	30-40	<0.005	1.39	<0.010	<0.03	32	31
EV-2	2	70-80	0.007	0.17	<0.010	<0.03	57	57
EV-2	3	20-40	0.006	0.33	<0.010	<0.03	37	37
EV-2	3	20-40	0.005	1.14	<0.010	<0.03	55	54
EV-2	3	60-70	<0.005	0.02	<0.010	<0.03	<10	<10
GD	1	0-20	<0.005	1.91	<0.010	<0.03	<10	<10
GD	1	35-45	<0.005	1.02	<0.010	<0.04	13	12
GD	1	70-80	0.01	1.42	0.013	0.25	172	170
GD	1	110-113	<0.005	0.03	<0.010	<0.03	<10	<10
GD	2	10-20	<0.005	<0.02	0.053	0.2	161	161
GD	2	40-60	<0.005	0.2	0.014	0.09	94	94
GD	3	20-30	<0.005	3.63	<0.010	0.05	18	14
GD	3	60-70	0.013	2.1	0.078	0.38	148	175
GD	3	75-95	<0.005	1.9	<0.010	<0.03	<10	<10
GD	3	75-95	<0.005	2.27	<0.010	<0.03	<10	<10
TD	1	0-20	<0.05	20.5	0.016	0.09	76	55
TD	1	25-50	0.022	0.02	0.131	0.39	218	217
TD	1	70-80	0.111	0.18	<0.010	1.5	575	573
TD	1	70-80	0.076	2.58	0.048	1.19	381	377
TD	1	110-120	0.226	5.66	<0.010	1.96	520	512
TD	2	10-20	<0.005	0.22	0.01	0.08	<10	<10
TD	2	45-60	0.123	4.12	0.103	2.33	303	296
TD	2	75-85	0.098	0.12	0.145	1.34	315	313
TD	3	20-30	<0.005	1.18	<0.010	0.06	18	17
TD	3	60-80	0.032	0.04	0.061	1.01	328	327

Table B-2) Continued

Deposit ID	Core ID	Depth (cm)	F2 C10-C16	F3 C16-C34	F4 C35-C50	F4 HTGC C34-C50+	% C50+	Soil Mois. (%w/w)
EV-2	1	0-30	3310	18400	8080	15200	19.2	24.6
EV-2	1	30-45	3530	18600	8180	15600	19.7	28.5
EV-2	1	45-60	3650	20800	9020	19200	23.4	29.3
EV-2	1	80-90	2890	14800	6480	12300	19.4	33.8
EV-2	2	0-25	3280	16800	7300	13100	17.5	30.3
EV-2	2	30-40	36.4	20000	8580	16800	20.5	30
EV-2	2	70-80	4210	21900	9510	17900	19.1	38.8
EV-2	3	20-40	3810	21700	8460	22300	28.4	33.7
EV-2	3	20-40	3950	19800	8600	17000	20.6	34.6
EV-2	3	60-70	4080	23300	10300	25000	28.1	41.4
GD	1	0-20	<50	765	319	526	16	5.74
GD	1	35-45	1660	13900	6290	14300	26.9	22.8
GD	1	70-80	3020	16700	7070	15900	24.6	23.6
GD	1	110-113	<50	303	160	257	16.7	6.22
GD	2	10-20	3520	21100	8830	16500	18.7	24.7
GD	2	40-60	2750	16400	7000	16300	26.3	25.4
GD	3	20-30	2020	15900	6970	14900	24.1	22.6
GD	3	60-70	1680	8380	3580	9580	30.5	23.1
GD	3	75-95	<50	337	199	327	18.7	4.89
GD	3	75-95	<50	205	121	193	18.2	4.94
TD	1	0-20	2350	16000	6820	14000	22.1	23.9
TD	1	25-50	4770	28200	12000	27500	25.5	27.1
TD	1	70-80	4470	24700	10700	21800	21.7	30
TD	1	70-80	3810	22400	9630	20000	22.4	28.8
TD	1	110-120	5080	28300	11800	24400	21.9	29.1
TD	2	10-20	2400	17900	7840	16900	24.4	26.2
TD	2	45-60	3350	17800	7810	20400	30.3	26.8
TD	2	75-85	4110	23000	9950	24700	28.4	25.8
TD	3	20-30	1920	14600	6510	14700	26.1	25
TD	3	60-80	3610	18300	7900	21500	31.3	23.3

Table B-3) Major Anions (IC). Values in mg L^{-1}

Deposit	Borehole	Depth	Filter Size (µm)	F	Cl	NO_2	NO_3	PO_4	SO_4	Br
EV-1	1	10	0.45	3.64	1037	< 0.05	< 0.05	< 0.05	2470	0.58
EV-1	1	10	0.45	3.5	1000	<0.1	<0.2	<0.1	2350	<0.2
EV-1	1	30	0.45	5.10	870	< 0.05	0.07	0.09	696	0.49
EV-1	1	30	0.45	5.15	862	<0.1	0.26	<0.1	686	0.52
EV-1	1	50	0.45	5.51	882	< 0.05	< 0.05	< 0.05	629	0.44
EV-1	1	50	0.45	5.52	874	<0.1	<0.2	<0.1	623	1.43
EV-1	1	90	0.45	2.97	807	< 0.05	0.26	< 0.05	532	0.60
EV-1	1	90	0.45	3.08	791	<0.1	1.32	<0.1	534	0.24
EV-1	1	120	0.45	2.38	865	< 0.05	0.18	< 0.05	1170	
EV-1	1	120	0.45	2.52	827	<0.1	0.84	<0.1	1080	<0.2
EV-1	2	10	0.45	0.96	1150	<0.1	<0.2	<0.1	4660	<0.2
EV-1	2	30	0.45	2.04	839	< 0.05	< 0.05	< 0.05	3489	0.55
EV-1	2	30	0.45	2	858	<0.1	<0.2	<0.1	3490	<0.2
EV-1	2	50	0.45	1.45	821	<0.1	0.32	0.1	2980	<0.2
EV-1	2	90	0.45	2.39	867	< 0.05	0.03	< 0.05	1570	0.55
EV-1	2	90	0.45	2.09	866	<0.1	<0.2	<0.1	1580	<0.2
EV-1	2	120	0.45	2.84	938	< 0.05	< 0.05	< 0.05	1980	0.64
EV-1	2	120	0.45	2.95	599	<0.1	<0.2	<0.1	1120	<0.2
EV-1	3	10	0.45	1.1	1200	<0.1	<0.2	<0.1	4400	<0.2
EV-1	3	30	0.45	1.85	831	<0.1	<0.2	0.11	2170	<0.2
EV-1	3	50	0.45	2.65	790	<0.1	<0.2	0.15	1370	0.28
EV-1	3	90	0.45	1.86	858	<0.1	<0.2	<0.1	2260	<0.2
EV-1	3	120	0.45	2.28	866	<0.1	<0.2	<0.1	1210	0.27
EV-1	4	10	0.45	1.08	1310	<0.1	<0.2	<0.1	4320	<0.2
EV-1	4	10	0.45	1.09	1340	<0.1	<0.2	<0.1	4430	<0.2
EV-1	4	30	0.45	1.83	769	<0.1	<0.2	0.13	2150	<0.2
EV-1	4	50	0.45	1.73	869	<0.1	<0.2	0.15	2360	<0.2
EV-1	4	90	0.45	1.64	814	<0.1	<0.2	<0.1	1900	<0.2
EV-1	4	90	0.45	1.61	784	<0.1	<0.2	<0.1	2020	<0.2
EV-1	4	120	0.45	1.48	790	<0.1	<0.2	<0.1	1810	<0.2
EV-1	4	150	0.45	2	808	<0.1	<0.2	0.1	1720	<0.2
EV-2	1	0	0.45	1.67	673	<0.1	<0.2	<0.1	2230	<0.2
EV-2	1	10	0.45	1.15	1380	<0.1	<0.2	<0.1	4420	<0.2
EV-2	1	60	0.45	1	1230	<0.1	<0.2	0.12	3370	<0.2
EV-2	1	85	0.45	2.78	1260	<0.1	<0.2	0.24	1740	0.3
EV-2	2	0	0.45	1.22	1800	<0.1	<0.2	<0.1	6410	<0.2
EV-2	2	10	0.45	1.17	984	<0.1	<0.2	0.13	3650	<0.2
EV-2	2	30	0.45	1.04	785	<0.1	<0.2	0.16	2660	<0.2
EV-2	2	60	0.45	1.09	745	<0.1	<0.2	0.17	2470	<0.2

Table B-3) Continued

Deposit	Borehole	Depth	Filter Size (µm)	F	Cl	NO_2	NO_3	PO_4	SO_4	Br
EV-2	2	70	0.45	1.72	829	<0.1	<0.2	0.12	2710	<0.2
EV-2	2	90	0.45	1.55	767	<0.1	<0.2	<0.1	2360	<0.2
EV-2	3	0	0.45	1.89	2160	<0.1	<0.2	<0.1	5170	<0.2
EV-2	3	10	0.45	1.89	1660	<0.1	<0.2	<0.1	4160	<0.2
EV-2	3	30	0.45	1.83	989	<0.1	<0.2	0.14	2710	<0.2
EV-2	3	30	0.45	2.39	868	<0.1	<0.2	<0.1	2280	<0.2
EV-2	3	60	0.45	1.76	774	<0.1	<0.2	0.13	2040	<0.2
EV-2	3	70	0.45	1.81	907	<0.1	<0.2	0.18	2420	<0.2
EV-2	3	90	0.45	1.54	872	<0.1	<0.2	0.14	2380	<0.2
EV-2	3	90	0.45	1.73	951	<0.1	<0.2	0.1	2620	<0.2
EV-2	4	0	0.45	1.5	1590	<0.1	<0.2	<0.1	5560	<0.2
EV-2	4	10	0.45	1.4	1500	<0.1	<0.2	<0.1	5110	<0.2
EV-2	4	30	0.45	1.3	910	<0.1	<0.2	<0.1	2810	<0.2
EV-2	4	60	0.45	1.45	745	<0.1	<0.2	<0.1	2660	<0.2
EV-2	4	90	0.45	1.07	812	<0.1	<0.2	<0.1	2780	<0.2
EV-2	4	120	0.45	1.19	811	<0.1	<0.2	<0.1	2600	<0.2
EV-2	4	150	0.45	1.19	771	<0.1	<0.2	<0.1	2490	<0.2
EV-2	4	180	0.45	1.02	767	<0.1	<0.2	<0.1	2500	<0.2
GD	1	40	0.45	0.9	124	<0.1	<0.2	<0.1	935	<0.2
GD	1	60	0.45	1.26	294	<0.1	<0.2	<0.1	842	<0.2
GD	1	80	0.45	2	383	<0.1	0.42	0.28	538	<0.2
GD	1	100	0.45	1.96	408	<0.1	<0.2	<0.1	434	<0.2
GD	2	5	0.45	1.3	105	0.53	31.7	<0.1	334	<0.2
GD	2	10	0.45	1.48	143	<0.1	<0.2	<0.1	424	<0.2
GD	2	60	0.45	1.53	181	<0.1	<0.2	<0.1	440	<0.2
GD	2	70	0.45	1.78	375	<0.1	<0.2	<0.1	447	<0.2
GD	2	100	0.45	2.01	437	<0.1	<0.2	<0.1	399	<0.2
GD	2	100	0.45	1.49	434	<0.1	<0.2	0.11	645	0.21
GD	3	0	0.45	1.26	83.1	<0.1	<0.2	<0.1	370	<0.2
GD	3	10	0.45	1.11	124	<0.1	<0.2	<0.1	607	<0.2
GD	3	70	0.45	1.56	225	0.83	6.68	<0.1	1000	<0.2
TD	1	0	0.45	1.04	501	<0.1	<0.2	<0.1	1120	<0.2
TD	1	10	0.45	2.19	477	<0.1	<0.2	0.23	381	<0.2
TD	1	70	0.45	2.9	464	<0.1	<0.2	0.22	81.8	0.22
TD	1	90	0.45	2.46	456	<0.1	<0.2	<0.1	1.06	0.21
TD	1	90	0.45	2.58	433	<0.1	<0.2	<0.1	8.52	0.21
TD	1	120	0.45	2.09	450	<0.1	<0.2	<0.1	15.9	0.2
TD	2	0	0.45	1.52	434	<0.1	<0.2	<0.1	1340	<0.2
TD	2	10	0.45	1.8	496	<0.1	<0.2	<0.1	756	<0.2
TD	2	60	0.45	2.35	460	<0.1	<0.2	0.18	148	<0.2

Table B-3) Continued

Deposit	Borehole	Depth	Filter Size (µm)	F	Cl	NO_2	NO_3	PO_4	SO_4	Br
TD	2	70	0.45	2.58	467	<0.1	<0.2	0.15	111	<0.2
TD	3	0	0.45	1.48	251	<0.1	<0.2	<0.1	1070	<0.2
TD	3	10	0.45	1.02	392	<0.1	<0.2	<0.1	1390	<0.2
TD	3	60	0.45	2.33	482	<0.1	<0.2	0.11	323	<0.2
TD	4	0	0.45	1.22	349	<0.1	<0.2	<0.1	1380	<0.2
TD	4	10	0.45	2.04	451	<0.1	<0.2	<0.1	921	<0.2
TD	4	65	0.45	1.99	443	<0.1	<0.2	<0.1	713	<0.2

Table B-4) Dissolved Cations (ICP-OES). Values in mg L^{-1}.

Deposit	Borehole	Depth	Filter Size (µm)	Preservation	Ca	K	Mg	Na	S
EV-1	1	10	0.45	HNO_3	46.2	40.5	32.3	1760	865
EV-1	1	10	0.45	HNO_3	39.8	37.7	29.1	1740	795
EV-1	1	30	0.45	HNO_3	9.48	22.9	7.79	1050	259
EV-1	1	30	0.45	HNO_3	7.97	21.4	7.32	944	227
EV-1	1	50	0.45	HNO_3	9.34	23.9	8.33	1110	236
EV-1	1	50	0.45	HNO_3	6.97	20	7.55	913	194
EV-1	1	90	0.45	HNO_3	10.8	15	8.24	1000	190
EV-1	1	90	0.45	HNO_3	10.4	14.7	8.17	1020	190
EV-1	1	90	0.45	HNO_3	8.39	13.7	7.64	907	157
EV-1	1	120	0.45	HNO_3	12.7	18	10.86	1260	227
EV-1	1	120	0.45	HNO_3	9.7	15	9.28	1020	191
EV-1	2	10	0.45	HNO_3	474	BDL	131	2280	1560
EV-1	2	30	0.45	HNO_3	365	55	68.23	1790	1230
EV-1	2	30	0.45	HNO_3	332	50.4	62.5	1740	1180
EV-1	2	50	0.45	HNO_3	286	51.5	55.7	1610	998
EV-1	2	90	0.45	HNO_3	91.3	26.9	28.3	1430	545
EV-1	2	90	0.45	HNO_3	93.5	26.8	29.1	1450	545
EV-1	2	90	0.45	HNO_3	110	30.5	32.8	1650	545
EV-1	2	90	0.45	HNO_3	74.7	22.6	24	1320	522
EV-1	2	120	0.45	HNO_3	55.9	29.8	38.8	1920	779
EV-1	2	120	0.45	HNO_3	45.3	25.4	32.1	1730	733
EV-1	3	10	0.45	HNO_3	382	BDL	132	2390	1510
EV-1	3	30	0.45	HNO_3	113	BDL	42.4	1470	721
EV-1	3	30	0.45	HNO_3	123	BDL	45.6	1540	758
EV-1	3	50	0.45	HNO_3	52.8	BDL	25.7	1200	462
EV-1	3	90	0.45	HNO_3	156	BDL	56.4	1620	812
EV-1	3	120	0.45	HNO_3	24.1	BDL	24.8	1420	414
EV-1	4	10	0.45	HNO_3	369	BDL	116	2430	1460
EV-1	4	30	0.45	HNO_3	129	BDL	41.3	1410	736
EV-1	4	50	0.45	HNO_3	159	BDL	46.7	1520	787
EV-1	4	90	0.45	HNO_3	113	BDL	40.8	1430	631
EV-1	4	120	0.45	HNO_3	111	BDL	40.7	1440	617
EV-1	4	120	0.45	HNO_3	115	BDL	41.2	1430	627
EV-1	4	150	0.45	HNO_3	91.5	BDL	37.4	1420	574
EV-2	1	0	0.2	HNO_3	178	45.7	41.8	1250	724
EV-2	1	10	0.2	HNO_3	448	61	92.4	2100	1520
EV-2	1	60	0.2	HNO_3	387	48.5	73.7	1970	1300
EV-2	2	0	0.2	HNO_3	372	101	153	3660	2110
EV-2	2	10	0.2	HNO_3	304	51.9	76.5	2130	1260
EV-2	2	30	0.2	HNO_3	246	BDL	58.6	1800	1050

Table B-4) Continued

Deposit	Borehole	Depth	Filter Size (µm)	Preservation	Ca	K	Mg	Na	S
EV-2	2	60	0.2	HNO_3	185	BDL	47.2	1570	840
EV-2	2	70	0.2	HNO_3	194	39.1	45.9	1560	920
EV-2	2	90	0.2	HNO_3	149	31.3	36.8	1490	801
EV-2	3	0	0.2	HNO_3	246	75	104	3660	1740
EV-2	3	10	0.2	HNO_3	188	BDL	66.4	2380	1180
EV-2	3	30	0.2	HNO_3	95.8	BDL	34	1630	759
EV-2	3	60	0.2	HNO_3	114	BDL	35.4	1490	690
EV-2	3	70	0.2	HNO_3	127	BDL	42.4	1690	802
EV-2	3	70	0.2	HNO_3	130	BDL	44.6	1780	835
EV-2	3	90	0.2	HNO_3	149	BDL	45.3	1720	820
EV-2	4	0	0.2	HNO_3	328	73.3	115	3310	1860
EV-2	4	10	0.2	HNO_3	316	BDL	76.4	2340	1270
EV-2	4	30	0.2	HNO_3	232	BDL	56	1780	949
EV-2	4	60	0.2	HNO_3	228	BDL	53.4	1590	901
EV-2	4	90	0.2	HNO_3	260	BDL	57.8	1660	940
EV-2	4	120	0.2	HNO_3	229	BDL	52.4	1630	873
EV-2	4	150	0.2	HNO_3	190	BDL	49.6	1630	840
EV-2	4	180	0.2	HNO_3	184	BDL	51.1	1680	853
EV-2	4	180	0.2	HNO_3	180	BDL	50.2	1660	842
GD	1	40	0.2	HNO_3	116	BDL	42.3	520	381
GD	1	60	0.2	HNO_3	63.4	BDL	26.2	540	274
GD	1	80	0.2	HNO_3	36.7	BDL	19.6	742	245
GD	1	100	0.2	HNO_3	22.1	BDL	13.4	666	106
GD	2	5	0.2	HNO_3	44.5	BDL	18.1	290	125
GD	2	10	0.2	HNO_3	43.8	BDL	16.8	343	140
GD	2	60	0.2	HNO_3	39.9	BDL	16.4	436	156
GD	2	70	0.2	HNO_3	31.2	BDL	16.1	718	152
GD	2	100	0.2	HNO_3	29.8	BDL	17.9	770	152
GD	3	0	0.2	HNO_3	37.6	BDL	17	263	139
GD	3	10	0.2	HNO_3	59.9	BDL	23.4	405	210
TD	1	0	0.2	HNO_3	41.2	BDL	27.9	990	383
TD	1	10	0.2	HNO_3	12.7	BDL	12.9	813	126
TD	1	70	0.2	HNO_3	7.71	BDL	9.59	711	27.7
TD	1	90	0.2	HNO_3	8.62	BDL	9.43	713	11.7
TD	1	90	0.2	HNO_3	8.66	BDL	9.47	707	12
TD	1	120	0.2	HNO_3	11.2	BDL	11.1	756	14.5
TD	2	0	0.2	HNO_3	63	BDL	39	982	462
TD	2	10	0.2	HNO_3	18.9	BDL	16.7	921	218
TD	2	70	0.2	HNO_3	10.6	BDL	11.6	773	37.5

Table B-4) Continued

Deposit	Borehole	Depth	Filter Size (µm)	Preservation	Ca	K	Mg	Na	S
TD	3	0	0.2	HNO_3	54.4	BDL	30.2	694	342
TD	3	10	0.2	HNO_3	77.6	BDL	43.2	1020	526
TD	3	60	0.2	HNO_3	11.2	BDL	11.9	826	89.8
TD	4	0	0.2	HNO_3	64	BDL	37.3	948	473
TD	4	10	0.2	HNO_3	23.6	BDL	19	973	296

Table B-5) Trace Elements (ICP-MS). Values in mg L^{-1}.

Deposit	Borehole	Depth	Filter Size (µm)	Preservation	Li	B	Na	Mg	Al	Si
EV-1	1	10	0.45	HNO_3	0.41	3.77	1625	32.1	1.2E-02	1.84
EV-1	1	10	0.45	HNO_3	0.42	3.80	1602	32.6	1.2E-02	1.86
EV-1	1	30	0.45	HNO_3	0.24	3.00	996	7.3	2.57	6.07
EV-1	1	50	0.45	HNO_3	0.23	2.92	991	7.7	7.18	14.33
EV-1	1	90	0.45	HNO_3	0.24	3.50	999	7.7	2.57	7.97
EV-1	1	120	0.45	HNO_3	0.27	3.60	1149	9.4	4.6E-02	4.32
EV-1	2	10	0.45	HNO_3	1.00	2.68	3152	156.9	9.2E-03	2.41
EV-1	2	30	0.45	HNO_3	0.59	3.12	1752	72.5	8.4E-03	2.01
EV-1	2	50	0.45	HNO_3	0.65	2.83	2236	74.1	6.7E-03	2.88
EV-1	2	90	0.45	HNO_3	0.37	3.84	1379	25.3	1.8E-02	3.70
EV-1	2	120	0.45	HNO_3	0.47	3.92	1735	36.7	1.2E-02	3.18
EV-1	3	10	0.45	HNO_3	1.06	2.81	3095	168.8	8.7E-03	2.09
EV-1	3	30	0.45	HNO_3	0.53	2.90	1875	46.5	7.7E-03	2.19
EV-1	3	30	0.45	HNO_3	0.52	2.98	1982	45.6	6.0E-03	2.06
EV-1	3	50	0.45	HNO_3	0.37	2.90	1383	20.8	1.20	3.74
EV-1	3	90	0.45	HNO_3	0.55	3.47	1758	54.2	9.7E-03	1.81
EV-1	3	120	0.45	HNO_3	0.34	3.97	1390	17.3	1.5E-02	2.67
EV-1	4	10	0.45	HNO_3	0.75	3.05	2331	115.0	3.0E-03	1.06
EV-1	4	30	0.45	HNO_3	0.43	2.91	1329	34.2	3.3E-03	1.53
EV-1	4	30	0.45	HNO_3	0.48	2.90	1792	46.3	3.2E-03	1.24
EV-1	4	50	0.45	HNO_3	0.49	3.04	1905	43.9	3.1E-03	1.25
EV-1	4	90	0.45	HNO_3	0.45	4.41	1397	35.3	3.0E-03	3.53
EV-1	4	120	0.45	HNO_3	0.43	4.55	1374	36.8	2.3E-03	3.39
EV-1	4	120	0.45	HNO_3	0.40	4.40	1386	30.2	4.0E-03	3.82
EV-2	1	10	0.2	HNO_3	0.73	5.62	2730	102.8	1.4E-03	2.33
EV-2	1	60	0.2	HNO_3	0.62	5.54	2759	56.8	4.8E-03	4.10
EV-2	1	85	0.2	HNO_3	0.53	4.99	2537	89.1	1.3E-02	1.75
EV-2	2	10	0.2	HNO_3	0.62	4.78	2207	81.2	2.5E-03	2.39
EV-2	2	30	0.2	HNO_3	0.49	3.85	1978	59.9	1.3E-03	3.35
EV-2	2	60	0.2	HNO_3	0.45	4.66	1707	46.8	1.6E-03	4.38
EV-2	2	70	0.2	HNO_3	0.40	4.27	1882	54.8	2.3E-03	2.10
EV-2	2	90	0.2	HNO_3	0.40	4.15	1674	39.0	1.7E-03	3.17
EV-2	3	10	0.2	HNO_3	0.60	4.35	2894	71.6	2.9E-03	2.67
EV-2	3	30	0.2	HNO_3	0.38	3.54	1780	35.1	2.9E-03	2.85
EV-2	3	60	0.2	HNO_3	0.40	4.55	1684	36.3	2.1E-03	3.92
EV-2	3	70	0.2	HNO_3	0.41	4.54	2059	45.4	6.3E-03	2.54
EV-2	3	70	0.2	HNO_3	0.42	4.03	2026	43.5	4.8E-03	2.24
EV-2	3	90	0.2	HNO_3	0.44	4.42	1984	44.8	2.1E-03	2.32
EV-2	4	10	0.2	HNO_3	0.50	5.72	2633	83.7	8.1E-04	2.79
EV-2	4	30	0.2	HNO_3	0.40	4.74	1988	57.7	7.0E-03	4.17

Table B-5) Continued

Deposit	Borehole	Depth	Filter Size (µm)	Preservation	Li	B	Na	Mg	Al	Si
EV-2	4	60	0.2	HNO_3	0.35	4.81	1942	53.7	4.2E-03	4.36
EV-2	4	90	0.2	HNO_3	0.36	4.89	1925	57.7	3.4E-03	3.67
EV-2	4	90	0.2	HNO_3	0.35	4.91	1697	55.2	3.6E-03	4.07
EV-2	4	120	0.2	HNO_3	0.33	4.76	1608	46.8	6.3E-03	4.15
EV-2	4	150	0.2	HNO_3	0.39	5.35	1627	50.4	3.4E-03	4.26
EV-2	4	180	0.2	HNO_3	0.40	5.62	1858	51.3	7.1E-03	3.81
GD	1	60	0.2	HNO_3	0.23	3.11	581	23.0	9.3E-03	1.83
GD	1	80	0.2	HNO_3	0.25	3.41	710	13.7	2.3E-02	3.73
GD	1	100	0.2	HNO_3	0.22	3.57	714	11.1	2.4E-02	3.25
GD	2	10	0.2	HNO_3	0.23	2.51	358	14.3	7.6E-03	2.72
GD	2	60	0.2	HNO_3	0.25	2.69	507	14.3	1.2E-02	2.83
GD	2	70	0.2	HNO_3	0.27	4.18	776	13.6	9.7E-03	3.78
GD	2	100	0.2	HNO_3	0.27	4.08	777	14.9	5.7E-03	3.13
GD	3	10	0.2	HNO_3	0.30	3.54	476	20.9	4.9E-03	2.01
TD	1	10	0.2	HNO_3	0.35	3.82	1098	25.2	8.0E-03	2.34
TD	1	70	0.2	HNO_3	0.18	3.31	700	7.5	2.2E+00	6.53
TD	1	90	0.2	HNO_3	0.18	3.53	759	6.9	1.9E-02	4.21
TD	1	90	0.2	HNO_3	0.17	3.52	752	6.9	2.7E-02	3.87
TD	1	120	0.2	HNO_3	0.18	3.53	706	8.2	1.6E-02	5.25
TD	2	10	0.2	HNO_3	0.28	3.59	901	13.6	4.3E-02	3.54
TD	2	70	0.2	HNO_3	0.21	3.43	859	8.5	1.9E-02	3.18
TD	3	10	0.2	HNO_3	0.43	3.16	983	37.4	4.5E-03	2.18
TD	3	60	0.2	HNO_3	0.24	3.29	860	8.8	2.6E-02	3.04
TD	3	70	0.2	HNO_3	0.30	2.91	1148	17.3	1.0E-02	2.34
TD	4	10	0.2	HNO_3	0.25	3.36	983	10.9	2.1E-02	2.85

Table B-5) Continued

Deposit	Borehole	Depth	Filter Size (µm)	Preservation	P	K	Ca	Sc	Ti
EV-1	1	10	0.45	HNO_3	0.06	BDL	42.24	6.7E-04	2.3E-03
EV-1	1	10	0.45	HNO_3	0.06	BDL	43.17	7.2E-04	2.1E-03
EV-1	1	30	0.45	HNO_3	0.11	BDL	8.41	2.7E-03	1.6E-02
EV-1	1	50	0.45	HNO_3	0.17	BDL	7.77	6.5E-03	4.4E-02
EV-1	1	90	0.45	HNO_3	0.17	BDL	8.87	3.2E-03	5.3E-02
EV-1	1	120	0.45	HNO_3	0.14	BDL	10.47	1.5E-03	3.0E-03
EV-1	2	10	0.45	HNO_3	0.02	53.04	599.39	7.2E-04	2.2E-03
EV-1	2	30	0.45	HNO_3	0.08	3.02	343.65	8.2E-04	2.2E-03
EV-1	2	50	0.45	HNO_3	0.02	44.74	332.90	8.6E-04	2.1E-03
EV-1	2	90	0.45	HNO_3	0.17	BDL	81.34	1.6E-03	2.2E-03
EV-1	2	120	0.45	HNO_3	0.15	BDL	50.26	1.4E-03	2.9E-03
EV-1	3	10	0.45	HNO_3	0.02	52.73	495.51	7.0E-04	2.5E-03
EV-1	3	30	0.45	HNO_3	0.02	38.20	142.42	7.8E-04	2.9E-03
EV-1	3	30	0.45	HNO_3	0.02	40.04	143.89	7.3E-04	2.7E-03
EV-1	3	50	0.45	HNO_3	0.03	61.64	62.82	1.6E-03	9.3E-03
EV-1	3	90	0.45	HNO_3	0.02	41.03	175.52	8.1E-04	2.5E-03
EV-1	3	120	0.45	HNO_3	0.05	18.01	26.97	1.1E-03	2.2E-03
EV-1	4	10	0.45	HNO_3	0.03	44.65	391.02	6.3E-04	2.7E-03
EV-1	4	30	0.45	HNO_3	0.02	34.50	137.07	6.8E-04	2.7E-03
EV-1	4	30	0.45	HNO_3	0.02	34.05	170.43	6.9E-04	2.2E-03
EV-1	4	50	0.45	HNO_3	0.02	35.84	165.72	7.0E-04	2.7E-03
EV-1	4	90	0.45	HNO_3	0.03	25.03	122.04	1.4E-03	2.8E-03
EV-1	4	120	0.45	HNO_3	0.04	25.12	118.62	1.3E-03	3.0E-03
EV-1	4	120	0.45	HNO_3	0.05	23.32	98.48	1.3E-03	2.6E-03
EV-2	1	10	0.2	HNO_3	0.04	44.09	429.15	8.9E-04	3.2E-03
EV-2	1	60	0.2	HNO_3	0.05	30.27	172.57	1.4E-03	3.3E-03
EV-2	1	85	0.2	HNO_3	0.06	45.34	313.79	7.3E-04	3.5E-03
EV-2	2	10	0.2	HNO_3	0.04	41.13	325.59	9.7E-04	4.5E-03
EV-2	2	30	0.2	HNO_3	0.04	28.92	258.00	1.4E-03	3.1E-03
EV-2	2	60	0.2	HNO_3	0.04	28.98	194.39	1.6E-03	3.8E-03
EV-2	2	70	0.2	HNO_3	0.03	34.20	217.21	9.6E-04	1.2E-03
EV-2	2	90	0.2	HNO_3	0.04	30.27	161.83	1.1E-03	1.6E-03
EV-2	3	10	0.2	HNO_3	0.03	34.69	206.08	8.9E-04	2.4E-03
EV-2	3	30	0.2	HNO_3	0.04	24.89	105.82	1.0E-03	2.6E-03
EV-2	3	60	0.2	HNO_3	0.05	28.95	124.37	1.4E-03	2.7E-03
EV-2	3	70	0.2	HNO_3	0.04	31.10	138.77	8.4E-04	2.5E-03
EV-2	3	70	0.2	HNO_3	0.05	34.39	139.38	8.2E-04	2.9E-03
EV-2	3	90	0.2	HNO_3	0.05	34.43	156.67	9.2E-04	1.8E-03
EV-2	4	10	0.2	HNO_3	0.03	38.68	337.92	9.7E-04	2.5E-03
EV-2	4	30	0.2	HNO_3	0.04	32.11	254.90	1.4E-03	4.1E-03

Table B-5) Continued

Deposit	Borehole	Depth	Filter Size (µm)	Preservation	P	K	Ca	Sc	Ti
EV-2	4	60	0.2	HNO_3	0.05	35.39	245.35	1.5E-03	3.9E-03
EV-2	4	90	0.2	HNO_3	0.04	32.09	276.42	1.2E-03	2.7E-03
EV-2	4	90	0.2	HNO_3	0.05	34.37	277.53	1.3E-03	4.4E-03
EV-2	4	120	0.2	HNO_3	0.10	32.25	238.67	1.1E-03	2.3E-03
EV-2	4	150	0.2	HNO_3	0.03	29.14	204.72	1.3E-03	2.2E-03
EV-2	4	180	0.2	HNO_3	0.03	31.63	197.07	1.1E-03	2.7E-03
GD	1	60	0.2	HNO_3	0.07	20.20	68.18	6.2E-04	1.9E-03
GD	1	80	0.2	HNO_3	0.10	18.04	32.10	9.5E-04	2.1E-03
GD	1	100	0.2	HNO_3	0.09	15.16	24.83	1.1E-03	1.6E-03
GD	2	10	0.2	HNO_3	0.07	15.03	47.54	7.3E-04	2.2E-03
GD	2	60	0.2	HNO_3	0.18	16.14	43.28	8.1E-04	2.8E-03
GD	2	70	0.2	HNO_3	0.10	17.41	34.70	1.2E-03	1.5E-03
GD	2	100	0.2	HNO_3	0.08	17.11	31.26	1.1E-03	1.8E-03
GD	3	10	0.2	HNO_3	0.05	18.18	65.99	6.5E-04	1.3E-03
TD	1	10	0.2	HNO_3	0.06	20.85	44.42	8.6E-04	1.3E-03
TD	1	70	0.2	HNO_3	0.09	13.87	9.44	2.7E-03	1.5E-02
TD	1	90	0.2	HNO_3	0.13	11.09	10.19	1.5E-03	2.6E-03
TD	1	90	0.2	HNO_3	0.11	11.26	10.31	1.4E-03	2.3E-03
TD	1	120	0.2	HNO_3	0.21	10.13	12.73	1.7E-03	2.2E-03
TD	2	10	0.2	HNO_3	0.14	16.32	21.65	9.5E-04	2.6E-03
TD	2	70	0.2	HNO_3	0.10	12.97	12.27	1.1E-03	1.8E-03
TD	3	10	0.2	HNO_3	0.10	23.80	83.24	6.3E-04	1.5E-03
TD	3	60	0.2	HNO_3	0.09	14.22	12.72	9.2E-04	1.5E-03
TD	3	70	0.2	HNO_3	0.08	18.43	31.70	8.3E-04	1.8E-03
TD	4	10	0.2	HNO_3	0.12	15.37	16.58	9.4E-04	1.7E-03

Table B-5) Continued

Deposit	Borehole	Depth	Filter Size (µm)	Preservation	V	Cr	Mn	Fe	Co
EV-1	1	10	0.45	HNO_3	2.9E-03	4.3E-03	2.2E-01	9.9E-03	5.8E-03
EV-1	1	10	0.45	HNO_3	3.2E-03	4.2E-03	2.2E-01	8.8E-03	5.9E-03
EV-1	1	30	0.45	HNO_3	1.6E-02	7.1E-03	1.7E-02	7.3E-01	2.8E-03
EV-1	1	50	0.45	HNO_3	2.7E-02	1.9E-02	2.3E-02	2.1E+00	3.5E-03
EV-1	1	90	0.45	HNO_3	1.0E-02	2.1E-02	2.0E-02	6.4E-01	2.7E-03
EV-1	1	120	0.45	HNO_3	6.8E-03	1.6E-02	1.7E-02	7.0E-02	2.8E-03
EV-1	2	10	0.45	HNO_3	2.9E-03	3.8E-02	5.2E-01	4.2E-02	1.6E-02
EV-1	2	30	0.45	HNO_3	5.7E-03	1.9E-03	2.2E-01	1.0E-02	8.0E-03
EV-1	2	50	0.45	HNO_3	6.5E-03	3.0E-02	1.3E-01	3.5E-02	6.3E-03
EV-1	2	90	0.45	HNO_3	1.7E-03	2.9E-03	5.5E-02	9.9E-01	5.5E-03
EV-1	2	120	0.45	HNO_3	1.9E-03	1.4E-03	4.8E-02	6.3E-01	5.6E-03
EV-1	3	10	0.45	HNO_3	2.7E-03	4.2E-02	8.5E-01	3.7E-02	1.6E-02
EV-1	3	30	0.45	HNO_3	6.5E-03	3.5E-02	1.0E-01	4.4E-02	4.9E-03
EV-1	3	30	0.45	HNO_3	6.7E-03	3.4E-02	1.0E-01	4.1E-02	5.1E-03
EV-1	3	50	0.45	HNO_3	1.2E-02	3.6E-02	3.5E-02	4.0E-01	2.7E-03
EV-1	3	90	0.45	HNO_3	5.2E-03	3.3E-02	1.9E-01	3.1E-02	5.9E-03
EV-1	3	120	0.45	HNO_3	2.5E-03	3.7E-02	2.6E-02	2.1E-02	3.3E-03
EV-1	4	10	0.45	HNO_3	2.8E-03	4.2E-02	7.8E-01	7.3E-03	1.7E-02
EV-1	4	30	0.45	HNO_3	6.3E-03	2.5E-02	7.0E-02	5.8E-03	3.6E-03
EV-1	4	30	0.45	HNO_3	5.4E-03	3.0E-02	8.6E-02	9.5E-03	4.1E-03
EV-1	4	50	0.45	HNO_3	6.2E-03	2.9E-02	8.4E-02	BDL	3.3E-03
EV-1	4	90	0.45	HNO_3	1.6E-03	2.9E-02	8.5E-02	9.6E-01	8.7E-03
EV-1	4	120	0.45	HNO_3	1.8E-03	2.7E-02	8.1E-02	1.1E+00	8.6E-03
EV-1	4	120	0.45	HNO_3	2.0E-03	2.8E-02	6.6E-02	8.2E-01	7.4E-03
EV-2	1	10	0.2	HNO_3	3.3E-03	3.5E-02	1.3E+00	1.2E-02	8.8E-02
EV-2	1	60	0.2	HNO_3	3.4E-03	3.9E-02	1.3E-01	6.2E-01	8.0E-03
EV-2	1	85	0.2	HNO_3	3.7E-03	4.0E-02	6.7E-01	1.8E-02	2.3E-02
EV-2	2	10	0.2	HNO_3	3.5E-03	3.0E-02	6.9E-01	2.1E-02	5.0E-02
EV-2	2	30	0.2	HNO_3	1.3E-03	2.5E-02	1.4E-01	1.1E+00	3.8E-03
EV-2	2	60	0.2	HNO_3	1.2E-03	2.4E-02	9.1E-02	1.4E+00	3.8E-03
EV-2	2	70	0.2	HNO_3	4.3E-03	2.3E-02	2.0E-01	1.2E-03	9.0E-03
EV-2	2	90	0.2	HNO_3	1.8E-03	2.4E-02	7.6E-02	4.9E-01	2.4E-03
EV-2	3	10	0.2	HNO_3	6.3E-03	3.5E-02	2.9E-01	6.2E-03	1.6E-02
EV-2	3	30	0.2	HNO_3	2.7E-03	2.7E-02	5.4E-02	2.5E-02	1.7E-03
EV-2	3	60	0.2	HNO_3	1.3E-03	2.6E-02	6.6E-02	3.7E-01	2.8E-03
EV-2	3	70	0.2	HNO_3	7.0E-03	2.7E-02	1.1E-01	BDL	5.4E-03
EV-2	3	70	0.2	HNO_3	8.3E-03	2.8E-02	7.9E-02	BDL	3.4E-03
EV-2	3	90	0.2	HNO_3	6.9E-03	2.7E-02	8.0E-02	BDL	3.2E-03
EV-2	4	10	0.2	HNO_3	5.3E-03	3.6E-02	5.8E-01	5.2E-03	4.7E-02
EV-2	4	30	0.2	HNO_3	1.3E-03	2.9E-02	1.3E-01	1.5E+00	2.5E-03

Table B-5) Continued

Deposit	Borehole	Depth	Filter Size (μm)	Preservation	V	Cr	Mn	Fe	Co
EV-2	4	60	0.2	HNO_3	1.0E-03	2.5E-02	1.1E-01	1.4E+00	1.7E-03
EV-2	4	90	0.2	HNO_3	2.4E-03	2.4E-02	1.9E-01	9.6E-01	9.0E-03
EV-2	4	90	0.2	HNO_3	1.8E-03	2.7E-02	1.4E-01	1.8E+00	4.1E-03
EV-2	4	120	0.2	HNO_3	1.7E-03	2.9E-02	1.4E-01	1.2E+00	4.3E-03
EV-2	4	150	0.2	HNO_3	3.0E-03	2.5E-02	1.8E-01	4.0E-01	1.1E-02
EV-2	4	180	0.2	HNO_3	3.4E-03	2.5E-02	2.3E-01	7.5E-02	1.6E-02
GD	1	60	0.2	HNO_3	6.5E-03	8.5E-03	1.6E-01	2.1E-02	9.9E-03
GD	1	80	0.2	HNO_3	1.1E-02	1.7E-02	7.3E-02	2.7E-02	4.5E-03
GD	1	100	0.2	HNO_3	1.1E-02	1.8E-02	5.4E-02	2.5E-02	3.7E-03
GD	2	10	0.2	HNO_3	2.4E-03	6.4E-03	2.0E-01	9.4E-02	5.1E-03
GD	2	60	0.2	HNO_3	4.5E-03	9.1E-03	2.1E-01	1.4E-01	1.2E-02
GD	2	70	0.2	HNO_3	1.4E-02	1.9E-02	8.2E-02	2.7E-02	3.9E-03
GD	2	100	0.2	HNO_3	1.4E-02	2.0E-02	8.3E-02	1.6E-02	8.9E-03
GD	3	10	0.2	HNO_3	1.1E-03	6.3E-03	2.2E-02	1.2E-02	6.1E-04
TD	1	10	0.2	HNO_3	4.0E-03	1.7E-02	2.5E-01	2.8E-02	8.0E-03
TD	1	70	0.2	HNO_3	2.4E-02	3.1E-02	3.0E-02	7.3E-01	1.9E-03
TD	1	90	0.2	HNO_3	1.1E-02	2.5E-02	2.4E-02	4.0E-02	1.1E-03
TD	1	90	0.2	HNO_3	1.1E-02	3.0E-02	2.5E-02	4.2E-02	1.1E-03
TD	1	120	0.2	HNO_3	8.7E-03	3.4E-02	3.3E-02	9.5E-02	2.4E-04
TD	2	10	0.2	HNO_3	1.2E-02	2.7E-02	5.2E-02	5.6E-02	3.6E-03
TD	2	70	0.2	HNO_3	1.8E-02	2.8E-02	3.1E-02	1.5E-02	2.7E-03
TD	3	10	0.2	HNO_3	3.6E-03	1.4E-02	1.7E-01	2.6E-03	4.7E-03
TD	3	60	0.2	HNO_3	1.8E-02	2.2E-02	2.5E-02	2.1E-02	1.7E-03
TD	3	70	0.2	HNO_3	1.9E-02	1.9E-02	7.5E-02	4.6E-03	3.3E-03
TD	4	10	0.2	HNO_3	1.7E-02	2.0E-02	2.5E-02	2.0E-02	1.3E-03

Table B-5) Continued

Deposit	Borehole	Depth	Filter Size (µm)	Preservation	Ni	Cu	Zn	As	Se
EV-1	1	10	0.45	HNO_3	2.2E-02	5.1E-02	5.2E-03	5.9E-03	8.4E-03
EV-1	1	10	0.45	HNO_3	2.3E-02	5.8E-02	4.9E-03	5.1E-03	8.3E-03
EV-1	1	30	0.45	HNO_3	1.4E-02	2.6E-02	2.6E-03	4.6E-03	1.4E-02
EV-1	1	50	0.45	HNO_3	1.6E-02	2.4E-02	2.9E-02	4.6E-03	1.6E-02
EV-1	1	90	0.45	HNO_3	1.9E-02	2.6E-02	5.8E-03	7.6E-03	2.1E-03
EV-1	1	120	0.45	HNO_3	1.7E-02	3.4E-02	3.4E-03	9.0E-03	2.6E-03
EV-1	2	10	0.45	HNO_3	5.8E-02	7.6E-02	1.9E-01	2.7E-03	1.9E-02
EV-1	2	30	0.45	HNO_3	2.9E-02	4.2E-02	7.5E-03	5.1E-03	1.3E-02
EV-1	2	50	0.45	HNO_3	2.6E-02	5.7E-02	8.0E-03	4.2E-03	2.0E-02
EV-1	2	90	0.45	HNO_3	2.5E-02	3.3E-02	5.6E-03	1.0E-02	2.9E-03
EV-1	2	120	0.45	HNO_3	2.4E-02	5.6E-02	5.3E-03	1.1E-02	4.3E-03
EV-1	3	10	0.45	HNO_3	4.6E-02	1.1E-01	1.1E-02	3.9E-03	2.0E-02
EV-1	3	30	0.45	HNO_3	2.0E-02	8.3E-02	7.7E-03	4.0E-03	1.5E-02
EV-1	3	30	0.45	HNO_3	2.0E-02	8.1E-02	1.4E-04	1.7E-03	1.7E-02
EV-1	3	50	0.45	HNO_3	1.5E-02	6.6E-02	BDL	1.9E-03	1.8E-02
EV-1	3	90	0.45	HNO_3	2.3E-02	8.2E-02	9.5E-04	4.6E-03	1.4E-02
EV-1	3	120	0.45	HNO_3	2.0E-02	5.8E-02	BDL	1.2E-02	9.8E-03
EV-1	4	10	0.45	HNO_3	4.5E-02	1.2E-01	1.8E-03	4.9E-03	2.1E-02
EV-1	4	30	0.45	HNO_3	1.6E-02	7.6E-02	2.2E-04	4.1E-03	1.6E-02
EV-1	4	30	0.45	HNO_3	1.8E-02	7.8E-02	BDL	3.1E-03	1.1E-02
EV-1	4	50	0.45	HNO_3	1.7E-02	8.7E-02	BDL	1.6E-03	9.9E-03
EV-1	4	90	0.45	HNO_3	3.0E-02	7.9E-02	BDL	9.8E-03	2.1E-03
EV-1	4	120	0.45	HNO_3	3.1E-02	8.2E-02	2.2E-03	1.1E-02	3.4E-03
EV-1	4	120	0.45	HNO_3	2.9E-02	6.6E-02	7.2E-03	1.0E-02	4.2E-03
EV-2	1	10	0.2	HNO_3	1.1E-01	1.1E-01	5.0E-03	4.4E-03	1.1E-02
EV-2	1	60	0.2	HNO_3	3.2E-02	1.3E-01	1.4E-03	1.2E-02	5.9E-03
EV-2	1	85	0.2	HNO_3	4.6E-02	1.6E-01	1.9E-03	3.3E-03	7.9E-03
EV-2	2	10	0.2	HNO_3	7.0E-02	1.5E-01	2.8E-03	4.7E-03	4.7E-03
EV-2	2	30	0.2	HNO_3	2.2E-02	1.3E-01	BDL	8.9E-03	BDL
EV-2	2	60	0.2	HNO_3	2.2E-02	1.1E-01	2.5E-03	1.3E-02	3.1E-03
EV-2	2	70	0.2	HNO_3	2.3E-02	5.1E-02	BDL	4.1E-03	4.7E-03
EV-2	2	90	0.2	HNO_3	1.8E-02	6.3E-02	BDL	6.2E-03	2.6E-03
EV-2	3	10	0.2	HNO_3	3.2E-02	1.0E-01	5.5E-04	5.7E-03	7.4E-03
EV-2	3	30	0.2	HNO_3	1.3E-02	9.9E-02	BDL	6.3E-03	5.4E-03
EV-2	3	60	0.2	HNO_3	1.6E-02	9.9E-02	BDL	8.5E-03	1.4E-03
EV-2	3	70	0.2	HNO_3	1.8E-02	1.1E-01	BDL	4.2E-03	2.4E-03
EV-2	3	70	0.2	HNO_3	1.5E-02	1.1E-01	BDL	6.7E-03	6.9E-03
EV-2	3	90	0.2	HNO_3	1.6E-02	6.6E-02	BDL	5.2E-03	6.8E-03
EV-2	4	10	0.2	HNO_3	7.2E-02	1.1E-01	2.0E-03	4.4E-03	4.8E-03
EV-2	4	30	0.2	HNO_3	1.9E-02	1.1E-01	BDL	1.0E-02	3.0E-03

Table B-5) Continued

Deposit	Borehole	Depth	Filter Size (µm)	Preser-vation	Ni	Cu	Zn	As	Se
EV-2	4	60	0.2	HNO_3	1.8E-02	1.2E-01	7.6E-04	1.2E-02	6.6E-03
EV-2	4	90	0.2	HNO_3	2.8E-02	1.0E-01	6.1E-04	9.5E-03	1.1E-03
EV-2	4	90	0.2	HNO_3	2.4E-02	1.3E-01	4.8E-03	1.4E-02	1.8E-03
EV-2	4	120	0.2	HNO_3	2.5E-02	5.0E-02	BDL	1.6E-02	7.6E-03
EV-2	4	150	0.2	HNO_3	2.7E-02	5.8E-02	1.8E-02	8.7E-03	4.0E-03
EV-2	4	180	0.2	HNO_3	3.6E-02	7.3E-02	2.2E-03	6.0E-03	5.8E-04
GD	1	60	0.2	HNO_3	3.4E-02	3.9E-02	BDL	3.1E-03	2.1E-03
GD	1	80	0.2	HNO_3	1.9E-02	4.3E-02	6.7E-03	6.9E-03	2.1E-03
GD	1	100	0.2	HNO_3	1.6E-02	3.1E-02	BDL	4.1E-03	BDL
GD	2	10	0.2	HNO_3	5.7E-02	2.0E-02	BDL	1.3E-03	2.8E-03
GD	2	60	0.2	HNO_3	6.2E-02	2.1E-02	BDL	1.3E-03	4.0E-04
GD	2	70	0.2	HNO_3	1.6E-02	2.2E-02	BDL	5.9E-03	4.6E-03
GD	2	100	0.2	HNO_3	2.3E-02	2.4E-02	BDL	4.3E-03	3.8E-03
GD	3	10	0.2	HNO_3	2.1E-02	1.9E-02	BDL	9.4E-04	8.7E-03
TD	1	10	0.2	HNO_3	2.7E-02	3.3E-02	BDL	3.0E-03	5.3E-03
TD	1	70	0.2	HNO_3	8.9E-03	2.6E-02	BDL	6.9E-03	1.9E-02
TD	1	90	0.2	HNO_3	7.4E-03	2.3E-02	BDL	7.1E-03	2.7E-03
TD	1	90	0.2	HNO_3	8.3E-03	2.1E-02	BDL	6.4E-03	2.3E-03
TD	1	120	0.2	HNO_3	4.3E-03	2.4E-02	BDL	5.0E-03	4.7E-03
TD	2	10	0.2	HNO_3	1.6E-02	3.1E-02	2.5E-02	1.6E-02	1.2E-01
TD	2	70	0.2	HNO_3	1.1E-02	2.5E-02	BDL	6.8E-03	6.5E-03
TD	3	10	0.2	HNO_3	2.7E-02	3.7E-02	BDL	1.2E-03	6.2E-03
TD	3	60	0.2	HNO_3	9.2E-03	2.8E-02	BDL	6.1E-03	4.9E-03
TD	3	70	0.2	HNO_3	1.4E-02	3.2E-02	BDL	3.5E-03	7.6E-04
TD	4	10	0.2	HNO_3	1.0E-02	3.2E-02	8.9E-04	5.1E-03	5.3E-04

Table B-5) Continued

Deposit	Borehole	Depth	Filter Size (µm)	Preservation	Sr	Mo	Ba	Hg
EV-1	1	10	0.45	HNO_3	1.74	1.0E-01	3.6E-02	3.5E-03
EV-1	1	10	0.45	HNO_3	1.76	1.0E-01	3.6E-02	7.4E-03
EV-1	1	30	0.45	HNO_3	0.43	1.4E-01	4.5E-02	1.3E-03
EV-1	1	50	0.45	HNO_3	0.44	1.6E-01	6.5E-02	5.1E-04
EV-1	1	90	0.45	HNO_3	0.48	1.0E-01	8.8E-02	BDL
EV-1	1	120	0.45	HNO_3	0.58	1.1E-01	8.0E-02	4.5E-04
EV-1	2	10	0.45	HNO_3	6.88	1.6E-02	2.7E-02	BDL
EV-1	2	30	0.45	HNO_3	5.03	9.0E-02	2.5E-02	BDL
EV-1	2	50	0.45	HNO_3	4.23	1.2E-01	2.9E-02	BDL
EV-1	2	90	0.45	HNO_3	1.84	9.5E-02	2.8E-02	2.2E-04
EV-1	2	120	0.45	HNO_3	2.26	9.2E-02	2.7E-02	9.2E-03
EV-1	3	10	0.45	HNO_3	7.05	1.6E-02	2.7E-02	BDL
EV-1	3	30	0.45	HNO_3	2.78	1.0E-01	3.3E-02	BDL
EV-1	3	30	0.45	HNO_3	2.84	1.0E-01	3.2E-02	BDL
EV-1	3	50	0.45	HNO_3	1.39	1.3E-01	4.4E-02	BDL
EV-1	3	90	0.45	HNO_3	3.06	7.9E-02	3.7E-02	BDL
EV-1	3	120	0.45	HNO_3	1.08	1.1E-01	4.2E-02	1.9E-03
EV-1	4	10	0.45	HNO_3	6.24	2.7E-02	2.3E-02	BDL
EV-1	4	30	0.45	HNO_3	2.50	9.2E-02	2.9E-02	BDL
EV-1	4	30	0.45	HNO_3	3.08	9.7E-02	3.0E-02	BDL
EV-1	4	50	0.45	HNO_3	2.91	1.1E-01	2.7E-02	BDL
EV-1	4	90	0.45	HNO_3	2.39	8.2E-02	2.7E-02	BDL
EV-1	4	120	0.45	HNO_3	2.33	7.4E-02	2.7E-02	BDL
EV-1	4	120	0.45	HNO_3	2.13	8.4E-02	2.8E-02	BDL
EV-2	1	10	0.2	HNO_3	5.19	8.6E-02	3.9E-02	BDL
EV-2	1	60	0.2	HNO_3	3.19	1.8E-01	2.7E-02	BDL
EV-2	1	85	0.2	HNO_3	4.52	1.4E-01	3.8E-02	BDL
EV-2	2	10	0.2	HNO_3	4.86	7.6E-02	2.5E-02	BDL
EV-2	2	30	0.2	HNO_3	3.80	9.7E-02	2.5E-02	BDL
EV-2	2	60	0.2	HNO_3	3.13	8.7E-02	2.6E-02	BDL
EV-2	2	70	0.2	HNO_3	3.47	9.5E-02	2.6E-02	1.0E-03
EV-2	2	90	0.2	HNO_3	2.90	8.8E-02	2.6E-02	BDL
EV-2	3	10	0.2	HNO_3	4.40	1.1E-01	2.7E-02	BDL
EV-2	3	30	0.2	HNO_3	2.28	1.1E-01	2.8E-02	BDL
EV-2	3	60	0.2	HNO_3	2.32	8.5E-02	2.8E-02	BDL
EV-2	3	70	0.2	HNO_3	2.75	1.0E-01	3.3E-02	BDL
EV-2	3	70	0.2	HNO_3	2.93	1.2E-01	3.1E-02	BDL
EV-2	3	90	0.2	HNO_3	3.02	1.1E-01	3.0E-02	BDL
EV-2	4	10	0.2	HNO_3	5.18	7.7E-02	2.5E-02	BDL
EV-2	4	30	0.2	HNO_3	3.91	7.8E-02	2.6E-02	BDL

Table B-5) Continued

Deposit	Borehole	Depth (cm)	Filter Size (µm)	Preservation	Sr	Mo	Ba	Hg
EV-2	4	60	0.2	HNO_3	3.76	6.6E-02	2.4E-02	BDL
EV-2	4	90	0.2	HNO_3	4.03	7.5E-02	2.7E-02	BDL
EV-2	4	90	0.2	HNO_3	4.00	7.6E-02	2.8E-02	BDL
EV-2	4	120	0.2	HNO_3	3.81	7.9E-02	2.8E-02	9.2E-04
EV-2	4	150	0.2	HNO_3	3.57	7.7E-02	2.8E-02	BDL
EV-2	4	180	0.2	HNO_3	3.64	7.2E-02	2.9E-02	BDL
GD	1	60	0.2	HNO_3	1.27	2.0E-02	3.4E-02	BDL
GD	1	80	0.2	HNO_3	0.87	5.4E-02	5.5E-02	BDL
GD	1	100	0.2	HNO_3	0.67	2.8E-02	9.8E-02	BDL
GD	2	10	0.2	HNO_3	0.78	5.0E-03	4.2E-02	BDL
GD	2	60	0.2	HNO_3	0.80	1.1E-02	4.0E-02	BDL
GD	2	70	0.2	HNO_3	0.86	6.8E-02	8.5E-02	2.3E-03
GD	2	100	0.2	HNO_3	0.88	5.3E-02	1.0E-01	BDL
GD	3	10	0.2	HNO_3	1.00	7.9E-04	3.5E-02	BDL
TD	1	10	0.2	HNO_3	1.30	4.2E-02	4.8E-02	BDL
TD	1	70	0.2	HNO_3	0.40	1.5E-01	3.0E-01	BDL
TD	1	90	0.2	HNO_3	0.41	4.0E-02	3.3E-01	1.5E-03
TD	1	90	0.2	HNO_3	0.41	3.8E-02	3.2E-01	BDL
TD	1	120	0.2	HNO_3	0.49	3.9E-03	3.4E-01	BDL
TD	2	10	0.2	HNO_3	0.76	6.3E-02	7.9E-02	BDL
TD	2	70	0.2	HNO_3	0.49	8.0E-02	2.9E-01	3.5E-03
TD	3	10	0.2	HNO_3	1.96	1.9E-02	4.4E-02	BDL
TD	3	60	0.2	HNO_3	0.49	1.2E-01	9.8E-02	BDL
TD	3	70	0.2	HNO_3	0.93	2.0E-01	5.2E-02	5.0E-04
TD	4	10	0.2	HNO_3	0.61	7.1E-02	5.8E-02	BDL

Table B-5) continued

Deposit	Borehole	Depth (cm)	Filter Size (µm)	Preservation	Pb	U
EV-1	1	10	0.45	HNO_3	7.8E-05	3.9E-03
EV-1	1	10	0.45	HNO_3	9.0E-05	3.8E-03
EV-1	1	30	0.45	HNO_3	6.4E-04	1.0E-02
EV-1	1	50	0.45	HNO_3	1.4E-03	1.4E-02
EV-1	1	90	0.45	HNO_3	6.1E-04	1.3E-02
EV-1	1	120	0.45	HNO_3	7.0E-05	1.5E-02
EV-1	2	10	0.45	HNO_3	1.2E-05	1.1E-03
EV-1	2	30	0.45	HNO_3	1.4E-04	4.9E-03
EV-1	2	50	0.45	HNO_3	2.5E-05	3.7E-03
EV-1	2	90	0.45	HNO_3	1.0E-04	5.9E-03
EV-1	2	120	0.45	HNO_3	1.9E-05	1.1E-02
EV-1	3	10	0.45	HNO_3	2.2E-05	1.2E-03
EV-1	3	30	0.45	HNO_3	BDL	3.8E-03
EV-1	3	30	0.45	HNO_3	BDL	3.8E-03
EV-1	3	50	0.45	HNO_3	1.3E-04	5.5E-03
EV-1	3	90	0.45	HNO_3	BDL	5.9E-03
EV-1	3	120	0.45	HNO_3	BDL	1.3E-02
EV-1	4	10	0.45	HNO_3	BDL	1.1E-03
EV-1	4	30	0.45	HNO_3	BDL	3.7E-03
EV-1	4	30	0.45	HNO_3	BDL	3.4E-03
EV-1	4	50	0.45	HNO_3	BDL	3.2E-03
EV-1	4	90	0.45	HNO_3	BDL	5.8E-03
EV-1	4	120	0.45	HNO_3	BDL	6.2E-03
EV-1	4	120	0.45	HNO_3	3.9E-06	7.1E-03
EV-2	1	10	0.2	HNO_3	BDL	4.0E-03
EV-2	1	60	0.2	HNO_3	BDL	7.4E-03
EV-2	1	85	0.2	HNO_3	2.7E-02	6.3E-03
EV-2	2	10	0.2	HNO_3	2.0E-05	5.4E-03
EV-2	2	30	0.2	HNO_3	BDL	2.0E-03
EV-2	2	60	0.2	HNO_3	BDL	3.5E-03
EV-2	2	70	0.2	HNO_3	BDL	3.6E-03
EV-2	2	90	0.2	HNO_3	BDL	3.5E-03
EV-2	3	10	0.2	HNO_3	BDL	5.5E-03
EV-2	3	30	0.2	HNO_3	BDL	2.2E-03
EV-2	3	60	0.2	HNO_3	BDL	3.6E-03
EV-2	3	70	0.2	HNO_3	BDL	5.8E-03
EV-2	3	70	0.2	HNO_3	5.5E-05	5.9E-03
EV-2	3	90	0.2	HNO_3	BDL	6.5E-03
EV-2	4	10	0.2	HNO_3	BDL	5.3E-03
EV-2	4	30	0.2	HNO_3	BDL	2.9E-03

Table B-5) Continued

Deposit	Borehole	Depth (cm)	Filter Size (µm)	Preservation	Pb	U
EV-2	4	60	0.2	HNO_3	1.9E-05	3.3E-03
EV-2	4	90	0.2	HNO_3	BDL	4.0E-03
EV-2	4	90	0.2	HNO_3	BDL	4.5E-03
EV-2	4	120	0.2	HNO_3	6.2E-05	4.6E-03
EV-2	4	150	0.2	HNO_3	6.7E-05	5.2E-03
EV-2	4	180	0.2	HNO_3	1.4E-04	6.3E-03
GD	1	60	0.2	HNO_3	5.5E-06	2.0E-03
GD	1	80	0.2	HNO_3	6.3E-04	1.5E-03
GD	1	100	0.2	HNO_3	BDL	2.1E-03
GD	2	10	0.2	HNO_3	2.5E-04	1.4E-03
GD	2	60	0.2	HNO_3	6.0E-04	2.1E-03
GD	2	70	0.2	HNO_3	BDL	2.6E-03
GD	2	100	0.2	HNO_3	4.3E-05	2.8E-03
GD	3	10	0.2	HNO_3	7.2E-05	1.9E-03
TD	1	10	0.2	HNO_3	3.6E-05	3.2E-03
TD	1	70	0.2	HNO_3	4.0E-04	5.4E-03
TD	1	90	0.2	HNO_3	6.2E-05	1.8E-03
TD	1	90	0.2	HNO_3	1.5E-04	1.7E-03
TD	1	120	0.2	HNO_3	9.2E-05	5.1E-04
TD	2	10	0.2	HNO_3	8.5E-04	3.4E-03
TD	2	70	0.2	HNO_3	6.9E-05	4.3E-03
TD	3	10	0.2	HNO_3	BDL	3.4E-03
TD	3	60	0.2	HNO_3	7.2E-05	5.6E-03
TD	3	70	0.2	HNO_3	7.6E-05	7.8E-03
TD	4	10	0.2	HNO_3	2.5E-04	4.5E-03

Table B-6) Summary of Total NA measured by FTIR (values in mg L^{-1})

Deposit	Borehole	Depth (cm)	Filter Size (µm)	Preservation	Total NA
EV-1	1	10	0.45	none	254
EV-1	1	30	0.45	none	78
EV-1	1	50	0.45	none	89
EV-1	1	90	0.45	none	65
EV-1	1	120	0.45	none	48
EV-1	2	10	0.45	none	171
EV-1	2	30	0.45	none	67
EV-1	2	50	0.45	none	56
EV-1	2	90	0.45	none	76
EV-1	2	120	0.45	none	67
EV-1	3	10	0.45	none	261
EV-1	3	30	0.45	none	97
EV-1	3	50	0.45	none	70
EV-1	3	90	0.45	none	76
EV-1	3	120	0.45	none	91
EV-1	4	10	0.45	none	218
EV-1	4	30	0.45	none	57
EV-1	4	50	0.45	none	64
EV-1	4	90	0.45	none	64
EV-1	4	120	0.45	none	45
EV-1	4	150	0.45	none	53
EV-2	1	10	0.45	none	110
EV-2	1	60	0.45	none	61
EV-2	2	10	0.45	none	70
EV-2	2	30	0.45	none	50
EV-2	2	60	0.45	none	39
EV-2	2	70	0.45	none	44
EV-2	2	90	0.45	none	47
EV-2	3	10	0.45	none	66
EV-2	3	30	0.45	none	56
EV-2	3	60	0.45	none	46
EV-2	3	70	0.45	none	49
EV-2	3	90	0.45	none	48
EV-2	4	10	0.45	none	50
EV-2	4	30	0.45	none	45
EV-2	4	60	0.45	none	48
EV-2	4	90	0.45	none	43
EV-2	4	120	0.45	none	44
EV-2	4	150	0.45	none	51
EV-2	4	180	0.45	none	49

Table B-6) Continued

Deposit	Borehole	Depth (cm)	Filter Size (µm)	Preservation	Total NA
GD	1	60	0.45	none	74
GD	1	100	0.45	none	54
GD	2	10	0.45	none	100
GD	2	60	0.45	none	85
GD	2	70	0.45	none	45
GD	2	100	0.45	none	54
GD	3	10	0.45	none	142
TD	1	10	0.45	none	55
TD	1	70	0.45	none	55
TD	1	90	0.45	none	57
TD	1	120	0.45	none	54
TD	2	10	0.45	none	44
TD	2	70	0.45	none	49
TD	3	10	0.45	none	100
TD	4	10	0.45	none	36

Table B-7) PREEQCi input file. Values in mmol L^{-1}

Location ID	#	Temp (°C)	pH	pe	Alk (meq L^{-1})	F	Cl	SO_4
EV-1-1-0-20	1	22.1	8.15	1.94E-02	9.99	0.191	29.26	25.76
EV-1-1-0-20	2	22.1	8.15	1.94E-02	9.99	0.191	29.26	25.76
EV-1-1-20-40	3	22.3	8.61	1.52E-02	8.99	0.268	24.53	7.25
EV-1-1-40-60	4	22.2	8.67	1.87E-02	11.39	0.290	24.88	6.54
EV-1-1-90	5	21.9	8.13	4.44E-03	16.39	0.156	22.76	5.54
EV-1-1-90	6	21.9	8.13	4.44E-03	16.39	0.156	22.76	5.54
EV-1-1-120	7	21.9	7.76	6.45E-03	16.19	0.125	24.39	12.23
EV-1-2-0-20	8	22.1	7.83	9.35E-03	2.60	0.051	32.44	48.51
EV-1-2-20-40	9	22.6	7.89	1.09E-02	3.00	0.108	23.65	36.32
EV-1-2-40-60	10	22.1	7.96	1.09E-02	3.40	0.076	23.16	31.02
EV-1-2-90	11	22.3	7.94	6.14E-03	9.99	0.126	24.45	16.30
EV-1-2-90	12	22.3	7.94	6.14E-03	9.99	0.126	24.45	16.30
EV-1-2-90	13	22.3	7.94	6.14E-03	9.99	0.126	24.45	16.30
EV-1-2-120	14	22.1	7.79	4.44E-03	13.39	0.149	26.46	20.57
EV-1-3-0-20	15	22.4	7.91	1.69E-02	4.20	0.058	33.85	45.80
EV-1-3-20-40	16	22.4	7.94	1.37E-02	4.80	0.097	23.44	22.59
EV-1-3-20-40	17	22.4	7.94	1.37E-02	4.80	0.097	23.44	22.59
EV-1-3-40-60	18	22.5	8.27	1.32E-02	5.79	0.139	22.28	14.26
EV-1-3-90	19	22.5	8.05	2.01E-02	6.19	0.098	24.20	23.53
EV-1-3-120	20	22.5	8.09	1.15E-02	13.99	0.120	24.43	12.60
EV-1-4-0-20	21	22.3	7.82	1.51E-02	4.00	0.057	36.95	44.97
EV-1-4-0-20	22	22.3	7.82	1.51E-02	4.00	0.057	37.80	46.12
EV-1-4-20-40	23	22.2	8.18	1.47E-02	3.40	0.096	21.69	22.38
EV-1-4-20-40	24	22.2	8.18	1.47E-02	3.40	0.096	21.69	22.38
EV-1-4-40-60	25	22.3	8.07	1.60E-02	3.60	0.091	24.51	24.57
EV-1-4-90	26	22.1	7.79	6.70E-03	8.79	0.086	22.96	19.78
EV-1-4-90	27	22.1	7.79	6.70E-03	8.79	0.085	22.11	21.03
EV-1-4-120	28	22.1	7.76	4.79E-03	8.99	0.078	22.28	18.84
EV-1-4-120	29	22.1	7.76	4.79E-03	8.99	0.078	22.28	18.84
EV-1-4-150	30	22.4	7.86	9.05E-03	10.79	0.105	22.79	17.91

Table B-7) Continued

Location ID	#	Temp (°C)	pH	pe	Alk (meq L^{-1})	F	Cl	SO_4
EV-2-1-10	1	22.9	7.74	1.14E-02	5.79	0.061	38.92	46.01
EV-2-1-60	2	22.7	7.87	1.70E-02	8.96	0.053	34.69	35.08
EV-2-1-85	3	22.2	8.34	2.31E-02	10.59	0.146	35.54	18.11
EV-2-2-10	4	22.9	7.52	5.24E-03	5.40	0.062	27.76	38.00
EV-2-2-30	5	22.5	7.74	1.38E-02	4.60	0.055	22.14	27.69
EV-2-2-60	6	23.2	7.61	5.03E-03	7.39	0.057	21.01	25.71
EV-2-2-70	7	22.9	7.83	8.56E-03	5.79	0.091	23.38	28.21
EV-2-2-90	8	22.6	7.82	4.86E-03	7.19	0.082	21.63	24.57
EV-2-3-10	9	23	7.74	9.72E-03	7.39	0.099	46.82	43.31
EV-2-3-30	10	22.3	7.8	1.57E-02	7.39	0.096	27.90	28.21
EV-2-3-30	11	22.3	7.8	1.57E-02	7.39	0.126	24.48	23.74
EV-2-3-60	12	22.9	7.74	1.14E-02	8.19	0.093	21.83	21.24
EV-2-3-70	13	22.7	7.82	2.17E-02	7.19	0.095	25.58	25.19
EV-2-3-70	14	22.7	7.82	2.17E-02	7.19	0.095	25.58	25.19
EV-2-3-90	15	23.1	7.79	1.82E-02	7.59	0.081	24.60	24.78
EV-2-3-90	16	23.1	7.79	1.82E-02	7.59	0.091	26.82	27.27
EV-2-4-10	17	23.8	7.5	8.16E-03	7.99	0.074	42.31	53.20
EV-2-4-30	18	24.3	7.46	1.07E-02	6.39	0.068	25.67	29.25
EV-2-4-60	19	23.3	7.6	6.45E-03	6.79	0.076	21.01	27.69
EV-2-4-90	20	22.5	7.45	9.99E-03	7.79	0.056	22.90	28.94
EV-2-4-90	21	22.5	7.45	9.99E-03	7.79	0.056	22.90	28.94
EV-2-4-120	22	22.5	7.52	6.79E-03	8.19	0.063	22.88	27.07
EV-2-4-150	23	22.9	7.47	9.62E-03	7.99	0.063	21.75	25.92
EV-2-4-180	24	22.7	7.52	1.13E-02	11.19	0.054	21.63	26.03
EV-2-4-180	25	22.7	7.52	1.13E-02	11.19	0.054	21.63	26.03

Table B-7) Continued

Location ID	#	Temp (°C)	pH	pe	Alk (meq L^{-1})	F	Cl	SO_4
GD-1-60	1	22.2	7.57	1.32E-02	6.79	0.066	8.29	8.77
GD-1-80	2	22.4	7.89	1.98E-02	10.39	0.105	10.80	5.60
GD-1-100	3	22.7	8.12	1.82E-02	12.79	0.103	11.51	4.52
GD-2-10	4	22.8	7.71	1.77E-02	6.79	0.078	4.03	4.41
GD-2-60	5	22.8	7.78	2.00E-02	8.79	0.081	5.11	4.58
GD-2-70	6	22.8	7.87	2.27E-02	12.59	0.094	10.58	4.65
GD-2-100	7	22.5	8.17	2.04E-02	14.99	0.106	12.33	4.15
GD-2-100	8	22.5	8.17	2.04E-02	14.99	0.078	12.24	6.71
GD-3-10	9	22.4	7.84	2.04E-02	4.60	0.058	3.50	6.32
TD-1-10	1	22.8	7.77	1.66E-02	9.19	0.115	13.45	3.97
TD-1-70	2	22.1	8.2	1.71E-02	17.98	0.153	13.09	0.85
TD-1-90	3	22.7	8.15	1.59E-02	18.78	0.129	12.86	0.01
TD-1-90	4	22.7	8.15	1.59E-02	18.78	0.136	12.21	0.09
TD-1-120	5	22.3	7.89	2.04E-02	19.98	0.110	12.69	0.17
TD-2-10	6	22.7	7.57	1.38E-02	8.99	0.095	13.99	7.87
TD-2-70	7	22.4	8.14	1.39E-02	17.38	0.136	13.17	1.16
TD-3-10	8	22.8	7.68	2.07E-02	7.79	0.054	11.06	14.47
TD-3-70	9	22.2	8.33	1.93E-02	14.99	0.123*	13.60*	3.36*
TD-4-10	10	22.8	7.81	1.29E-02	14.19	0.107	12.72	9.59

*Values taken from TD-3-60

Table B-7) Continued

Location ID	#	Br	Ca	Mg	Na	Al	Si	P
EV-1-1-0-20	1	7.20E-03	1.15	1.329	76.56	4.39E-04	6.54E-02	2.07E-03
EV-1-1-0-20	2	7.20E-03	1.15	1.329	76.56	4.55E-04	6.61E-02	2.07E-03
EV-1-1-20-40	3	6.15E-03	0.24	0.320	45.67	9.54E-02	2.16E-01	3.53E-03
EV-1-1-40-60	4	5.51E-03	0.23	0.343	48.28	2.66E-01	5.10E-01	5.63E-03
EV-1-1-90	5	7.46E-03	0.27	0.339	43.50	9.53E-02	2.84E-01	5.51E-03
EV-1-1-90	6	7.46E-03	0.26	0.336	44.37	9.53E-02	2.84E-01	5.51E-03
EV-1-1-120	7		0.32	0.447	54.81	1.71E-03	1.54E-01	4.59E-03
EV-1-2-0-20	8	1.25E-03	11.83	5.389	99.17	3.39E-04	8.58E-02	5.73E-04
EV-1-2-20-40	9	6.91E-03	9.11	2.807	77.86	3.11E-04	7.15E-02	2.55E-03
EV-1-2-40-60	10	1.25E-03	7.14	2.291	70.03	2.50E-04	1.02E-01	7.50E-04
EV-1-2-90	11	6.84E-03	2.28	1.164	62.20	6.52E-04	1.32E-01	5.47E-03
EV-1-2-90	12	6.84E-03	2.33	1.197	63.07	6.52E-04	1.32E-01	5.47E-03
EV-1-2-90	13	6.84E-03	2.74	1.349	71.77	6.52E-04	1.32E-01	5.47E-03
EV-1-2-120	14	8.04E-03	1.39	1.596	83.51	4.36E-04	1.13E-01	4.92E-03
EV-1-3-0-20	15	1.25E-03	9.53	5.430	103.96	3.21E-04	7.43E-02	6.31E-04
EV-1-3-20-40	16	1.25E-03	2.82	1.744	63.94	2.87E-04	7.79E-02	5.07E-04
EV-1-3-20-40	17	1.25E-03	3.07	1.876	66.99	2.22E-04	7.34E-02	5.60E-04
EV-1-3-40-60	18	3.50E-03	1.32	1.057	52.20	4.44E-02	1.33E-01	9.88E-04
EV-1-3-90	19	1.25E-03	3.89	2.320	70.47	3.61E-04	6.43E-02	6.96E-04
EV-1-3-120	20	3.38E-03	0.60	1.020	61.77	5.64E-04	9.50E-02	1.60E-03
EV-1-4-0-20	21	1.25E-03	9.21	4.772	105.70	1.09E-04	3.77E-02	1.06E-03
EV-1-4-0-20	22	1.25E-03	9.21	4.772	105.70	1.09E-04	3.77E-02	1.06E-03
EV-1-4-20-40	23	1.25E-03	3.22	1.699	61.33	1.22E-04	5.44E-02	8.04E-04
EV-1-4-20-40	24	1.25E-03	3.22	1.699	61.33	1.17E-04	4.41E-02	5.97E-04
EV-1-4-40-60	25	1.25E-03	3.97	1.921	66.12	1.13E-04	4.46E-02	6.76E-04
EV-1-4-90	26	1.25E-03	2.82	1.678	62.20	1.12E-04	1.26E-01	9.17E-04
EV-1-4-90	27	1.25E-03	2.82	1.678	62.20	1.12E-04	1.26E-01	9.17E-04
EV-1-4-120	28	1.25E-03	2.77	1.674	62.64	8.64E-05	1.21E-01	1.16E-03
EV-1-4-120	29	1.25E-03	2.87	1.695	62.20	8.64E-05	1.21E-01	1.16E-03
EV-1-4-150	30	1.25E-03	2.28	1.538	61.77	1.47E-04	1.36E-01	1.64E-03

Table B-7) Continued

Location ID	#	Br	Ca	Mg	Na	Al	Si	P
EV-2-1-10	1	1.25E-03	11.18	3.80	91.34	5.28E-05	8.29E-02	1.37E-03
EV-2-1-60	2	1.25E-03	9.66	3.03	85.69	1.79E-04	1.46E-01	1.56E-03
EV-2-1-85	3	3.75E-03	6.14*	2.41*	78.29*	4.70E-04	6.24E-02	1.85E-03
EV-2-2-10	4	1.25E-03	7.58	3.15	92.65	9.23E-05	8.51E-02	1.37E-03
EV-2-2-30	5	1.25E-03	6.14	2.41	78.29	4.70E-05	1.19E-01	1.16E-03
EV-2-2-60	6	1.25E-03	4.62	1.94	68.29	5.92E-05	1.56E-01	1.27E-03
EV-2-2-70	7	1.25E-03	4.84	1.89	67.86	8.44E-05	7.47E-02	8.18E-04
EV-2-2-90	8	1.25E-03	3.72	1.51	64.81	6.34E-05	1.13E-01	1.41E-03
EV-2-3-10	9	1.25E-03	4.69	2.73	103.52	1.09E-04	9.52E-02	9.81E-04
EV-2-3-30	10	1.25E-03	2.39	1.40	70.90	1.09E-04	1.01E-01	1.28E-03
EV-2-3-30	11	1.25E-03	2.39	1.40	70.90	1.09E-04	1.01E-01	1.28E-03
EV-2-3-60	12	1.25E-03	2.84	1.46	64.81	7.79E-05	1.39E-01	1.68E-03
EV-2-3-70	13	1.25E-03	3.17	1.74	73.51	2.34E-04	9.03E-02	1.36E-03
EV-2-3-70	14	1.25E-03	3.24	1.83	77.42	1.77E-04	7.99E-02	1.76E-03
EV-2-3-90	15	1.25E-03	3.72	1.86	74.82	7.81E-05	8.25E-02	1.72E-03
EV-2-3-90	16	1.25E-03	3.72	1.86	74.82	7.81E-05	8.25E-02	1.72E-03
EV-2-4-10	17	1.25E-03	7.88	3.14	101.78	2.99E-05	9.94E-02	9.28E-04
EV-2-4-30	18	1.25E-03	5.79	2.30	77.42	2.59E-04	1.49E-01	1.27E-03
EV-2-4-60	19	1.25E-03	5.69	2.20	69.16	1.56E-04	1.55E-01	1.57E-03
EV-2-4-90	20	1.25E-03	6.49	2.38	72.21	1.25E-04	1.31E-01	1.20E-03
EV-2-4-90	21	1.25E-03	6.49	2.38	72.21	1.35E-04	1.45E-01	1.75E-03
EV-2-4-120	22	1.25E-03	5.71	2.16	70.90	2.32E-04	1.48E-01	3.32E-03
EV-2-4-150	23	1.25E-03	4.74	2.04	70.90	1.26E-04	1.52E-01	8.54E-04
EV-2-4-180	24	1.25E-03	4.59	2.10	73.08	2.64E-04	1.36E-01	1.13E-03
EV-2-4-180	25	1.25E-03	4.49	2.06	72.21	2.64E-04	1.36E-01	1.13E-03

*Values taken from EV-2-2-30

Table B-7) Continued

Location ID	#	Br	Ca	Mg	Na	Al	Si	P
GD-1-60	1	1.25E-03	1.58	1.08	23.49	3.46E-04	6.51E-02	2.41E-03
GD-1-80	2	1.25E-03	0.92	0.81	32.27	8.39E-04	1.33E-01	3.32E-03
GD-1-100	3	1.25E-03	0.55	0.55	28.97	8.82E-04	1.16E-01	2.80E-03
GD-2-10	4	1.25E-03	1.09	0.69	14.92	2.81E-04	9.70E-02	2.22E-03
GD-2-60	5	1.25E-03	1.00	0.67	18.96	4.60E-04	1.01E-01	5.90E-03
GD-2-70	6	1.25E-03	0.78	0.66	31.23	3.58E-04	1.35E-01	3.33E-03
GD-2-100	7	1.25E-03	0.74	0.74	33.49	2.12E-04	1.11E-01	2.60E-03
GD-2-100	8	2.63E-03	0.74	0.74	33.49	2.12E-04	1.11E-01	2.60E-03
GD-3-10	9	1.25E-03	1.49	0.96	17.62	1.82E-04	7.15E-02	1.74E-03
TD-1-10	1	1.25E-03	0.32	0.53	35.36	2.97E-04	8.34E-02	1.79E-03
TD-1-70	2	2.75E-03	0.19	0.39	30.93	8.23E-02	2.33E-01	3.02E-03
TD-1-90	3	2.63E-03	0.22	0.39	31.01	7.18E-04	1.50E-01	4.11E-03
TD-1-90	4	2.63E-03	0.22	0.39	30.75	1.00E-03	1.38E-01	3.50E-03
TD-1-120	5	2.50E-03	0.28	0.46	32.88	6.01E-04	1.87E-01	6.74E-03
TD-2-10	6	1.25E-03	0.47	0.69	40.06	1.58E-03	1.26E-01	4.66E-03
TD-2-70	7	1.25E-03	0.26	0.48	33.62	7.04E-04	1.13E-01	3.09E-03
TD-3-10	8	1.25E-03	1.94	1.78	44.37	1.68E-04	7.75E-02	3.35E-03
TD-3-70	9	1.25E-03*	0.28*	0.49*	35.93*	3.72E-04	8.33E-02	2.72E-03
TD-4-10	10	1.25E-03	0.59	0.78	42.32	7.66E-04	1.01E-01	3.77E-03

*Values taken from TD-3-60

Table B-7) Continued

Location ID	#	K	Mn	Fe	Ni	Cu	Zn
EV-1-1-0-20	1	1.036	3.95E-03	1.77E-04	3.69E-04	8.05E-04	8.01E-05
EV-1-1-0-20	2	1.036	3.99E-03	1.58E-04	3.86E-04	9.10E-04	7.54E-05
EV-1-1-20-40	3	0.586	3.12E-04	1.30E-02	2.41E-04	4.16E-04	4.01E-05
EV-1-1-40-60	4	0.611	4.19E-04	3.84E-02	2.68E-04	3.82E-04	4.38E-04
EV-1-1-90	5	0.384	3.70E-04	1.14E-02	3.27E-04	4.12E-04	8.87E-05
EV-1-1-90	6	0.376	3.70E-04	1.14E-02	3.27E-04	4.12E-04	8.87E-05
EV-1-1-120	7	0.460	3.08E-04	1.25E-03	2.85E-04	5.42E-04	5.20E-05
EV-1-2-0-20	8	1.356	9.45E-03	7.56E-04	9.91E-04	1.19E-03	2.97E-03
EV-1-2-20-40	9	0.077	4.06E-03	1.87E-04	4.92E-04	6.60E-04	1.15E-04
EV-1-2-40-60	10	1.144	2.28E-03	6.32E-04	4.49E-04	8.99E-04	1.23E-04
EV-1-2-90	11	0.688	9.96E-04	1.77E-02	4.25E-04	5.20E-04	8.53E-05
EV-1-2-90	12	0.685	9.96E-04	1.77E-02	4.25E-04	5.20E-04	8.53E-05
EV-1-2-90	13	0.780	9.96E-04	1.77E-02	4.25E-04	5.20E-04	8.53E-05
EV-1-2-120	14	0.762	8.82E-04	1.12E-02	4.13E-04	8.82E-04	8.12E-05
EV-1-3-0-20	15	1.349	1.54E-02	6.58E-04	7.89E-04	1.67E-03	1.64E-04
EV-1-3-20-40	16	0.977	1.83E-03	7.87E-04	3.47E-04	1.31E-03	1.18E-04
EV-1-3-20-40	17	1.024	1.83E-03	7.27E-04	3.47E-04	1.28E-03	2.17E-06
EV-1-3-40-60	18	1.577	6.29E-04	7.13E-03	2.54E-04	1.04E-03	
EV-1-3-90	19	1.049	3.51E-03	5.49E-04	3.85E-04	1.30E-03	1.46E-05
EV-1-3-120	20	0.461	4.75E-04	3.81E-04	3.39E-04	9.11E-04	
EV-1-4-0-20	21	1.142	1.42E-02	1.31E-04	7.70E-04	1.83E-03	2.80E-05
EV-1-4-0-20	22	1.142	1.42E-02	1.31E-04	7.70E-04	1.83E-03	2.80E-05
EV-1-4-20-40	23	0.882	1.27E-03	1.04E-04	2.80E-04	1.20E-03	3.40E-06
EV-1-4-20-40	24	0.871	1.56E-03	1.70E-04	3.06E-04	1.23E-03	
EV-1-4-40-60	25	0.917	1.53E-03		2.94E-04	1.37E-03	
EV-1-4-90	26	0.640	1.54E-03	1.73E-02	5.11E-04	1.25E-03	
EV-1-4-90	27	0.640	1.54E-03	1.73E-02	5.11E-04	1.25E-03	
EV-1-4-120	28	0.642	1.47E-03	2.00E-02	5.23E-04	1.29E-03	3.44E-05
EV-1-4-120	29	0.642	1.47E-03	2.00E-02	5.23E-04	1.29E-03	3.44E-05
EV-1-4-150	30	0.596	1.20E-03	1.47E-02	4.88E-04	1.04E-03	1.11E-04

Table B-7) Continued

Location ID	#	K	Mn	Fe	Ni	Cu	Zn
EV-2-1-10	1	1.13	2.43E-02	2.16E-04	1.94E-03	1.67E-03	7.66E-05
EV-2-1-60	2	0.77	2.30E-03	1.12E-02	5.52E-04	2.04E-03	2.16E-05
EV-2-1-85	3	1.16	1.21E-02	3.19E-04	7.83E-04	2.51E-03	2.93E-05
EV-2-2-10	4	1.05	1.26E-02	3.69E-04	1.20E-03	2.38E-03	4.27E-05
EV-2-2-30	5	0.74	2.50E-03	1.99E-02	3.77E-04	1.97E-03	
EV-2-2-60	6	0.74	1.66E-03	2.43E-02	3.83E-04	1.67E-03	3.84E-05
EV-2-2-70	7	0.87	3.61E-03	2.10E-05	3.95E-04	8.07E-04	
EV-2-2-90	8	0.77	1.37E-03	8.71E-03	3.00E-04	9.84E-04	
EV-2-3-10	9	0.89	5.28E-03	1.11E-04	5.42E-04	1.63E-03	8.48E-06
EV-2-3-30	10	0.64	9.88E-04	4.40E-04	2.22E-04	1.56E-03	
EV-2-3-30	11	0.64	9.88E-04	4.40E-04	2.22E-04	1.56E-03	
EV-2-3-60	12	0.74	1.20E-03	6.66E-03	2.81E-04	1.56E-03	
EV-2-3-70	13	0.80	2.06E-03		3.05E-04	1.66E-03	
EV-2-3-70	14	0.88	1.44E-03		2.61E-04	1.76E-03	
EV-2-3-90	15	0.88	1.46E-03		2.66E-04	1.04E-03	
EV-2-3-90	16	0.88	1.46E-03		2.66E-04	1.04E-03	
EV-2-4-10	17	0.99	1.05E-02	9.39E-05	1.23E-03	1.65E-03	3.13E-05
EV-2-4-30	18	0.82	2.28E-03	2.71E-02	3.30E-04	1.70E-03	
EV-2-4-60	19	0.91	1.92E-03	2.43E-02	3.09E-04	1.85E-03	1.16E-05
EV-2-4-90	20	0.82	3.39E-03	1.71E-02	4.82E-04	1.57E-03	9.25E-06
EV-2-4-90	21	0.88	2.52E-03	3.23E-02	4.04E-04	1.97E-03	7.28E-05
EV-2-4-120	22	0.82	2.62E-03	2.16E-02	4.18E-04	7.90E-04	
EV-2-4-150	23	0.75	3.28E-03	7.25E-03	4.66E-04	9.09E-04	2.78E-04
EV-2-4-180	24	0.81	4.17E-03	1.34E-03	6.20E-04	1.15E-03	3.40E-05
EV-2-4-180	25	0.81	4.17E-03	1.34E-03	6.20E-04	1.15E-03	3.40E-05

Table B-7) Continued

Location ID	#	K	Mn	Fe	Ni	Cu	Zn
GD-1-60	1	0.52	2.91E-03	3.81E-04	5.76E-04	6.20E-04	
GD-1-80	2	0.46	1.33E-03	4.89E-04	3.22E-04	6.75E-04	1.02E-04
GD-1-100	3	0.39	9.85E-04	4.40E-04	2.75E-04	4.84E-04	
GD-2-10	4	0.38	3.73E-03	1.68E-03	9.73E-04	3.18E-04	
GD-2-60	5	0.41	3.75E-03	2.47E-03	1.05E-03	3.37E-04	
GD-2-70	6	0.45	1.49E-03	4.77E-04	2.72E-04	3.48E-04	
GD-2-100	7	0.44	1.52E-03	2.89E-04	3.97E-04	3.80E-04	
GD-2-100	8	0.44	1.52E-03	2.89E-04	3.97E-04	3.80E-04	
GD-3-10	9	0.46	3.95E-04	2.13E-04	3.54E-04	2.98E-04	
TD-1-10	1	0.53	4.56E-03	4.96E-04	4.55E-04	5.16E-04	
TD-1-70	2	0.35	5.46E-04	1.30E-02	1.52E-04	4.11E-04	
TD-1-90	3	0.28	4.41E-04	7.20E-04	1.26E-04	3.55E-04	
TD-1-90	4	0.29	4.54E-04	7.59E-04	1.41E-04	3.35E-04	
TD-1-120	5	0.26	6.04E-04	1.70E-03	7.29E-05	3.73E-04	
TD-2-10	6	0.42	9.40E-04	1.01E-03	2.76E-04	4.92E-04	3.81E-04
TD-2-70	7	0.33	5.65E-04	2.62E-04	1.88E-04	3.94E-04	
TD-3-10	8	0.61	3.06E-03	4.74E-05	4.62E-04	5.81E-04	
TD-3-70	9	0.47	1.37E-03	8.18E-05	2.38E-04	4.97E-04	
TD-4-10	10	0.39	4.54E-04	3.61E-04	1.70E-04	5.07E-04	1.36E-05

Table B-7) Continued

Location ID	#	As	Se	Sr	Ba	H_2S
EV-1-1-0-20	1	7.91E-05	1.06E-04	1.99E-02	2.60E-04	0.001544
EV-1-1-0-20	2	6.79E-05	1.05E-04	2.01E-02	2.61E-04	0.001544
EV-1-1-20-40	3	6.13E-05	1.83E-04	4.92E-03	3.30E-04	0.002959
EV-1-1-40-60	4	6.12E-05	2.04E-04	5.07E-03	4.76E-04	0.015311
EV-1-1-90	5	1.01E-04	2.71E-05	5.44E-03	6.41E-04	0.002316
EV-1-1-90	6	1.01E-04	2.71E-05	5.44E-03	6.41E-04	0.002316
EV-1-1-120	7	1.21E-04	3.35E-05	6.64E-03	5.79E-04	0.000836
EV-1-2-0-20	8	3.59E-05	2.42E-04	7.85E-02	1.94E-04	0.000161
EV-1-2-20-40	9	6.85E-05	1.59E-04	5.74E-02	1.84E-04	0.000322
EV-1-2-40-60	10	5.54E-05	2.47E-04	4.83E-02	2.14E-04	0.000386
EV-1-2-90	11	1.39E-04	3.67E-05	2.10E-02	2.07E-04	0.000515
EV-1-2-90	12	1.39E-04	3.67E-05	2.10E-02	2.07E-04	0.000515
EV-1-2-90	13	1.39E-04	3.67E-05	2.10E-02	2.07E-04	0.000515
EV-1-2-120	14	1.44E-04	5.45E-05	2.58E-02	1.95E-04	0.000869
EV-1-3-0-20	15	5.15E-05	2.49E-04	8.04E-02	1.99E-04	0.00029
EV-1-3-20-40	16	5.28E-05	1.91E-04	3.17E-02	2.41E-04	0.000708
EV-1-3-20-40	17	2.22E-05	2.19E-04	3.24E-02	2.36E-04	0.000708
EV-1-3-40-60	18	2.49E-05	2.23E-04	1.59E-02	3.19E-04	0.001094
EV-1-3-90	19	6.19E-05	1.77E-04	3.49E-02	2.72E-04	0.000483
EV-1-3-120	20	1.55E-04	1.24E-04	1.23E-02	3.09E-04	0.001769
EV-1-4-0-20	21	6.48E-05	2.69E-04	7.13E-02	1.70E-04	0.000257
EV-1-4-0-20	22	6.48E-05	2.69E-04	7.13E-02	1.70E-04	0.000257
EV-1-4-20-40	23	5.53E-05	2.05E-04	2.85E-02	2.09E-04	0.000772
EV-1-4-20-40	24	4.20E-05	1.45E-04	3.51E-02	2.21E-04	0.000772
EV-1-4-40-60	25	2.10E-05	1.26E-04	3.33E-02	1.96E-04	0.000933
EV-1-4-90	26	1.31E-04	2.69E-05	2.73E-02	1.94E-04	0.000836
EV-1-4-90	27	1.31E-04	2.69E-05	2.73E-02	1.94E-04	0.000836
EV-1-4-120	28	1.49E-04	4.32E-05	2.66E-02	2.00E-04	0.000676
EV-1-4-120	29	1.49E-04	4.32E-05	2.66E-02	2.00E-04	0.000676
EV-1-4-150	30	1.33E-04	5.28E-05	2.43E-02	2.02E-04	0.000869

Table B-7) Continued

Location ID	#	As	Se	Sr	Ba	H_2S
EV-2-1-10	1	5.93E-05	1.40E-04	5.93E-02	2.82E-04	0.00029
EV-2-1-60	2	1.54E-04	7.51E-05	3.64E-02	1.99E-04	0.000708
EV-2-1-85	3	4.40E-05	1.00E-04	5.16E-02	2.73E-04	0.000676*
EV-2-2-10	4	6.31E-05	5.99E-05	5.55E-02	1.82E-04	0.000129
EV-2-2-30	5	1.19E-04		4.34E-02	1.85E-04	0.000483
EV-2-2-60	6	1.79E-04	3.91E-05	3.58E-02	1.92E-04	0.00045
EV-2-2-70	7	5.51E-05	5.99E-05	3.96E-02	1.86E-04	0.00029
EV-2-2-90	8	8.25E-05	3.25E-05	3.31E-02	1.92E-04	0.000643
EV-2-3-10	9	7.55E-05	9.42E-05	5.02E-02	1.93E-04	0.00029
EV-2-3-30	10	8.39E-05	6.90E-05	2.60E-02	2.02E-04	0.000515
EV-2-3-30	11	8.39E-05	6.90E-05	2.60E-02	2.02E-04	0.000515
EV-2-3-60	12	1.14E-04	1.71E-05	2.65E-02	2.07E-04	0.000643
EV-2-3-70	13	5.61E-05	3.05E-05	3.14E-02	2.37E-04	0.000354
EV-2-3-70	14	8.96E-05	8.78E-05	3.34E-02	2.29E-04	0.000354
EV-2-3-90	15	6.90E-05	8.63E-05	3.45E-02	2.15E-04	0.00029
EV-2-3-90	16	6.90E-05	8.63E-05	3.45E-02	2.15E-04	0.00029
EV-2-4-10	17	5.83E-05	6.09E-05	5.91E-02	1.81E-04	6.43E-05
EV-2-4-30	18	1.34E-04	3.79E-05	4.46E-02	1.86E-04	0.000322
EV-2-4-60	19	1.55E-04	8.32E-05	4.29E-02	1.77E-04	0.000386
EV-2-4-90	20	1.27E-04	1.33E-05	4.59E-02	1.95E-04	0.000225
EV-2-4-90	21	1.84E-04	2.32E-05	4.57E-02	2.05E-04	0.000225
EV-2-4-120	22	2.11E-04	9.68E-05	4.34E-02	2.06E-04	0.000354
EV-2-4-150	23	1.16E-04	5.03E-05	4.07E-02	2.03E-04	0.000257
EV-2-4-180	24	7.98E-05	7.30E-06	4.16E-02	2.12E-04	0.000225
EV-2-4-180	25	7.98E-05	7.30E-06	4.16E-02	2.12E-04	0.000225

*Value averaged from EV-2-1-60 and EV-2-2-90

Table B-7) Continued

Location ID	#	As	Se	Sr	Ba	H_2S
GD-1-60	1	4.11E-05	2.62E-05	1.45E-02	2.49E-04	6.43E-05
GD-1-80	2	9.20E-05	2.69E-05	9.87E-03	4.04E-04	1.93E-04*
GD-1-100	3	5.48E-05		7.69E-03	7.14E-04	3.22E-04
GD-2-10	4	1.77E-05	3.58E-05	8.85E-03	3.06E-04	1.29E-04
GD-2-60	5	1.70E-05	5.10E-06	9.15E-03	2.90E-04	2.57E-04
GD-2-70	6	7.89E-05	5.77E-05	9.77E-03	6.16E-04	2.57E-04
GD-2-100	7	5.79E-05	4.81E-05	1.00E-02	7.52E-04	4.83E-04
GD-2-100	8	5.79E-05	4.81E-05	1.00E-02	7.52E-04	4.83E-04
GD-3-10	9	1.26E-05	1.11E-04	1.14E-02	2.53E-04	2.25E-04
TD-1-10	1	3.98E-05	6.69E-05	1.48E-02	3.46E-04	6.43E-05
TD-1-70	2	9.24E-05	2.39E-04	4.55E-03	2.19E-03	8.36E-04
TD-1-90	3	9.52E-05	3.43E-05	4.65E-03	2.37E-03	1.19E-03
TD-1-90	4	8.48E-05	2.89E-05	4.64E-03	2.35E-03	1.19E-03
TD-1-120	5	6.68E-05	6.00E-05	5.57E-03	2.50E-03	3.54E-04
TD-2-10	6	2.16E-04	1.57E-03	8.65E-03	5.77E-04	9.65E-05
TD-2-70	7	9.10E-05	8.21E-05	5.59E-03	2.10E-03	6.11E-04
TD-3-10	8	1.57E-05	7.89E-05	2.24E-02	3.23E-04	1.61E-04
TD-3-70	9	4.63E-05	9.60E-06	1.07E-02	3.82E-04	2.90E-04
TD-4-10	10	6.87E-05	6.74E-06	6.96E-03	4.19E-04	4.50E-04

*Value average of GD-1-60 and GD-1-100

Table B-8) Charge balance error and saturation indices from PREEQCi

Location ID	#	charge	Percent Error	Calcite	Dolomite	Gypsum	Siderite
EV-1-1-0-20	1	-8.41E-03	-5.13	0.55	1.26	-1.08	-1.00
EV-1-1-0-20	2	-8.41E-03	-5.13	0.55	1.26	-1.08	-1.05
EV-1-1-20-40	3	-6.02E-04	-0.64	0.43	1.09	-2.05	1.16
EV-1-1-40-60	4	1.27E-03	1.31	0.54	1.36	-2.12	1.66
EV-1-1-90	5	-4.99E-03	-5.34	0.31	0.82	-2.09	1.03
EV-1-1-90	6	-4.15E-03	-4.41	0.30	0.80	-2.11	1.03
EV-1-1-120	7	-8.38E-03	-7.07	-0.06	0.12	-1.79	-0.26
EV-1-2-0-20	8	3.07E-03	1.34	0.56	0.87	0.01	-1.23
EV-1-2-20-40	9	2.51E-03	1.43	0.63	0.85	-0.13	-1.66
EV-1-2-40-60	10	1.47E-03	0.93	0.68	0.94	-0.25	-1.00
EV-1-2-90	11	2.69E-03	2.08	0.73	1.27	-0.88	0.89
EV-1-2-90	12	3.73E-03	2.87	0.74	1.29	-0.87	0.89
EV-1-2-90	13	1.37E-02	9.84	0.81	1.40	-0.82	0.89
EV-1-2-120	14	9.22E-03	5.69	0.45	1.05	-1.07	0.62
EV-1-3-0-20	15	5.77E-03	2.51	0.77	1.38	-0.10	-1.01
EV-1-3-20-40	16	6.01E-04	0.44	0.47	0.81	-0.70	-0.74
EV-1-3-20-40	17	4.48E-03	3.20	0.50	0.88	-0.67	-0.77
EV-1-3-40-60	18	1.99E-03	1.81	0.60	1.20	-1.12	0.60
EV-1-3-90	19	6.50E-03	4.40	0.81	1.49	-0.58	-0.72
EV-1-3-120	20	1.76E-03	1.42	0.47	1.28	-1.53	-0.54
EV-1-4-0-20	21	4.07E-03	1.75	0.65	1.09	-0.12	-1.81
EV-1-4-0-20	22	8.89E-04	0.38	0.64	1.08	-0.11	-1.82
EV-1-4-20-40	23	2.17E-03	1.66	0.61	1.02	-0.64	-1.53
EV-1-4-20-40	24	2.18E-03	1.67	0.61	1.02	-0.64	-1.32
EV-1-4-40-60	25	1.56E-03	1.09	0.60	0.97	-0.54	-1000.00
EV-1-4-90	26	5.36E-04	0.40	0.59	1.05	-0.74	0.69
EV-1-4-90	27	-1.12E-03	-0.83	0.58	1.03	-0.72	0.68
EV-1-4-120	28	3.25E-03	2.47	0.58	1.02	-0.76	0.74
EV-1-4-120	29	3.06E-03	2.33	0.59	1.04	-0.74	0.74
EV-1-4-150	30	5.80E-04	0.44	0.68	1.27	-0.86	0.76

Table B-8) Continued

Location ID	#	charge	Percent Error	Calcite	Dolomite	Gypsum	Siderite
EV-2-1-10	1	-1.43E-02	-6.36	0.81	1.25	-0.03	-1.53
EV-2-1-60	2	-1.94E-03	-0.97	1.11	1.81	-0.14	0.50
EV-2-1-85	3	1.43E-02	8.65	1.52	2.74	-0.49	-0.57
EV-2-2-10	4	6.12E-03	3.08	0.44	0.59	-0.22	-1.49
EV-2-2-30	5	1.42E-02	8.85	0.55	0.79	-0.35	0.44
EV-2-2-60	6	2.41E-03	1.64	0.53	0.78	-0.48	0.60
EV-2-2-70	7	-3.42E-03	-2.25	0.64	0.96	-0.44	-2.37
EV-2-2-90	8	-1.93E-03	-1.36	0.63	0.96	-0.57	0.33
EV-2-3-10	9	-2.18E-02	-9.15	0.55	0.96	-0.41	-1.72
EV-2-3-30	10	-1.27E-02	-7.97	0.40	0.65	-0.74	-1.00
EV-2-3-30	11	-3.03E-04	-0.20	0.43	0.71	-0.77	-0.97
EV-2-3-60	12	1.63E-03	1.20	0.52	0.84	-0.72	0.21
EV-2-3-70	13	9.58E-04	0.62	0.55	0.94	-0.65	-1000.00
EV-2-3-70	14	5.29E-03	3.33	0.56	0.97	-0.64	-1000.00
EV-2-3-90	15	5.13E-03	3.30	0.62	1.04	-0.59	-1000.00
EV-2-3-90	16	-2.12E-03	-1.31	0.61	1.01	-0.57	-1000.00
EV-2-4-10	17	-3.21E-02	-12.83	0.54	0.79	-0.15	-2.01
EV-2-4-30	18	3.97E-03	2.38	0.40	0.52	-0.37	0.44
EV-2-4-60	19	2.75E-03	1.81	0.56	0.81	-0.38	0.55
EV-2-4-90	20	2.29E-03	1.43	0.51	0.67	-0.32	0.28
EV-2-4-90	21	2.38E-03	1.48	0.51	0.67	-0.32	0.56
EV-2-4-120	22	2.33E-03	1.50	0.56	0.78	-0.39	0.48
EV-2-4-150	23	3.69E-03	2.43	0.43	0.59	-0.47	-0.04
EV-2-4-180	24	2.45E-03	1.56	0.60	0.96	-0.49	-0.62
EV-2-4-180	25	1.29E-03	0.83	0.59	0.94	-0.50	-0.62

Table B-8) Continued

Location ID	#	charge	Percent Error	Calcite	Dolomite	Gypsum	Siderite
GD-1-60	1	-3.33E-03	-5.73	0.18	0.28	-1.09	-1.13
GD-1-80	2	3.73E-03	5.63	0.48	0.99	-1.49	-0.59
GD-1-100	3	-1.87E-03	-2.95	0.58	1.27	-1.78	-0.40
GD-2-10	4	-8.29E-04	-2.26	0.27	0.43	-1.40	-0.27
GD-2-60	5	-4.02E-04	-0.92	0.39	0.70	-1.45	0.02
GD-2-70	6	2.02E-03	3.11	0.48	1.00	-1.62	-0.55
GD-2-100	7	1.19E-03	1.69	0.81	1.73	-1.72	-0.52
GD-2-100	8	-3.82E-03	-5.11	0.77	1.64	-1.56	-0.54
GD-3-10	9	2.21E-03	5.43	0.32	0.53	-1.17	-1.21
TD-1-10	1	6.95E-03	10.38	-0.12	0.09	-2.06	-0.69
TD-1-70	2	-1.99E-04	-0.31	0.37	1.17	-2.91	1.20
TD-1-90	3	7.38E-04	1.16	0.44	1.25	-4.76	-0.07
TD-1-90	4	9.73E-04	1.55	0.44	1.25	-3.81	-0.04
TD-1-120	5	1.52E-03	2.27	0.31	0.95	-3.43	0.14
TD-2-10	6	4.02E-03	5.08	-0.23	-0.20	-1.69	-0.62
TD-2-70	7	2.45E-03	3.62	0.44	1.26	-2.66	-0.54
TD-3-10	8	4.64E-03	4.99	0.35	0.75	-0.93	-1.95
TD-3-70	9	2.53E-03	3.53	0.54	1.44	-2.22	-0.98
TD-4-10	10	-7.33E-04	-0.83	0.26	0.75	-1.56	-0.75

Table B-8) Continued

Location ID	#	Fluorite	Goethite	Pyrite	FeS
EV-1-1-0-20	1	-0.65	4.75	13.44	-2.43
EV-1-1-0-20	2	-0.65	4.70	13.32	-2.51
EV-1-1-20-40	3	-0.81	7.89	17.53	0.50
EV-1-1-40-60	4	-0.77	8.44	19.76	1.79
EV-1-1-90	5	-1.20	6.47	16.54	0.04
EV-1-1-90	6	-1.22	6.47	16.54	0.04
EV-1-1-120	7	-1.42	4.44	13.31	-2.04
EV-1-2-0-20	8	-0.94	4.47	11.73	-2.92
EV-1-2-20-40	9	-0.32	4.11	12.22	-2.96
EV-1-2-40-60	10	-0.68	4.83	12.89	-2.36
EV-1-2-90	11	-0.62	6.20	14.61	-0.79
EV-1-2-90	12	-0.61	6.20	14.61	-0.79
EV-1-2-90	13	-0.55	6.20	14.60	-0.79
EV-1-2-120	14	-0.75	5.49	14.15	-1.14
EV-1-3-0-20	15	-0.92	4.66	12.65	-2.51
EV-1-3-20-40	16	-0.81	4.90	13.10	-2.20
EV-1-3-20-40	17	-0.77	4.87	13.09	-2.22
EV-1-3-40-60	18	-0.73	6.84	14.95	-0.81
EV-1-3-90	19	-0.68	5.05	13.03	-2.34
EV-1-3-120	20	-1.21	4.92	13.59	-2.17
EV-1-4-0-20	21	-0.94	3.69	11.80	-3.28
EV-1-4-0-20	22	-0.95	3.69	11.80	-3.28
EV-1-4-20-40	23	-0.75	4.74	12.75	-2.82
EV-1-4-20-40	24	-0.75	4.95	12.95	-2.61
EV-1-4-40-60	25	-0.73	-1000.00	-1000.00	-1000.00
EV-1-4-90	26	-0.89	5.74	14.21	-0.99
EV-1-4-90	27	-0.91	5.74	14.18	-1.01
EV-1-4-120	28	-0.97	5.72	14.10	-1.01
EV-1-4-120	29	-0.96	5.72	14.10	-1.01
EV-1-4-150	30	-0.80	5.88	14.31	-0.99

Table B-8) Continued

Location ID	#	Fluorite	Goethite	Pyrite	FeS
EV-2-1-10	1	-0.80	3.68	11.89	-3.12
EV-2-1-60	2	-0.93	5.77	14.10	-1.17
EV-2-1-85	3	-0.12	5.56	13.40	-2.33
EV-2-2-10	4	-0.91	3.28	11.16	-3.34
EV-2-2-30	5	-1.02	5.71	13.82	-1.14
EV-2-2-60	6	-1.10	5.41	13.58	-1.21
EV-2-2-70	7	-0.68	2.99	11.08	-4.00
EV-2-2-90	8	-0.85	5.56	13.89	-1.29
EV-2-3-10	9	-0.75	3.37	11.70	-3.37
EV-2-3-30	10	-0.94	4.17	12.46	-2.68
EV-2-3-30	11	-0.67	4.19	12.41	-2.69
EV-2-3-60	12	-0.84	5.23	13.48	-1.55
EV-2-3-70	13	-0.81	-1000.00	-1000.00	-1000.00
EV-2-3-70	14	-0.80	-1000.00	-1000.00	-1000.00
EV-2-3-90	15	-0.88	-1000.00	-1000.00	-1000.00
EV-2-3-90	16	-0.80	-1000.00	-1000.00	-1000.00
EV-2-4-10	17	-0.83	2.60	10.39	-4.06
EV-2-4-30	18	-0.90	5.08	13.30	-1.32
EV-2-4-60	19	-0.78	5.39	13.48	-1.26
EV-2-4-90	20	-0.99	4.74	12.95	-1.62
EV-2-4-90	21	-0.99	5.01	13.15	-1.38
EV-2-4-120	22	-0.93	5.04	13.55	-1.27
EV-2-4-150	23	-1.00	4.45	12.70	-1.92
EV-2-4-180	24	-1.15	3.82	12.01	-2.66
EV-2-4-180	25	-1.16	3.82	12.01	-2.66

Table B-8) Continued

Location ID	#	Fluorite	Goethite	Pyrite	FeS
GD-1-60	1	-1.17	3.57	11.02	-3.35
GD-1-80	2	-0.97	4.59	12.20	-2.74
GD-1-100	3	-1.20	5.16	12.85	-2.48
GD-2-10	4	-1.07	4.73	12.12	-2.45
GD-2-60	5	-1.10	5.05	12.72	-2.09
GD-2-70	6	-1.13	4.52	12.43	-2.64
GD-2-100	7	-1.06	5.07	13.02	-2.52
GD-2-100	8	-1.37	5.05	13.00	-2.54
GD-3-10	9	-1.23	4.21	11.69	-3.12
TD-1-10	1	-1.32	4.31	11.77	-2.92
TD-1-70	2	-1.26	6.75	15.02	-0.71
TD-1-90	3	-1.34	5.38	14.18	-1.75
TD-1-90	4	-1.29	5.40	14.28	-1.68
TD-1-120	5	-1.37	5.02	13.16	-2.05
TD-2-10	6	-1.40	3.99	11.70	-2.81
TD-2-70	7	-1.24	4.91	13.04	-2.53
TD-3-10	8	-1.38	2.96	10.73	-3.98
TD-3-70	9	-1.35	4.92	12.47	-3.10
TD-4-10	10	-1.25	4.15	12.30	-2.79

Table B-9) Whole Rock Elemental Data

Location ID	Si	Al	Fe	Mg	Ca	Na	K	Ti	P	Mn	Cr
EV-1-1-0-20	268700	97200	23200	5300	3900	2700	18100	4900	300	500	103
EV-1-1-20-40	225900	117700	25800	5700	3600	3000	19100	4800	300	500	109
EV-1-1-40-60	240100	117900	25100	5700	3500	3200	19800	4900	300	500	109
EV-1-1-40-60	225000	107200	24600	5400	3500	3000	18100	4700	300	500	103
EV-1-1-40-60	240100	117900	25100	5700	3500	3200	19800	4900	300	500	109
EV-1-1-90	274100	94500	22000	4800	3400	2400	17400	4800	300	500	96
EV-1-1-120	276600	91100	21900	4700	3400	2400	17700	4900	300	500	103
EV-1-3-90	272100	97800	22200	4900	4200	2200	18200	4900	300	500	89
EV-1-4-150	271000	97800	22500	4900	4100	2200	18000	4900	300	500	103
EV-2-4-0	277000	86800	20200	4400	4300	2500	16500	5100	300	500	82
EV-2-4-10	277500	89200	20300	4400	4400	2200	16600	5000	300	500	75
EV-2-4-30	276900	89400	20400	4300	4400	1900	16400	5100	300	500	96
EV-2-4-60	275200	89900	20300	4300	4500	1800	16700	5000	300	500	89
EV-2-4-90	277600	89100	20200	4300	4600	1800	16500	5000	300	500	82
EV-2-4-90	277800	88600	20300	4300	4600	1800	16700	5000	300	500	89
EV-2-4-120	279200	88100	20100	4300	4400	1800	16400	5000	300	500	75
EV-2-4-150	277500	89400	20600	4500	4400	1900	16800	5000	300	500	82
EV-2-4-180	276100	88400	20200	4300	4400	1900	16700	4900	300	500	96
GD-2-5	347300	58200	13100	2600	1600	700	11800	5500	200	300	68
GD-2-10	290100	86400	19900	3900	2400	1100	15900	5000	300	500	89
GD-2-10	291700	86600	19900	3900	2500	1200	16600	4900	300	500	96
GD-2-60	285800	87600	20100	4100	2900	1400	16300	5000	300	500	89
GD-2-100	274500	88600	20700	4200	2900	1600	16600	5000	300	500	89
GD-2-100	275600	88600	20400	4200	2800	1500	16200	5000	300	500	82
GD-1-40	313600	72000	16500	3300	2400	1000	13900	6800	200	400	68
GD-3-70	282300	84700	19700	4000	2900	1300	15700	4900	300	500	96
TD-2-0	270100	94200	21300	4500	2800	1600	17100	5000	300	500	89
TD-2-10	267800	95100	21500	4500	2900	1700	17000	5200	300	500	96
TD-2-60	270900	92200	20800	4400	2900	1900	16800	5100	300	500	82
TD-2-60	271800	92100	20800	4300	2900	1900	16800	5000	300	500	103
TD-2-80	279600	92100	20100	4300	3100	1800	17100	4700	300	500	89
TD-1-120	291000	88200	19300	4200	2800	1700	16800	4700	300	500	82
TD-3-70	268400	94600	20900	4600	3200	1900	17400	5000	300	500	96
TD-3-70	268400	94600	20900	4600	3200	1900	17400	5000	300	500	96
TD-4-10	299000	79900	17700	3700	2600	1500	14700	7100	300	400	75

Table B-9) Continued

Location ID	Ba	V	Mo	Pb	Zn	Ni	As	C	S	H_2O
EV-1-1-0-20	445	118	0.6	11.5	37	20.2	2.2	69100	3700	84200
EV-1-1-20-40	451	139	1	13	40	25.6	2	94400	4400	105200
EV-1-1-40-60	439	131	0.7	12.1	36	20.8	1.6	66400	2900	104700
EV-1-1-40-60	429	141	1.3	12.8	39	27.6	2.2	127100	6500	97400
EV-1-1-40-60	439	131	0.7	12.1	36	20.8	1.6	66400	2900	104700
EV-1-1-90	434	113	0.8	11.2	37	20.7	2	67600	3600	84800
EV-1-1-120	441	111	0.7	10.7	36	20.3	2	71700	3800	81500
EV-1-3-90	435	115	0.7	11.2	35	19.6	1.9	62300	3200	86500
EV-1-4-150	424	116	0.7	10.9	34	19.1	1.8	63100	3500	87400
EV-2-4-0	426	108	1	10.4	32	18.2	2	80300	4700	82000
EV-2-4-10	425	109	0.9	11.5	36	19.9	1.6	77700	4700	78600
EV-2-4-30	433	111	0.9	11.1	35	19.9	1.8	77000	4300	80700
EV-2-4-60	455	111	1	10.6	34	20	1.5	77800	4400	82800
EV-2-4-90	427	108	0.9	10.7	34	18.9	1.9	78000	4300	79700
EV-2-4-90	423	109	0.8	10.5	34	19.2	1.6	77700	4000	80300
EV-2-4-120	411	108	0.9	11.5	36	20.7	1.9	76700	3800	80500
EV-2-4-150	428	106	0.8	11.1	35	20.1	2	78100	4800	77100
EV-2-4-180	424	110	0.9	11.2	36	20.8	2	78800	4800	82400
GD-2-5	345	70	0.5	8.3	27	14.3	1.7	39900	1900	57200
GD-2-10	434	105	0.9	12.2	37	20	1.8	62800	3300	79900
GD-2-10	442	107	0.9	12.4	38	20.6	2	63000	3300	74700
GD-2-60	420	109	0.7	11.8	37	15.3	1.7	69900	4000	77100
GD-2-100	426	111	1	11.4	36	20.4	1.8	87600	5100	78300
GD-2-100	426	112	1	11.3	36	19.9	2	85400	5100	79500
GD-1-40	363	93	0.7	10.3	31	18.5	2	64500	3400	65100
GD-3-70	420	105	0.9	11.2	34	18.8	2.1	85100	4600	76300
TD-2-0	434	119	1	12.6	36	24	1.9	84000	4400	79600
TD-2-10	420	120	1.1	13.1	38	22.6	2.1	81700	3900	84400
TD-2-60	421	117	1.1	12	36	22.2	1.9	83000	4700	83300
TD-2-60	409	114	0.9	12.7	36	22.1	2.2	81300	5200	82500
TD-2-80	414	110	1	11	34	19.2	1.7	78100	4700	72200
TD-1-120	430	106	0.8	10.5	34	17.2	2	61400	3600	74000
TD-3-70	432	118	1.4	11.6	36	23.1	2.1	87200	5000	77800
TD-3-70	432	118	1.4	11.6	36	23.1	2.1	87200	5000	77800
TD-4-10	379	100	0.9	10.8	32	19.3	1.6	70000	3600	71400